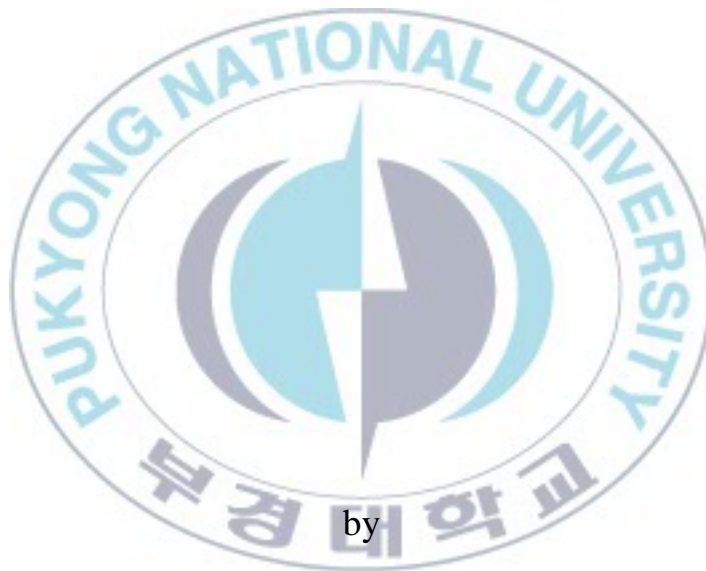


Thesis for Degree of Doctor of Philosophy

Development of Controller for Digital Gas Metal Arc Welding System



by

Seung-Mok Shin

Department of Mechanical Engineering

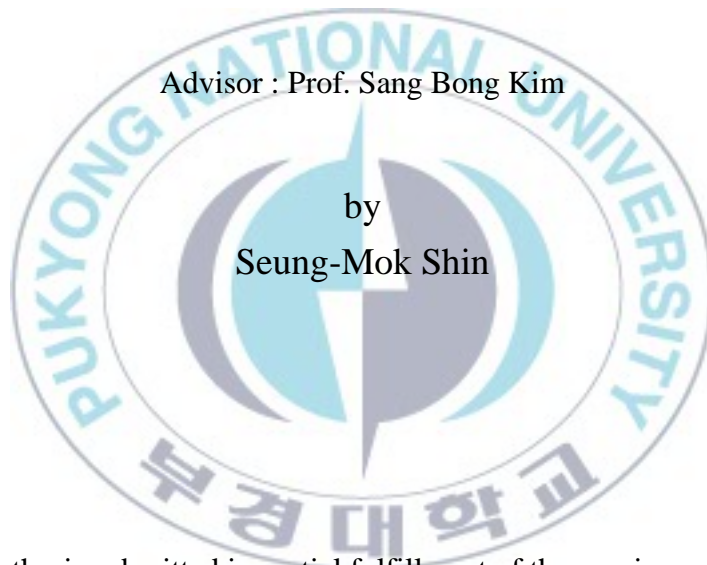
The Graduate School

Pukyong National University

August 2012

Development of Controller for Digital Gas Metal Arc Welding System

디지털 가스금속아크용접시스템을 위한
컨트롤러 개발



Advisor : Prof. Sang Bong Kim

by
Seung-Mok Shin

A thesis submitted in partial fulfillment of the requirements
for the degree of

Doctor of Philosophy

In the Department of Mechanical Engineering, The Graduate School,
Pukyong National University

August 2012

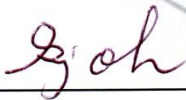
Development of Controller for Digital Gas Metal Arc Welding System

A dissertation
by
Seung-Mok Shin

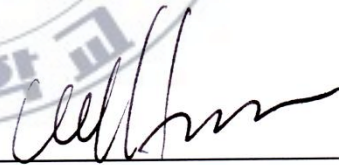
Approved as to styles and contents by:



(Chairman) **Yeon Wook Choe**



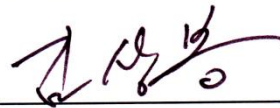
(Member) **Sea June Oh**



(Member) **Hwan Seong Kim**



(Member) **Hak Kyeong Kim**



(Member) **Sang Bong Kim**

June, 2012

Acknowledgements

This dissertation could not have been completed without the help and continuous support from professors, colleagues, friends, and family to whom I am most grateful.

First and foremost, I would like to express my sincere gratitude to my supervisor, Prof. Sang Bong Kim, Pukyong National University. He has been a constant source inspiration and ideas, given me great challenges and been very supportive with all kinds of help.

I would like to appreciate to my dissertation committee, Prof. Yeon Wook Choe, Pukyong National University, Prof. Sea June Oh and Prof. Hwan Seong Kim, Korea Maritime University, and Prof. Hak Kyeong Kim, Pukyong National University, for their detailed comments and suggestion during the final phases of the preparation of this dissertation.

I am also grateful to Pandu Sandi Pratama and Phuc Think Doan for giving me a lot of valuable, interesting and enjoyable discussions, which have contributed substantially to this dissertation.

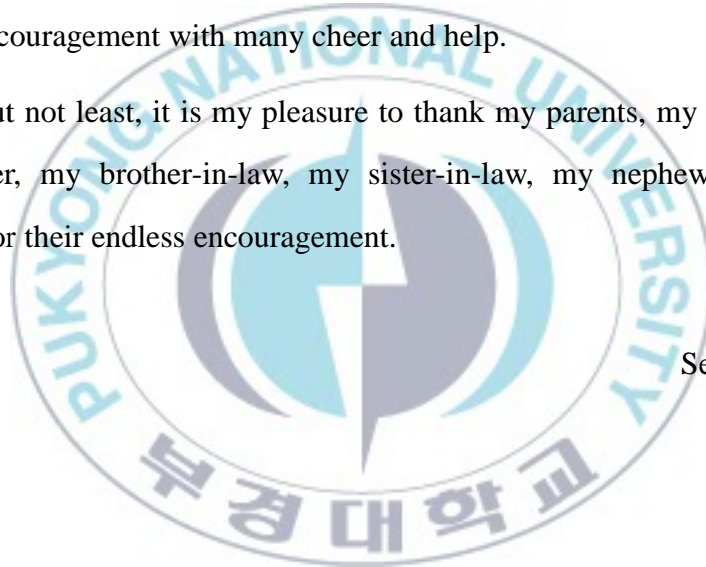
I would like to thank all the members of CIMEC lab for giving me a comfortable and active environment for pursuing my research : Prof. M. S. Shin, Prof. H. U. Ahn, Prof. C. W. Lee, Dr. J. W. Lee, Dr. N. S. Jung, Dr. H. R. Yoo, Dr. J. H. Suh, Dr. D. K. Kim, Dr. S. J. Park, S. K. Kim, Y. M. Park, W. Y. Jeong, M. J. Bae, J. G. Kim, H. J. Im, J. W. Kim and others. And thanks are also due to

all of students, Bui Thanh Luan, Hoang Giang, Patil Chetanraj D from Indonesia and Vietnam for their great encouragement.

I gratefully appreciate the Korea East West Power Company through the Instrumentation & Control department for their support.

This thesis is dedicated to my wife Jie Hye Yoon who has sacrificed thousands of hours of her time to allow me the chance to learn and research and to my children, Soo Hyeon Shin, Seong Hyeon Shin and Ju Hyeon Shin for their endless encouragement with many cheer and help.

Last but not least, it is my pleasure to thank my parents, my parents-in-law, my brother, my brother-in-law, my sister-in-law, my nephews and my all relatives for their endless encouragement.



Seung-Mok Shin

Contents

Acknowledgement	i
Contents.....	iii
Abstract	vi
List of Figures	ix
List of Tables	xiii
Nomenclature.....	xiv
Chapter 1 : Introduction.....	1
1.1. Background and motivation	1
1.2. Review of previous studies	4
1.3. Problem statements	5
1.4. Objective and researching method	7
1.5. Content and summary of contributions	7
Chapter 2 : Theoretical background and system design.....	10
2.1. Basic concepts of welding machines.....	10
2.2. Mathematical modeling.....	15
2.2.1. Dynamics.....	17
2.2.2. Force affecting droplet dynamics	19
2.2.3. Reset conditions	21
2.2.4. DC motor of Wire Feeding Unit (WFU)	25
2.3. Hardware configuration of the proposed system.	27
2.3.1. Shielding gas	28
2.3.2. Gas Metal Arc Welding Power Supply	30
2.3.3. Wire Feeding Unit (WFU)	41
2.3.4. Travel beam.....	41

Chapter 3 : Control design using self-tuning Fuzzy PID.....	43
3.1. Introduction	43
3.2. Model of WFU	44
3.3. Controller design.....	47
3.3.1. Normalization.....	50
3.3.2. Fuzzification.....	50
3.3.3. Fuzzy rule and fuzzy inference	52
3.3.4. Defuzzification.....	54
3.4. Simulation and experimental results	55
3.4.1. Identification of parameters for transfer function	55
3.4.2. Simulation and experimental results	57
3.5. Summary	67
Chapter 4 : Control design using Fuzzy Sliding Mode Control.....	68
4.1. Introduction	68
4.2. Controller design	69
4.2.1. Design of Voltage Controller for Gas metal Arc Welding Power Supply	69
4.2.2. Design of Current Controller for Wire Feeding Unit.....	70
4.3. Simulation and experimental results	76
4.3.1. Identification of parameters for the transfer function	76
4.3.2. Simulation results.....	77
4.3.3. Experimental results.....	82
4.4. Summary	90
Chapter 5 :Kalman filter.....	91
5.1. Introduction	91
5.2. Kalman filter design	92
5.3. Simulation results.....	98
5.3.1. Kalman filter applied in self-tuning Fuzzy PID controller.	101
5.3.2. Kalman filter applied on Fuzzy Sliding Mode Control.....	108

5.4. Summary 114

Chapter 6 : Conclusions and future works. 115

6.1. Conclusions 115

6.2. Future works..... 118

References 119

Publications and conferences128

Appendix131



Development of Controller for Digital Gas Metal Arc Welding System

Seung-Mok Shin

Department of Mechanical Engineering, Graduate School,
Pukyong National University

Abstract

Welding is widely used in several industrial fields such as shipbuilding industries, automobile industries, railway equipment, aircraft, spacecraft and components manufacturing business. Specially, Gas Metal Arc Welding (GMAW) is the most popular welding machine which is used in various industries. It can be used to weld most of commercial metals and alloys. The GMAW process can be done in all positions with higher welding speed, and deeper penetration of the weld rather than other welding method. Furthermore, GMAW process makes automation in welding process becomes easier by combining this process with mobile robot. The development of electronic and electrical technology drags the development of GMAW. The previous control system of GMAW has problems such as no guarantee of stability due to the fixed parameters in PID controller, no guarantee of stability due to the difference between predicted trajectory and actual trajectory in MPC and chattering

phenomenon in SMC. To solve the problems of conventional controllers and increase the quality of welding process, it is necessary to present modeling and to develop new and improved control algorithms for automatic digital Gas Metal Arc Welding (GMAW) process. Therefore, the following tasks are implemented in this dissertation. Firstly, the hardware configuration of GMAW system is proposed. The system consists of shielding gas, Gas Metal Arc Welding Power Supply (PS-GMAW), Wire Feeding Unit (WFU) and travel beam. The PS-GMAW consists of rectifier, inverter, transformer, sensors, control board, DC motor driver and IGBT driver. A control system is based on DSP TMS320F28335 technology. Then, based on the proposed GMAW system, the mathematical modeling of GMAW system is presented. Based on this mathematical modeling, the control algorithm is proposed. To verify the proposed controller, this mathematical modeling also is used in simulation. Secondly, self-tuning Fuzzy Proportional–Integral–Derivative (PID) controller is designed and applied to control the welding current to be constant by controlling the wire-feed speed of the Wire Feeding Unit (WFU). The automatic parameter self-tuning by fuzzy algorithm in the Fuzzy PID controller can solve the problem with limitation of stability due to fixed parameters in PID controllers. Thirdly, Fuzzy Sliding Mode Control (FSMC) is proposed to enhance the quality of the welding result. By fuzzifying the sliding surface, the feedback control gain from the fuzzy inference rule base is obtained. Moreover, based on dynamics modeling of Wire Feeding Unit (WFU), Fuzzy Sliding Mode Control (FSMC) is proposed to change the electrode feed rate in order to achieve the output welding current to the setting value. The FSMC can solve the chattering

phenomenon of SMC. Based on modeling of GMAW Power Supply (PS-GMAW), P controller is proposed to keep the output welding voltage of GMAW Power Supply to the setting value. Finally, the Kalman filter algorithm is proposed. This algorithm is suitable to estimate the value with noisy information. This dissertation presents a method to dynamically observe two important variables of a GMAW process, i.e. arc voltage and welding current. The proposed controller can easily control the welding output using the values estimated by Kalman filter algorithm.

Simulation and experimental results show that the welding current and voltage of the digital GMAW system are successfully controlled by the proposed controllers. Therefore, the simulation and experimental results shows the effectiveness and applicability of the proposed controllers for the digital GMAW system.

Keywords: Gas Metal Arc Welding machine, Fuzzy PID, Fuzzy Sliding Mode Control, Kalman filter.

List of Figures

Chapter 2 : Theoretical background and system design

Fig. 2.1 SMAW welding process.....	12
Fig. 2.2 GTAW welding process	13
Fig. 2.3 GMAW welding process	14
Fig. 2.4 Schematic diagram of GMAW process.....	15
Fig. 2.5 Pendant drop modeled as a mass-spring-damper system.....	21
Fig. 2.6 Schematics of DC motor.....	25
Fig. 2.7 Gas Metal Arc Welding equipment.....	28
Fig. 2.8 Shielding gas.....	29
Fig. 2.9 Bead contour penetration	29
Fig. 2.10 Block diagram of PS-GMAW	30
Fig. 2.11 Schematic circuit of GMAW.....	31
Fig. 2.12 Low frequency rectifier.....	32
Fig. 2.13 IGBT inverter.....	33
Fig. 2.14 High frequency transformer.....	34
Fig. 2.15 High frequency rectifier.....	35
Fig. 2.16 IGBT driver circuit.....	36
Fig. 2.17 Current sensor and signal conditioner circuit	37
Fig. 2.18 Voltage sensor and signal conditioner circuit	37
Fig. 2.19 DC motor driver circuit.....	38
Fig. 2.20 TMS320F28X EVM Rev.1.1 and TMS320F28335 V1.4	40
Fig. 2.21 DSP pin configuration.....	40
Fig. 2.22 Wire Feeding Unit (WFU)	41
Fig. 2.23 Travel beam.....	42
Fig. 2.24 GMAW system for experiment.....	42

Chapter 3 : Control design using self-tuning Fuzzy PID

Fig. 3.1 Block diagram for an open loop transfer function of the WFU	46
Fig. 3.2 Conventional PID controller	48
Fig. 3.3 Self-tuning Fuzzy PID controller	49
Fig. 3.4 Fuzzy logic control structure	50
Fig. 3.5 Membership functions of input (e, \dot{e})	51
Fig. 3.6 Membership functions of output (K_p, K_i and K_d)	51
Fig. 3.7 Rule surface views	54
Fig. 3.8 Tuning gains	59
Fig. 3.9 Control voltage of Wire Feeding Unit in simulation	60
Fig. 3.10 Output current in simulation	61
Fig. 3.11 Welding current error in simulation	62
Fig. 3.12 Disturbance applied to GMAW system	63
Fig. 3.13 Simulation results for developed GMAW with disturbance	64
Fig. 3.14 Tuning-gains with disturbance	65
Fig. 3.15 Experimental results for developed GMAW	66
Fig. 3.16 Welding result by FPID	66
Fig. 3.17 Welding result by PID	67

Chapter 4 : Control design using Fuzzy Sliding Mode Control

Fig. 4.1 Membership functions	74
Fig. 4.2 Rule surface of SFMC	75
Fig. 4.3 Block diagram of GMAW control system.	75
Fig. 4.4 Control voltage of Wire Feeding Unit in simulation	78
Fig. 4.5 Output current in simulation.	79
Fig. 4.6 Welding current error in simulation.	80
Fig. 4.7 Sliding surface in simulation.	81
Fig. 4.8 Output welding voltage and current in simulation	82
Fig. 4.9 Control input voltage of Wire Feeding Unit using PID controller	83
Fig. 4.10 Welding current and welding voltage using PID controller.	84

Fig. 4.11 Welding current error using PID controller.....	85
Fig. 4.12 Wire Feeding Unit control input of voltage using FSMC.....	86
Fig. 4.13 Welding current and welding voltage using FSMC	87
Fig. 4.14 Welding current error using FSMC.....	88
Fig. 4.15 Sliding surface	89
Fig. 4.16 Welding results of GMAW.....	89

Chapter 5 :Kalman filter

Fig. 5.1 Block diagram of GMAW system applying Kalman filter to self-tuning Fuzzy PID controller.....	101
Fig. 5.2 Control input voltage of Wire Feeding Unit with/ without applying Kalman filter to self-tuning Fuzzy PID controller in simulation	102
Fig. 5.3 Output current in simulation with/ without applying Kalman filter to self-tuning Fuzzy PID controller.....	103
Fig. 5.4 Welding current error with/ without applying Kalman filter applied to self-tuning Fuzzy PID controller in simulation.....	104
Fig. 5.5 PS-GMAW voltage controller with/ without applying Kalman filter to self-tuning Fuzzy PID controller in simulation.....	105
Fig. 5.6 Arc voltage in simulation with/ without applying Kalman filter to self-tuning Fuzzy PID controller	106
Fig. 5.7 Arc voltage error in simulation with/ without applying Kalman filter to self-tuning Fuzzy PID controller.....	107
Fig. 5.8 Block diagram of GMAW system applying Kalman filter to Fuzzy Sliding Mode Control.....	108
Fig. 5.9 Wire Feeding Unit control voltage with/ without applying Kalman filter to Fuzzy Sliding Mode Control in simulation.....	109
Fig. 5.10 Output current in simulation with/ without applying Kalman filter to Fuzzy Sliding Mode Control in simulation.....	110
Fig. 5.11 Welding current error in simulation with/ without applying Kalman filter to Fuzzy Sliding Mode Control	111
Fig. 5.12 Arc voltage in simulation with/ without applying Kalman filter to	

Fuzzy Sliding Mode Control.....112
Fig. 5.13 Arc voltage in simulation with/ without applying Kalman filter to
Fuzzy Sliding Mode Control113



List of Tables

Chapter 1 : Introduction

Table 1.1 Problems of conventional controllers	6
--	---

Chapter 2 : Theoretical background and system design

Table 2.1 GMA welding natural metal transfer modes.	24
--	----

Chapter 3 : Control design using self-tuning Fuzzy PID

Table 3.1 Rule bases for determining gain K_p	52
---	----

Table 3.2 Rule bases for determining gain K_{ii}	53
--	----

Table 3.3 Rule bases for determining gain K_{td}	53
--	----

Table 3.4 Numerical values of DC motor of WFU	56
---	----

Table 3.5 Welding condition for the experiment	58
--	----

Chapter 4 : Control design using Fuzzy Sliding Mode Control

Table 4.1 Rule base of FSMC	74
-----------------------------------	----

Table 4.2 Numerical values and initial conditions	77
---	----

Chapter 5 : Kalman filter

Table 5.1 Parameter values for simulation.	99
---	----

Chapter 6 : Conclusions and future works

Table 6.1 Advantages of proposed controllers	117
--	-----

Nomenclatures

Variables	Descriptions	Units
b_d	damping coefficient	[Ns/m]
b_m	damping ratio of mechanical system	[Nms]
b'	conversion ratio from angular velocity into linear velocity	
CT	distance from contact tip to work piece	[m]
C_d	drag coefficient	
D	duty cycle	
D_{roll}	diameter of wire electrode roll	[m]
D_{mtr}	rotor diameter of motor	[m]
D_{ratio}	ratio of diameter between motor and feed roll	[m]
E	secondary voltage drop	[V]
E_a	arc length factor	[V/m]
e	back emf	[V]
e_i	current error of welding machine	[A]
\dot{e}_i	derivative of the current error	[A/s]
e_u	arc voltage error of PS-GMAW	[V]
F_d	force due to aerodynamic drag	[N]
F_e	force due to electromagnetic induction	[N]
F_m	force due to momentum	[N]
F_g	force due to gravity	[N]
F_s	surface tension force	[N]
F_{tot}	total force acting in droplet detachment	[N]

g	acceleration of gravity	[m/s ²]
H	heat input	[J]
I_s	setting current for welding machines	[A]
I_w	welding current	[A]
i	armature current	[A]
J_m	moment inertia of the motor	[kgm ²]
J_L	moment inertia of the wire feed roll	[kgm ²]
K_{gear}	gear box ratio	
K_P	proportional gain of conventional PID	
K_I	integral gain of conventional PID	
K_D	derivative gain of conventional PID	
K_{pp}	proportional gain of proposed P controller	
K_{tp}	proportional tuning-gain of Fuzzy PID controller	
K_{ti}	integral tuning-gain of Fuzzy PID controller	
K_{td}	derivative tuning-gain of Fuzzy PID controller	
K_{pf}	proportional gain of Fuzzy PID controller	
K_{if}	integral gain of Fuzzy PID controller	
K_{df}	derivative gain of Fuzzy PID controller	
k_d	spring constant	[N/m]
k_e	motor constant	[Vs/rad]
k_T	armature constant	[Nm/A]
L_{am}	electric inductance of armature	[H]
L_s	inductance	[H]
l_{arc}	arc length	[m]
l_s	stick out	[m]
\dot{l}_s	stick put velocity	[m/s]
M_L	mass of feed roll	[kg]

M_R	melting rate	[m ³ /s]
M_{Ri}	ration of melting rate related to current	[m ³ /sA]
M_{Rv}	ration of melting rate related to voltage	[m ³ /sV]
n_p	number of primary winding	
n_s	number of secondary winding	
P	input power	[watt]
R_{arc}	arc resistance	[Ω]
R_{am}	electric resistance of armature	[Ω]
R_L	electrode resistance	[Ω]
R_s	source resistance	[Ω]
r_d	droplet radius	[m]
R_a	entry radius of current path	[m]
r_a	exit radius of current path	[m]
r_o	electrode radius	[m]
T_m	motor torque	[Nm]
T	sampling time	[s]
U_b	relative fluid to drop velocity	[m/s]
U_u	PS-GMAW voltage controller	
u_i	current controller	
V_{AC}	AC input voltage of rectifier	[V]
V_{arc}	arc voltage	[V]
V_{DC}	DC output voltage of rectifier	[V]
V_d	stick out voltage	[V]
V_m	motor supply voltage	[V]
V_{oc}	open circuit voltage	[V]
V_o	arc voltage constant	[V]
V_s	setting voltage for welding machines	[V]

V_T	relative travel velocity	[m/s]
V_{Tout}	output voltage of transformer	[V]
V_{Tin}	input voltage of transformer	[V]
V_t	output voltage of transformer	[V]
W_f	electrode feed rate	[m/s]
x_d	droplet displacement	[m]
\dot{x}_d	droplet velocity	[m/s]
\ddot{x}_d	droplet acceleration	[m/s ²]
α	angle between the arc axis and the vertical	[°]
ΔD	welding voltage disturbance	[V]
ΔG	welding current disturbance	[V]
γ	surface tension constant	[N/m ²]
ρ	resistivity of the electrode	[Ω /m]
ρ_p	plasma density	[kg/m ³]
ρ_ω	electrode density	[kg/m ³]
μ_0	permeability of free space	[kg m/A ² s ²]
μ	magnetic permeability	[kg m/A ² s ²]
θ	rotor angle	[rad]
$\dot{\theta}$	angular velocity of the motor	[rad/s]
$\ddot{\theta}$	angular acceleration of the motor	[rad/s ²]
$\ddot{\theta}_L$	angular acceleration of the wire feed roll	[rad/s ²]

Chapter 1. Introduction

1.1 Background and motivation

Manufacturing industries in South Korea gives 27.9% of the Gross Domestic Product (GDP) and absorbs 37.9% of employment [7]. In manufacturing industry, welding industry is the most important industry because the raw materials are not useful unless they are molded and welded well.

In 2006, total product amount of South Korean welding industry was USD 2.77 billion [7]. The amount has increase gradually during the past four years due to rapid development of the manufacturing industry in South Korea during this decade.

South Korea's shipbuilding industry is largest in the world. The amount of welding usage in the shipbuilding industry is 57% of total amount in the overall major industries [7]. Lloyd's World Shipbuilding Statistics, shows that the total ship production in South Korea was increased dramatically from 1990 to 2005. In 2005, South Korean, Japanese and Chinese shipbuilders secured 37%, 24% and 16.6% of world shipbuilding orders, respectively [29].

The second major industries using welding machines in their production process are automobile industries. Automobile industry of South Korea was the fifth largest in the world in terms of production volume and the sixth largest in term of export volume in 2010 [12]. During the last three decades beginning in the 1970s, South Korea's automotive industry has risen from a small

government-controlled parochial industry to a significant player in the global markets. Three major companies Hyundai Motor Company, Kia Motors Corporation, and Daewoo Motor Corporation accounted for about 90 percent of the South Korean market, while the remaining was supplied by minor producers and importers.

The other industries using welding machines in their production are Railway equipment manufacturing business, aircraft, spacecraft and components manufacturing business.

The export amount of the welding industries grew dramatically at an annual average of 21% from 2004 to 2008. While the export amount was 2 times of the import amount in 2004, the export amount was confirmed to be 3.5 times of the import amount in 2008 [7].

The most popular welding machine in South Korean manufacturing industries is Gas Metal Arc Welding (GMAW). The GMAW is applied to most industries due to its versatility and specific advantages such as [15]:

- GMAW is the only consumable electrode welding process that can be used for welding all commercial metals and alloys.
- GMAW welding can be done in all positions unlike in submerged metal arc welding.
- Because of the continuous electrode feed, the metal deposition rates in GMAW are significantly higher than shielded metal arc welding (SMAW).

- Due to higher metal filler deposition rates, welding speed in GMAW can be higher than that in SMAW.
- Because the wire feed is continuous in GMAW, continuous welding is possible.
- GMAW has no restriction on the length of the electrode as in SMAW.
- With spray transfer in GMAW, deeper penetration of the weld is possible compared to SMAW.
- Due to the absence of slag, GMAW has less problems for cleaning.
- Furthermore, the welding process can be combined with mobile robot [3,35,49].

In order to increase product quality, a good quality welding machine must be developed. Due to the development of electronic and electrical technology, more advanced technology has been applied to increase the quality of welding machines [22]. The GMAW system included fast inverter module and a relative powerful controller system, which was supposed to control the welding process through the inverter module. Even though inverter technology and controller were used in older machines, the computation capability was limited, and the control algorithms were based on traditional transformer welding machines. To develop the new inverter with powerful computational capability, better control algorithms are needed.

1.2 Review of previous studies

The principles of gas metal arc welding began to be understood in the early 19th century after Humphry Davy discovered the short pulsed electric arcs in 1800. Vasily Petrov independently produced the continuous electric arc in 1802 soon followed by Davy[61]. Until 1880, the electric arc technology has been developed with the aim of industrial usage. At first, carbon electrodes were used in carbon arc welding. By 1890, metal electrodes were invented by Nikolay Slavyanov and C. L. Coffin[62]. In 1920, GMAW was invented by P. O. Nobel of General Electric. It used a bare electrode wire and direct current, and used arc voltage to regulate the feed rate.

In 1948, the GMAW was finally developed by the Battelle Memorial Institute. It used a smaller diameter electrode and a constant voltage power source which had been developed by H.E. Kennedy. It offered a high deposition rate, but the cost of inert gases is high and limited to use to non-ferrous materials. In 1953, carbon dioxide as a welding atmosphere was used. GMAW became more popular since it made welding steel more economical. In 1958 and 1959, the short-arc variation of GMAW was released. It increased welding versatility and made the welding of thin materials possible while it relies on smaller electrode wires and more advanced power supplies. The spray-arc transfer variation was developed in the early 1960s when experimenters added small amounts of oxygen to inert gases. More recently, pulsed current has been applied, giving rise to a new method called the pulsed spray-arc variation.

Nowadays, researching the GMAW process involves a large number of

topics. These topics can be divided into control of the process, and investigation and modeling of the physics characterizing the process. The control area can be divided into control of the weld pool, and control of the arc and the electrode. The quality of the weld is related to weld pool geometry such as penetration, the heating and cooling of the workpiece. Control of the arc and the electrode can also be related to the quality of the weld. The area of this research is closely concerned with control algorithms for electrode melting, drop detachment and stabilization of arc length.

In Gas Metal Arc Welding system, arc voltage and welding current are the main controllable parameters to get the best welding result [32]. Welding voltage is directly related to metal transfer mode [2] and welding current is directly related to droplet generation [23], deposition rates, depth and width of weld penetration and size of the weld bead [16]. Finally, both parameters affect many features of weld such as weld geometry, weld metallurgical characteristics, weld stability, weld defect and strength [39, 45].

1.3 Problem statements

Several control approaches are implemented to control the welding process of GMAW. Two PI controllers were applied by K. L. Moore et al. [32], M. Abdelrahman [33] and F. Ding et al. [17] to control welding process. X. Huang and S. Chen [56], M. Jafari et al. [34] and P. V. Junhor et al. [44] proposed Support Vector Machine(SVM) based fuzzy modeling. Y. M. Zang et al. [58] and Y. M. Chae et al. [59] proposed novel control method to control the welding

output. However, since the system is nonlinear, it is difficult to tune parameters to get the result in whole range operation in those kinds of classical control methods. M. M. Anzehee et al. [39] proposed Model Predictive Control (MPC) to improve the control performance. The problem is that MPC has no guarantee for closed-loop system to be stable if the predicted trajectory is different from the actual trajectory. C. Y. Lee et al. [11], M. D. Ngo et al. [37] and W. H. Chu et al. [54] proposed sliding mode control to control GMAW. In sliding mode control, chattering phenomenon in digital application excites high frequency unmodeled dynamics which are undesired in the control system [6].

Table 1.1 shows the problems of conventional controllers.

Table 1.1 Problems of conventional controllers

Conventional controller	Problems
PI control by K. L. Moore et al. SVM fuzzy modeling by X. Huang and S. Chen Novel control method by Y. M. Zang et al.	Fixed controller parameters : difficult to tune under system parameter variations in real time
MPC by M. M. Anzehee et al.	No guarantee of stability for closed-loop system
Sliding mode control by M. D. Ngo et al.	Chattering phenomenon

To solve the conventional controller's problems, the new controllers are needed to solve the above problems.

1.4 Objective and researching method

The objective of this dissertation is to present modeling and innovative control algorithms for digital GMAW system. To do this, the following tasks are done. Firstly, hardware configuration and mathematical modeling of GMAW system is proposed. Secondly, a simple algorithm of welding current controller using self-tuning Fuzzy Proportional–Integral–Derivative (PID) controller is proposed. Thirdly, a welding current controller and an arc voltage controller using Fuzzy Sliding Mode Control are proposed. Finally, the Kalman filter algorithm to estimate the wire feed rate using welding current and arc voltage information is proposed and applied to the above two controllers.

Simulation and experimental results show that the welding current and voltage of the digital GMAW system are successfully controlled by the proposed controllers. Therefore, the simulation and experimental results shows the effectiveness and applicability of the proposed controllers for the digital GMAW system.

1.5 Content and summary of contributions

Chapter 1: Introduction

This chapter introduces the research background and motivation, objective and research method of this dissertation, and the outline of content and summary of contribution of this dissertation.

Chapter 2: Theoretical background and system design

This chapter explains the basic concepts, mathematical modeling and hardware configuration of GMAW.

Chapter 3: Controller design using self-tuning Fuzzy PID

This chapter introduces welding current control using self-tuning Fuzzy PID and conventional PID controller method based on the modeling of Wire Feeding Unit (WFU). Simulation and experimental results of the self-tuning Fuzzy PID controller are compared to those of conventional PID controller.

Chapter 4: Control design using Fuzzy Sliding Mode Control

This chapter introduces welding current controller using Fuzzy Sliding Mode Control based on the modeling of WFU and welding voltage control using of PS-GMAW using P controller. The control system is tested through simulation and experiment to verify the effectiveness of control system. Simulation and experimental results of the self-tuning Fuzzy Sliding Mode Control are compared to those of conventional PID controller.

Chapter 5: Kalman filter

This chapter introduces Kalman filter algorithm for estimating the welding current and welding voltage in GMAW system with noisy condition. Furthermore, by the estimated value of Kalman filter, the arc voltage and the welding current are controlled using self-tuning Fuzzy PID controller and Fuzzy Sliding Mode Controller. To verify the effectiveness of Kalman filter, simulation

and experiment are done.

Chapter 6: Conclusions and future works

The conclusions for each chapter are summarized and discussed. Moreover, suggestions for the future work on GMAW control related topics are presented.



Chapter 2. Theoretical background and system design

This chapter describes the basic concepts of welding machines, mathematical modeling of GMAW system and the prototype of Gas Metal Arc Welding system for experiment. The overall objective of this dissertation is to improve the weld quality by developing an advanced control scheme for the GMAW process. One way to find such controller scheme is, first, to develop a mathematical modeling to describe the process, and then, based on the modeling, a controller for the process is designed. Moreover, the hardware configuration of the GMAW system is described.

2.1 Basic concepts of welding machines

Welding is a common process to join metals in industrial activity. The American Welding Society (AWS) defines welding as “a kind of a joining process that produces coalescence of materials by heating them to the welding temperature, with or without the application of pressure or by the application of filler” [1].

The physics of welding deals with the complex physical phenomena associated with welding, including electricity, heat, magnetism, light and sound. In particular, many welding processes require the application of heat or pressure, or both, to produce a suitable bond between the

parts being joined. A common means of heating for welding is done by the flow of current through electrical contact resistance at the joined surfaces of two work pieces.

Several kinds of welding process that acquire heat from the outside can be described as follows:

- Arc Welding
- Resistance Welding
- Electro-Slag Welding
- Oxyfuel Gas Welding
- Thermit Welding
- Diffusion Welding
- Electron Beam Welding
- Laser Beam Welding
- Friction Welding
- Ultrasonic Welding
- Spot, Seam and Projection Welding
- Flash, Upset and Percussion Welding

Moreover, welding method using arc welding consists of

- Shielded Metal Arc Welding (SMAW)
- Gas Tungsten Arc Welding (GTAW)
- Gas Metal Arc Welding (GMAW)
- Flux-Cored Arc Welding (FCAW)
- Submerged Arc Welding (SAW)

- Electro-gas Welding (EGW)
- Plasma Arc Welding (PAW)

In 1881, the electric arc welding method for steel known as carbon arc welding, using carbon electrodes was created. The advances in arc welding continued with the invention of metal electrodes in the late 19th century which gave a more stable arc. This welding method is called Stick Metal Arc Welding (SMAW). In SMAW process at Fig. 2.1, a consumable electrode with a dry flux coating and a metal core is used [1]. When an electrical arc is established between the electrode and workpiece, it melts the workpiece, the solid metal core of the electrode and the flux coating. As the flux coating burns away, gas is released and protects the welding process from the ambient air. The gas becomes an active component in the stick welding process. A layer of slag, covering and protecting the welded area, is produced from the burning flux coating. Stick welding is a simple process that can be carried out using some inexpensive equipment. However, compared to the other arc welding methods, its weld quality is not as good as the other arc welding method.

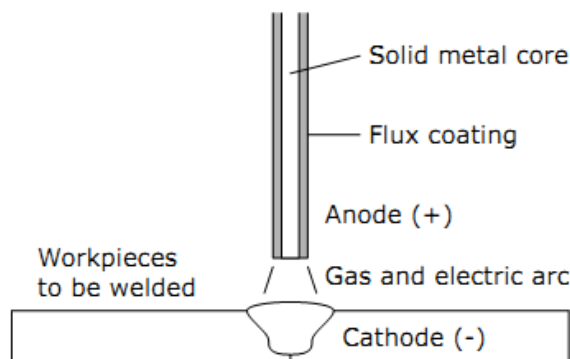


Fig. 2.1 SMAW welding process

There are better methods which are not time-consuming due to change of electrode pieces such as Gas Tungsten Arc Welding (GTAW) and Metal Inert Gas (MIG) [21]. In GTAW, an electrode consisting of pure tungsten or some alloy that includes tungsten is used. Because the electrode has high melting point, the electrode in GTAW is not supposed to be melted. Thus, in the GTAW process, only the workpiece is melted. Similarly in SMAW process, a gas is used to protect the weld area from contamination. However, the gas is externally supplied to the process. GTAW produces a high quality of welds, but it is slow. So it is not suitable for many industrial applications requiring high welding speed. Fig. 2.2 illustrates the GTAW process [1].

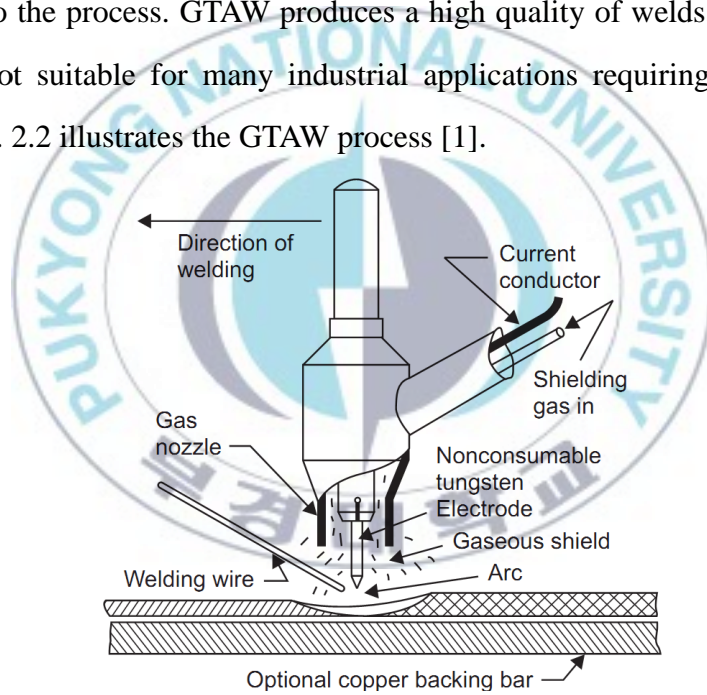


Fig. 2.2 GTAW welding process

Since the inert gases are expensive to produce, Metal Active Gas (MAG) or Gas Metal Arc Welding (GMAW) was invented, where a chemical gas such as carbon dioxide (CO_2) is used. In GMAW, a consumable electrode is used. The

electrical arc is generated between the consumable electrode usually acting as the anode and the workpiece acting as the cathode. The energy produced in the arc melts the electrode, and causes drop growth and drop detachment from the tip of the electrode. The electrode is replaced by new electrode material, often referred to as the wire. The wire electrode material is pushed forward by a wire feed system. Similarly in GTAW, the process is protected from the ambient air using a shielding gas. Typically, pure argon or a mixed gas of argon and CO₂ is used. Fig. 2.3 describes the GMAW process involving the electrical arc [1, 57].

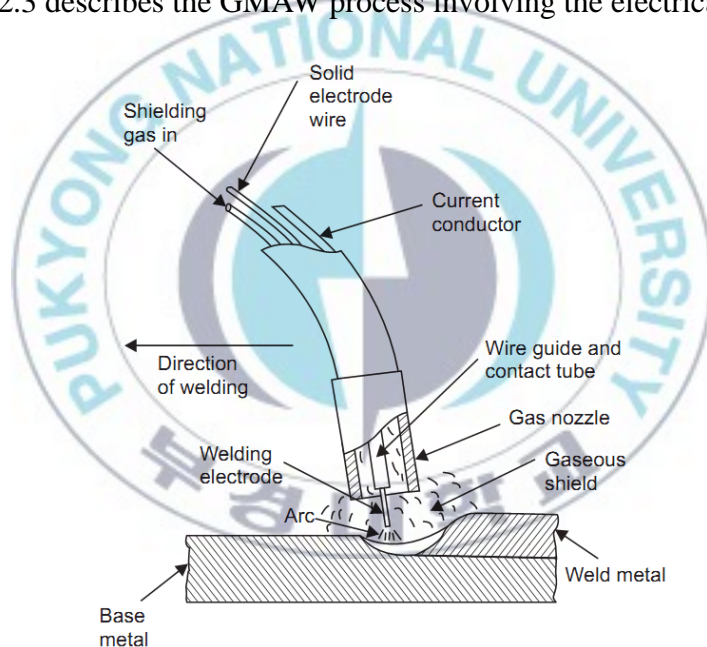


Fig. 2.3 GMAW welding process

The focus of this dissertation is on Gas Metal Arc Welding (GMAW). The American Welding Society (AWS) defined Gas Metal Arc Welding (GMAW) to be “an arc welding process that uses an arc between a continuous filler metal

electrode and the weld pool. The process is used with shielding from an externally supplied gas and without the application of pressure[1].

2.2 Mathematical modeling

Mathematical modeling from [15, 20, 25, 27, 31] are applied in this dissertation. To present the model, first, schematic diagram of GMAW process for obtaining the modeling equations is given. Secondly, the equations describing the dynamics of droplet and the forces acting on the drop are given. Thirdly, the reset condition that governs droplet detachment is given. Finally, the DC motor modeling for Wire Feeding Unit is given.

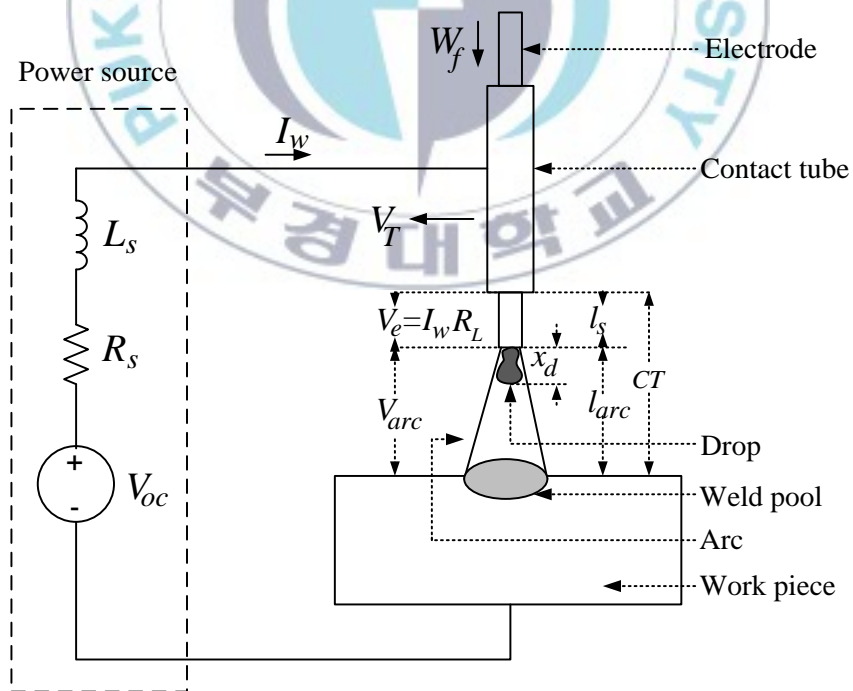


Fig. 2.4 Schematic diagram of GMAW process

The schematic diagram of GMAW process is shown in Fig. 2.4. Symbols in Fig. 2.4 are denoted as follows:

V_{oc} : open circuit voltage [V]

R_s : source resistance [Ω]

L_s : inductance [H]

I_w : welding current [A]

W_f : electrode feed rate [m/s]

V_T : relative travel velocity [m/s]

V_e : stick out voltage [V]

R_L : electrode resistance [Ω]

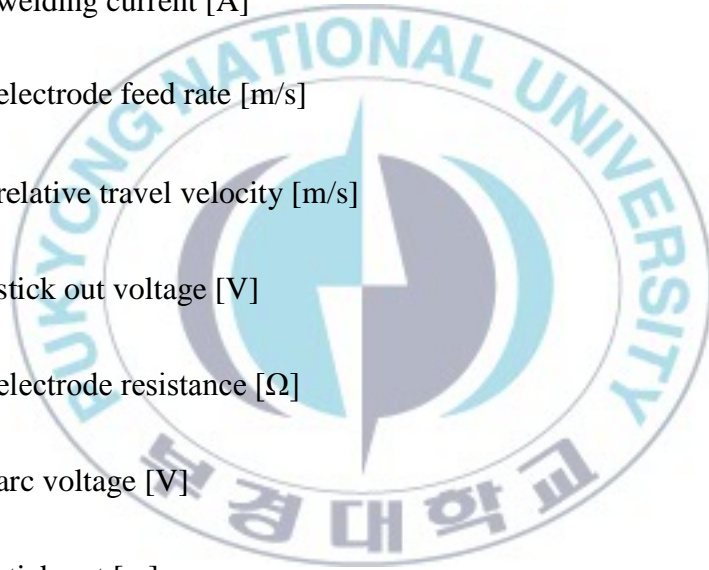
V_{arc} : arc voltage [V]

l_s : stick out [m]

x_d : droplet displacement [m]

l_{arc} : arc length [m]

CT : distance from contact tip to work piece [m]



2.2.1 Dynamics

- Welding current

Welding current is important factor in welding process. Based on Kirchhoff's current law, the mathematical modeling of current in GMAW process in Fig. 2.4 are:

$$\dot{I}_w = \frac{V_{oc} - R_L I_w - V_{arc} - R_s I_w}{L_s} \quad (2.1)$$

The welding current is directly related to heat transfer [47]. In the case of arc welding, the energy input is usually the arc energy input. Arc energy input, H [J/m], is the quantity of energy transferred per unit length of weld from a traveling heat source. Thus, the energy input is defined as the ratio of the total input power, P [W], of the heat source to its relative travel velocity, V_T [m/s].

$$H = P / V_T \quad (2.1)$$

If the heat source is an arc, the heat input energy is obtained as

$$H = I_w E / V_T \quad (2.2)$$

$$E = V_e + V_{arc} \quad (2.3)$$

where E is secondary voltage drop [W].

- Arc voltage

The voltage drop across the arc is directly proportional to arc length. Hence, the arc voltage is controlled by changing the arc length. There is a minimum voltage for striking the arc, and the open-circuit voltage of the power supply is obviously higher than the arc-striking voltage. The arc voltage, V_{arc} , is denoted by:

$$V_{arc} = V_o + R_{arc} I_w + E_{arc} (CT - l_s) \quad (2.4)$$

V_o is arc voltage constant and its value is 12V, R_{arc} is arc resistance [Ω], E_{arc} is arc length factor and its value is 1500V/m, CT is distance from contact tip to work piece [m] and l_s is stick out [m].

- Melting rate

The heat energy in an arc is generated by electrical reactions at the anode and cathode regions within the plasma. This energy melts the electrode. The melting rate is primarily affected by the welding current [50]. The melting rate, M_R [m/s], is given as [41]:

$$M_R = M_{Ri} I_w - M_{Rv} V_{arc} \quad (2.5)$$

where M_{Ri} and M_{Rv} are the ratios of the melting-rate related to the welding current and welding voltage, respectively.

- Stick out

In welding process, electrode extension or stick out determines the welding current and arc voltage. The stick out velocity, \dot{l}_s [m/s], is calculates using

equation:

$$\dot{l}_s = W_f - M_R \quad (2.6)$$

The stick out resistance, R_L [Ω], is defined by:

$$R_L = \rho[l_s + 0.5(r_d + x_d)] \quad (2.7)$$

Stick out resistance depends on resistivity of the electrode, ρ [Ω/m], stick out length, l_s [m], droplet radius, r_d [m], and droplet displacement, x_d [m]. Its value of stick out resistance is changed depending on the arc length, l_{arc} .

2.2.2 Force affecting droplet dynamics

The melted drop is detached from the contact point through the electric arc column when the static equilibrium of the forces, acting on the arc, is broken. There are four forces to be acting on the droplet as follows [19]:

- a. Force due to electromagnetic induction (Lorenz):

A current-carrying conductor establishes a magnetic field around the conductor. Due to the welding current, the electromagnetic force, F_e [N], is given by

$$F_e = \frac{\mu}{4\pi} I_w^2 \ln \left| \frac{r_a^2}{R_a} \right| \quad (2.8)$$

where μ is magnetic permeability [$\text{kg m/A}^2 \text{s}^2$], I_w is welding current [A], r_a is exit radius of current path [m] and R_a is entry radius of current path [m].

b. Force due to aerodynamic drag:

The gas flow (atmosphere) around and within the arc induces aerodynamic drag, F_d [N], on the droplet given by

$$F_d = \frac{C_d [r_d^2 - r_\omega^2] \pi \rho_p U_b^2}{2} \quad (2.9)$$

where C_d is drag coefficient, r_ω is electrode radius [m], ρ_p is the plasma density [kg/m^3], r_d is the droplet radius [m] and U_b is relative fluid to drop velocity [m/s]. This force is higher with higher droplet radius and gas velocity.

c. Force due to momentum :

The force due to momentum, F_m [N], is given by:

$$F_m = M_R \rho_\omega W_f \quad (2.10)$$

where ρ_ω is electrode density [kg/m^3] and W_f is electrode feed rate [m/s].

d. Force due to gravity:

The gravitational force, F_g [N], is given by:

$$F_g = m_d g \cos \alpha \quad (2.11)$$

where m_d is the mass of the droplet and g is the vertical component of the acceleration due to gravity (9.81 m/sec^2), and α is the angle between the arc axis and the vertical.

The total force acting in pendant drop is:

$$F_{tot} = F_e + F_d + F_m + F_g \quad (2.12)$$

2.2.3 Reset conditions

The pendent drop contracts at the start of the pulse and becomes unstable when the diameter of the droplet attains some critical value. Furthermore, the drop velocity at detachment is controlled by Lorentz force.

The droplet is characterized as a typical spring-mass damper mechanical system, analogous to water droplets as shown in Fig. 2.5 [20, 24].

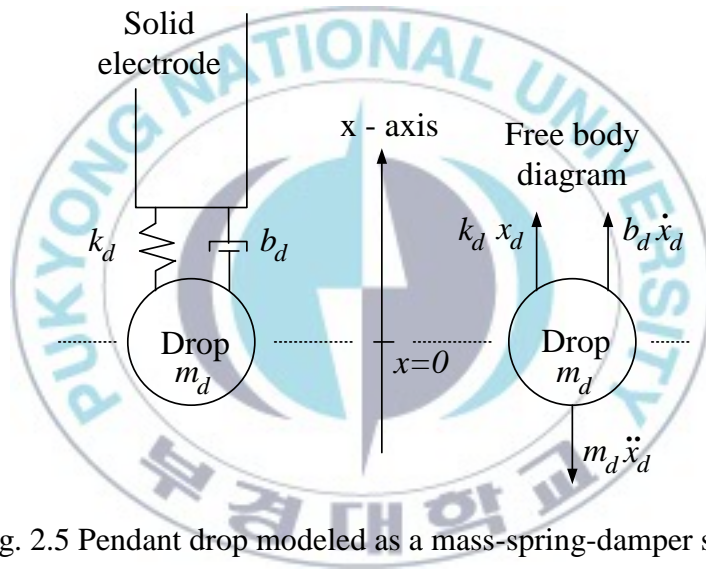


Fig. 2.5 Pendant drop modeled as a mass-spring-damper system

A derivation of a dynamic growth and detachment droplet model by using a second order spring-mass model:

$$F_{tot} = m_d \ddot{x}_d + b_d \dot{x}_d + k_d x_d \quad (2.13)$$

where m_d is mass of droplet [kg], \ddot{x}_d is droplet acceleration [m/s^2], b_d is

damping coefficient [Ns/m], \dot{x}_d is droplet velocity [m/s], k_d is spring constant [N/m], and x_d is droplet displacement [m].

Rewriting the above results in:

$$\ddot{x}_d = \frac{F_{tot} - b_d \dot{x}_d - k_d x_d}{m_d} \quad (2.14)$$

There are two criterions that causing reset condition as follows:

- Due to imbalance
- It's happen when total force acting in pendant drop, F_{tot} , is larger than tensions force, F_s .

$$F_{tot} > F_s \quad (2.15)$$

- Surface tension is important in metal transfer. In free-flight transfer, it is the principal force that prevents droplet detachment, and in dip (short-circuit) transfer, it is the force that pulls the droplet into the weld pool. Using the static analysis of the drop retaining force in globular transfer, the surface tension (force), F_s [N], is obtained as:

$$F_s = 2\pi r_\omega \gamma \quad (2.16)$$

where r_ω is electrode radius [m], and γ is surface tension constant [N/m²].

- Due to shape ability

$$r_d > \frac{\pi(r_d + r_w)}{1.25 \left(\frac{x_d + r_d}{r_d} \right) \left(1 + \frac{\mu_0 I_w^2}{2\pi^2 \gamma (r_d + r_w)} \right)^{\frac{1}{2}}} \quad (2.17)$$

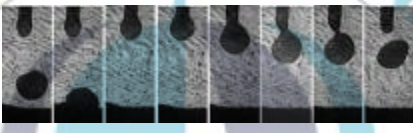
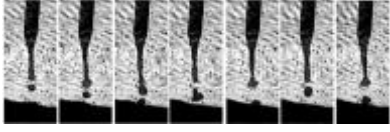
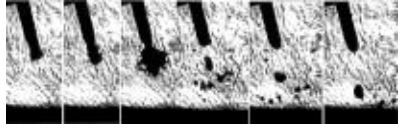
where μ_0 is permeability of free space [kg m/A² s²].

Due to several forces that affecting droplet dynamics and reset condition, there are several kinds of metal transfer mode in GMAW system. This metal transfer mode affects the welding result [5,43]. Table 2.1 shows the relation between the main force acting on the metal droplet with the metal transfer modes [42].

The contact transfer mode is characterized by parameter settings for a short arc with a very high electrode feed rate (over 10–12 m/min), to produce a welding current 250–350A. As the transfer is governed by a strong electromagnetic force, the droplets are of small size with a high transfer rate minimizing the surface tension effect. There is a high level of spatter.

Globular metal transfer is encountered when operating with low to moderate current and moderate to high voltage. Large droplets, reaching diameters of 1.5–3 times the wire diameter, and very low droplet transfer rates, in the rate of 1–10 droplets per second, characterize this transfer mode.

Table 2.1 GMA welding natural metal transfer modes.

Group of modes	Transfer mode	Appearance	Main governing force (effect)
Contact transfer	Short-circuiting		Surface tension and electromagnetic pinch effect
	Bridging		Surface tension
	Forced short-circuiting		Strongly pronounced electromagnetic pinch effect
Free-flight transfer	Globular		Gravitational force
	Repelled globular		Gravitational force and repelling forces
	Projected spray		Electromagnetic force
	Streaming spray		Electromagnetic force
	Rotating spray		Electromagnetic force
	Explosive		Electromagnetic force and chemical reactions

2.2.4 DC motor of Wire Feeding Unit (WFU)

In GMAW system, changing the wire-feed rate regulates the arc length [26]. The wire feed motor used is generally a DC servomotor. DC motors provide excellent speed control for acceleration and deceleration with effective and simple torque control. The fact that the power supply of a DC motor connects directly to the field of the motor can allow precise voltage control, which is necessary for speed and torque control applications. Mathematical modeling of DC motor is applied in this dissertation [55].

Fig. 2.6 shows schematics of DC motor.

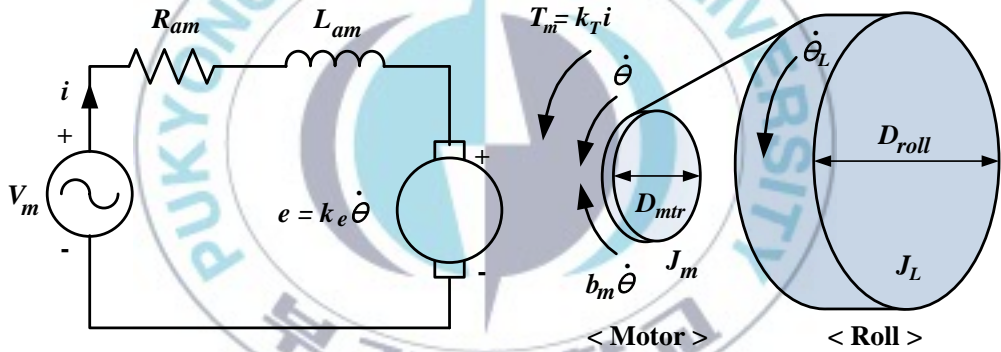


Fig. 2.6 Schematics of DC motor

The motor torque, T_m , is related to the armature current, i , by armature constant, k_T .

$$T_m = k_T i \quad (2.18)$$

The back emf, e , is related to the rotational velocity by the following

equations:

$$e = k_e \dot{\theta} \quad (2.19)$$

From Fig. 2.6, the following equations are obtained based on Newton's law combined with Kirchhoff's law:

$$\begin{aligned} J_L \ddot{\theta}_L + J_m \ddot{\theta} + b_m \dot{\theta} &= k_T i \\ \ddot{\theta}_L &= \ddot{\theta} \times D_{ratio}, \quad D_{ratio} = \frac{D_{mtr}}{D_{roll}} \end{aligned} \quad (2.20)$$

$$J_L = \frac{M_L \times (D_{roll} / 2)^2}{2}$$

$$L_{am} \frac{di}{dt} + R_{am} i = V_m - k_e \dot{\theta} \quad (2.21)$$

where J_m is moment inertia of the motor [$\text{kg m}^2/\text{s}^2$], J_L is moment inertia of the wire feed roll [$\text{kg m}^2/\text{s}^2$], b_m is damping ratio of the mechanical system [Nms], L_{am} is electric inductance of armature [H], R_{am} is electric resistance of armature [Ω], V_m is motor supply voltage [V], k_e is motor constant [Vs/rad], $\dot{\theta}$ is angular velocity of the motor [rad/s], and $\ddot{\theta}$ is angular acceleration of the motor [rad/s^2], $\ddot{\theta}_L$ is angular acceleration of the wire feed roll [rad/s^2], M_L is the mass of the wire feed roll [kg], D_{mtr} is rotor diameter of the motor [m], D_{roll} is diameter of the wire feed roll [m], D_{ratio} is ratio of D_{mtr} to D_{roll} .

Using Laplace transforms, the above modeling equations can be expressed in

terms of Laplace variable, s .

$$s(D_{ratio}J_Ls + J_m s + b_m)\dot{\theta}(s) = k_T I(s) \quad (2.22)$$

$$(L_{am}s + R_{am})I(s) = V_m - k_e \dot{\theta}(s) \quad (2.23)$$

Eliminating $I(s)$ can get the following open-loop transfer function from its supply voltage as the input to the angular velocity of the motor of WFU as the output.

$$\frac{\dot{\theta}}{V_m} = \frac{k_T}{(D_{ratio}J_Ls + J_m s + b_m)(L_{am}s + R_{am}) + k_e k_T} \quad (2.24)$$

$$\frac{\dot{\theta}}{V_m} = \frac{k_T}{(D_{ratio}J_L + J_m)L_{am}s^2 + (L_{am}b_m + D_{ratio}R_{am}J_L + R_{am}J_m)s + (R_{am}b_m + k_e k_T)} \quad (2.25)$$

Note that as the electrode wire diameter is increased while maintaining the same electrode feed rate, higher welding current is required. Also, higher welding current (with all the other variables being kept constant) results in:

- Higher deposition rates.
- Increased depth and width of weld penetration.
- Increased size of the weld bead.

2.3 Hardware configuration of the proposed system

A schematic drawing of developed GMAW is shown in Fig. 2.7. This GMAW system consists of CO₂ shielding gas, Gas Metal Arc Welding Power Supply (PS-GMAW), Wire Feeding Unit (WFU) and Travel Beam.

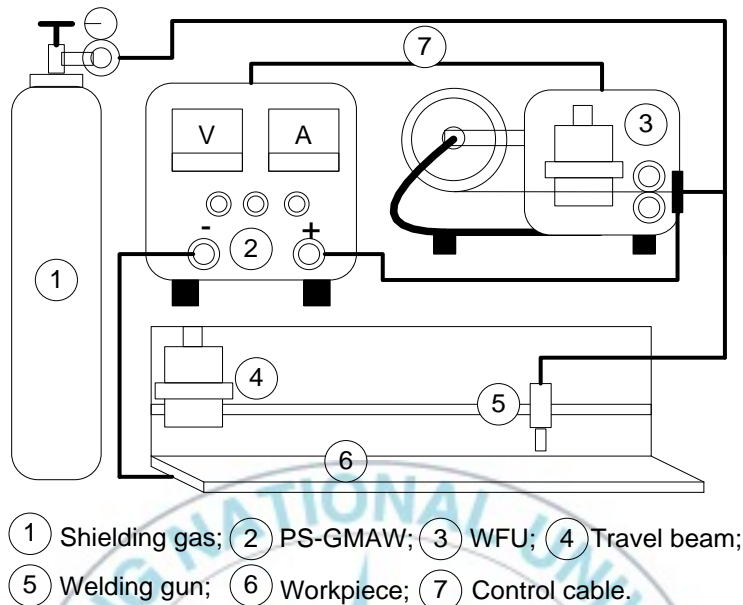


Fig. 2.7 Gas Metal Arc Welding equipment

2.3.1 Shielding gas

The primary function of the shielding gas is to exclude the atmosphere from contact with the molten weld metal. This is necessary because most metals, when they are heated to their melting point in air, exhibit a strong tendency to form oxides and nitrides. Oxygen also reacts with carbon in molten steel to form carbon monoxide and carbon dioxide. These varied reaction products may result in weld deficiencies such as trapped slag, porosity and weld metal embrittlement. Reaction products are easily formed in the atmosphere unless precautions are taken to exclude nitrogen and oxygen.



Fig. 2.8 Shielding gas

The shielding gas and flow rate also affects the arc characteristics, mode of metal transfer, penetration and weld bead profile, speed of welding, undercutting tendency, cleaning action and weld metal mechanical properties [60]. The effects of different shielding gases in bead contour penetration are shown in Fig. 2.9.

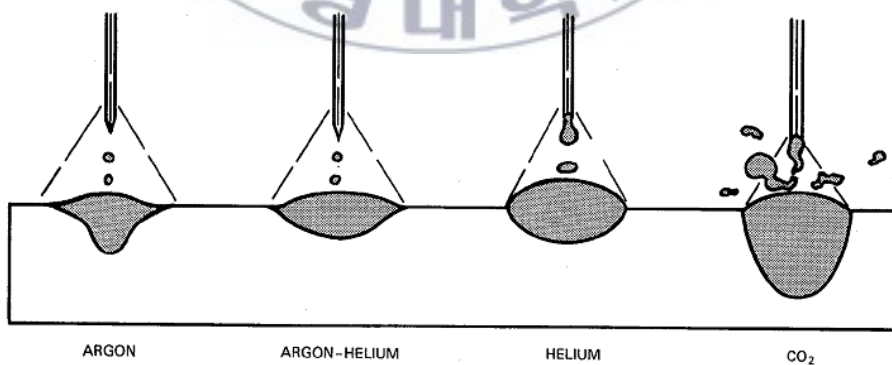


Fig. 2.9 Bead contour penetration

In this experiment, carbon dioxide (CO₂) gas was used. CO₂ is a reactive gas widely used in its pure form for gas metal arc welding of carbon and low alloy steels. The CO₂ shielded arc produces a weld bead of excellent penetration with a rough surface profile.

2.3.2 Gas Metal Arc Welding Power Supply (PS-GMAW)

The block diagram of GMAW power supply is shown in Fig. 2.10. Power supply with 220VAC and 50/60Hz is rectified using full wave rectifier, and then DC link capacitor smooths the rectified DC voltage. Two pairs of IGBT with full bridge configuration invert the smoothed DC voltage into 20kHz AC voltage. Two pairs of IGBT with full bridge configuration invert the smoothed DC voltage into 20kHz AC voltage.

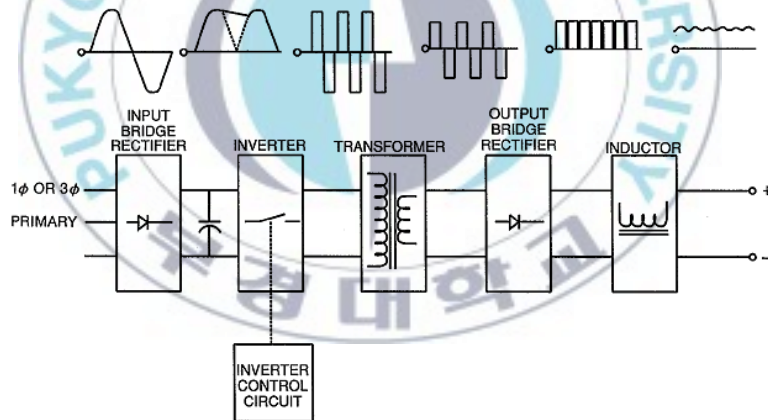


Fig. 2.10 Block diagram of PS-GMAW

The output voltage can be controlled by changing the duty cycle of PWM for IGBT's gate trigger. High frequency step down transformer with ferrite core reduces the output voltage to 16VAC – 36VAC, and then this output voltage is rectified by one pair of high frequency diode.

The schematic circuit of GMAW power supply is shown in Fig. 2.11.

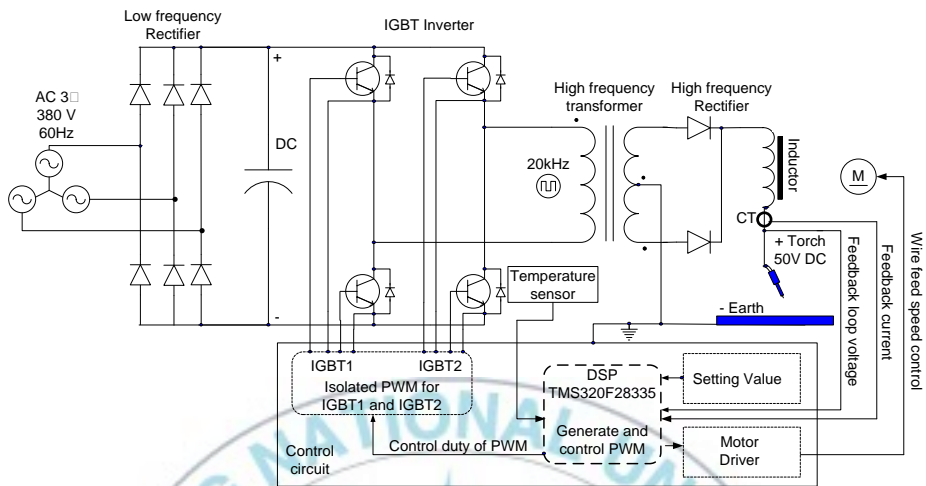


Fig. 2.11 Schematic circuit of GMAW

Each parts of Gas Metal Arc Welding Power Supply (PS-GMAW) are considered as below:

a. Low frequency Rectifier

The power supply 380V AC 3 Φ 60 Hz is rectified using 3 phase rectifier 6RI100E-808 as shown in Fig. 2.12. This diode module has specification:

- Repetitive peak voltage : 800V
- Average output current : 100A
- Forward voltage : 1.15V

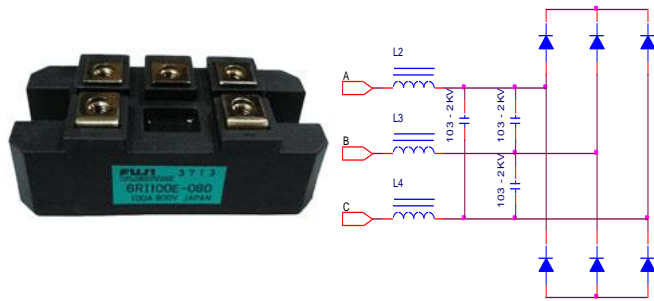


Fig. 2.12 Low frequency rectifier

The output of the rectifier is smoothed using 900V 4700 μ F capacitor. The maximum output current of rectifier can be calculated using the following equations:

$$V_{DC} = \sqrt{2}V_{AC} \quad (2.26)$$

$$V_{DC} = \sqrt{2} \cdot 380 \text{ VDC} = 537 \text{ VDC} \quad (2.27)$$

where V_{DC} is DC output voltage of rectifier (VDC) and V_{AC} is AC input voltage of rectifier (VAC).

b. IGBT inverter

The output of rectifier then is inverted by IGBT inverter. SKM75GB063D as shown in Fig. 2.13 has specification:

- Collector to emitter peak voltage (V_{CES}) : 600V
- Collector peak current (I_C) : 100A at T_C 25°C, 75A at T_C 75°C
- Diode peak current (I_F) : 75A at T_C 25°C, 50A at T_C 75°C

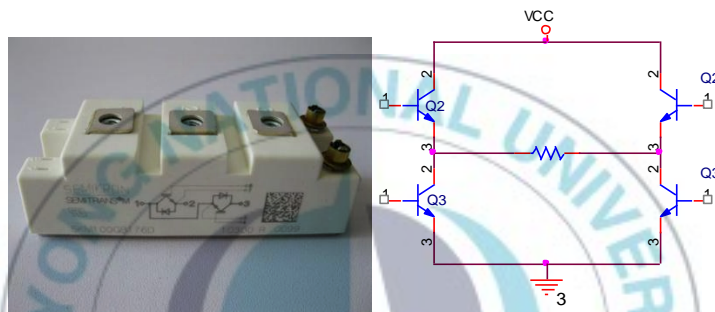


Fig. 2.13 IGBT inverter

The output voltage of welding machines by changing duty cycle of inverter can be controlled.

c. High frequency transformer

High frequency transformer is shown in Fig. 2.14. This transformer uses ferrite core that has high magnetic permeability coupled and low electrical conductivity which prevents eddy currents. Because the core has high permeability, the number of coils can be reduced since the core can be magnetized easily. So, the total size of transformer can be reduced significantly. Furthermore, because the number of coils is reduced, the chopper loss is also

reduced, and the total efficiency of high frequency transformer is higher than that of low frequency transformer.

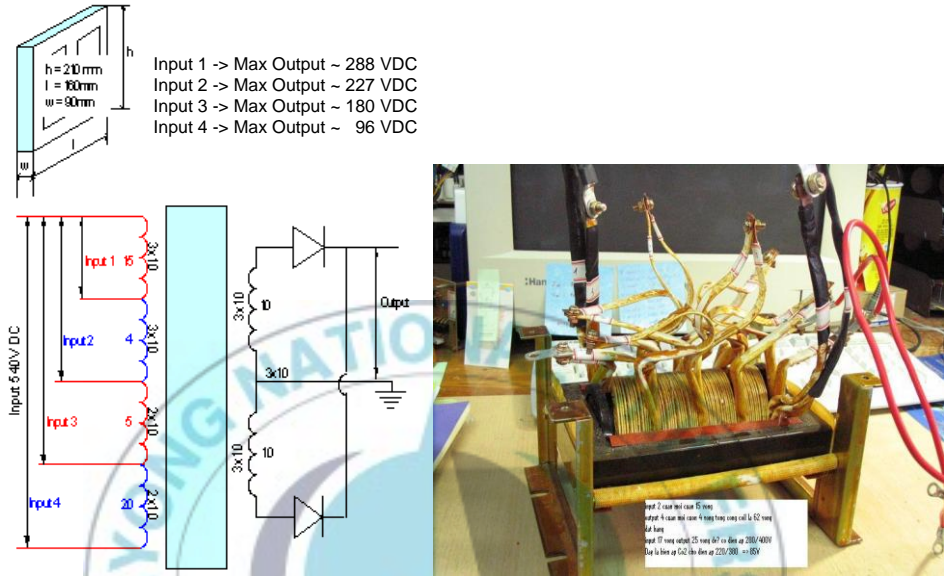


Fig. 2.14 High frequency transformer

The output of high frequency transformer can be calculated as:

$$V_{T_{out}} = V_{T_{in}} \times \frac{n_s}{n_p} \times 82\% \quad (2.28)$$

where $V_{T_{out}}$ is output voltage of transformer [V], $V_{T_{in}}$ is input voltage of transformer [V], n_p is number of primary winding, and n_s is number of secondary winding.

Input 4 in Fig. 2.14 is used in this dissertation. So, the maximum output of the transformer is 96VDC.

d. High frequency rectifier

The output of transformer is rectified using ultra fast soft recovery diode module DBC2F200N4 as shown in Fig. 2.15. This diode has specification:

- Repetitive reverse voltage : 600V
- Low forward voltage drop : 1.5V
- Average forward current : 200A at $T_C = 100^\circ\text{C}$
- Ultra-fast reverse recovery time : 180ns



Fig. 2.15 High frequency rectifier

e. IGBT drive

Output PWM voltage signal from DSP should be magnified before it connected to IGBT. To trigger an IGBT properly, at least +12 VDC PWM signal is needed. To make sure that the IGBT turns off properly, it must be triggered with negative voltage -15V. In the full bridge inverter using IGBT, each ground reference of each IGBT must be insulated each other to avoid short circuit. Because of those reasons, IGBT driver is needed.

Fig. 2.16 shows IGBT drive circuit. The PWM signal from pin TLP1 triggers IC TLP250 through 470 Ω resistor. TLP250 is a photocoupler that insulates input

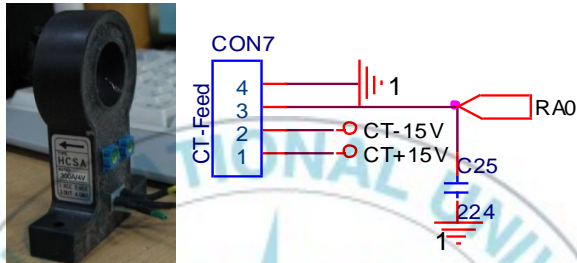
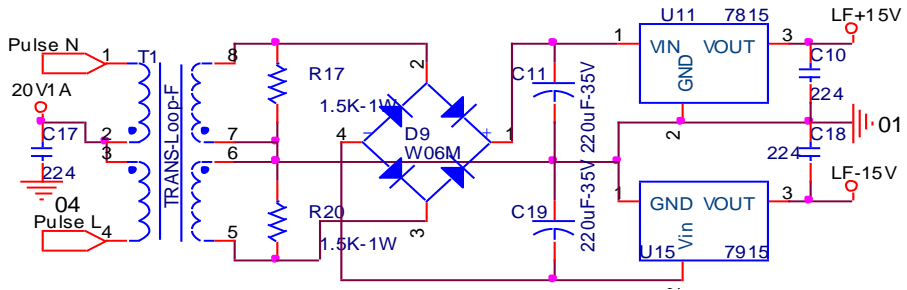


Fig. 2.17 Current sensor and signal conditioner circuit

g. Voltage sensor

For sensing the voltage, the circuit as shown in Fig. 2.18 is needed. To insulate the DSP and high voltage, ISO124P is used.

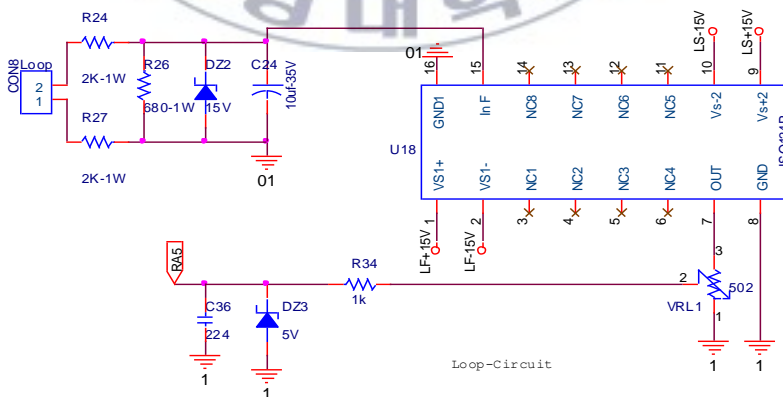


Fig. 2.18 Voltage sensor and signal conditioner circuit

h. DC motor drive

Similarly with IGBT drive, the DC motor driver circuit in Fig. 2.19 separates the PWM input from DSP and motor drive optically using IC TLP250. IC IR2105 for driving MOSFET IRF540 is used. This IC has 2 outputs that invert each other. When the input signal is high, the output signal HO is high and LO is low. In this case, Q2 turns on, Q3 turns off and output motor is connected to +24V. On the other hand, when the input signal is low, the output signal HO is low and LO is high. In this case, Q2 turns off, Q3 turns on and output motor is connected to ground. The motor speed depends on duty cycle of PWM.

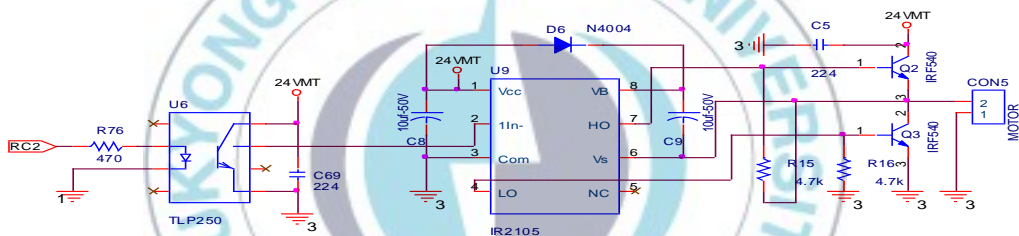


Fig. 2.19 DC motor drive circuit

i. Main controller DSP TMS320F28335

DSP TMS320F28335 as main controller in Fig. 2.20 is used. This DSP has specifications:

- High-performance static CMOS technology
 - Up to 150 MHz (6.67-ns cycle time)
 - 1.9-V/1.8 -V Core, 3.3-V I/O design
- On-chip memory 256K x 16 flash, 34K x 16 SARAM

- Boot ROM (8K x 16)
- Enhanced control peripherals
 - Up to 18 PWM outputs
 - Up to 6 HRPWM outputs with 150 ps MEP
- Resolution
 - Up to 6 event capture inputs
 - Up to 2 quadrature encoder interfaces
 - Up to 8 32-bit/nine 16-bit timers
- Serial port peripherals
 - Up to 2 CAN modules
 - Up to 3 SCI (UART) modules
 - Up to 2 McBSP modules (configurable as SPI)
 - One SPI module
 - One inter-integrated-circuit (I2C) bus
- 12-Bit ADC, 16 channels
 - 80-ns conversion rate
 - 2 x 8 channel input multiplexer
 - Two sample-and-hold
 - Single/simultaneous conversions
 - Internal or external reference



Fig. 2.20 TMS320F28X EVM Rev.1.1 and TMS320F28335 V1.4

TMS320F28335 V1.4 in Fig. 2.20 is used. This module includes power supply connection, clock, supply regulator and connectors. In order to make connection easy, TMS320F28X EVM Rev .1.1 is used. This module includes power supply, active filter for ADC, connectors for serial port peripherals and connectors for I/O.

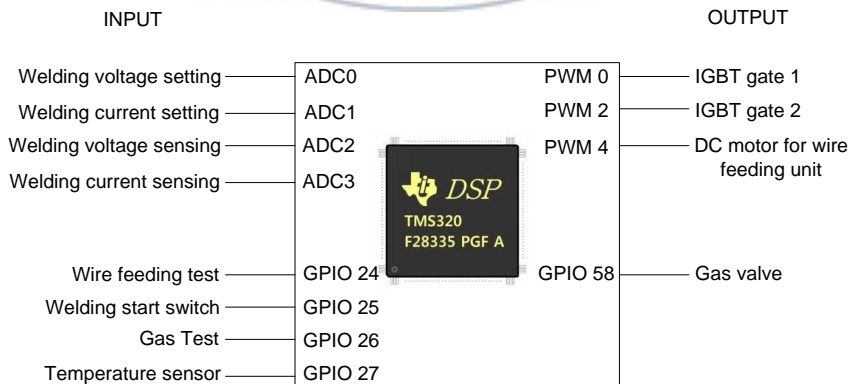


Fig. 2.21 DSP pin configuration

2.3.3 Wire Feeding Unit (WFU)

The Wire Feeding Unit in Fig. 2.22 consists of an electric motor, drive rolls, and accessories for maintaining electrode alignment and pressure. This unit is integrated with speed control in PS-GMAW. The electrode feed motor is 24V direct current (DC) motor. The wire feed speed of Wire Feeding Unit (WFU) has range from about 1.9 to 30m/min.



Fig. 2.22 Wire Feeding Unit (WFU)

2.3.4 Travel beam

Travel beam in Fig. 2.23 consists of the frame, DC motor, motor driver, and torch holder. Primary function of travel beam is to hold the torch and move along the axis with constant speed. This travel beam also keeps the distance between contact tip and workpiece constant. The axis length of travel beam is 1.5m. The travel beam have separate controller to maintain the travel speed.

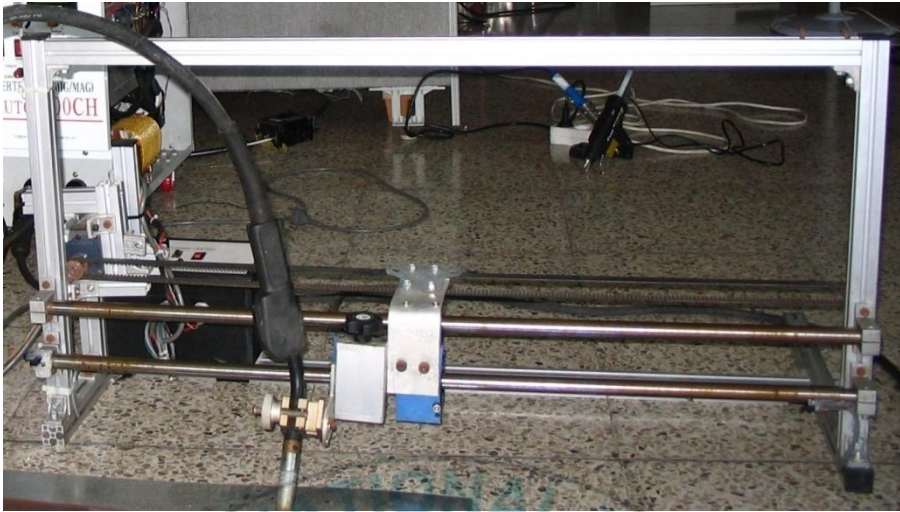


Fig. 2.23 Travel beam

The complete system of GMAW system is shown in Fig. 2.24

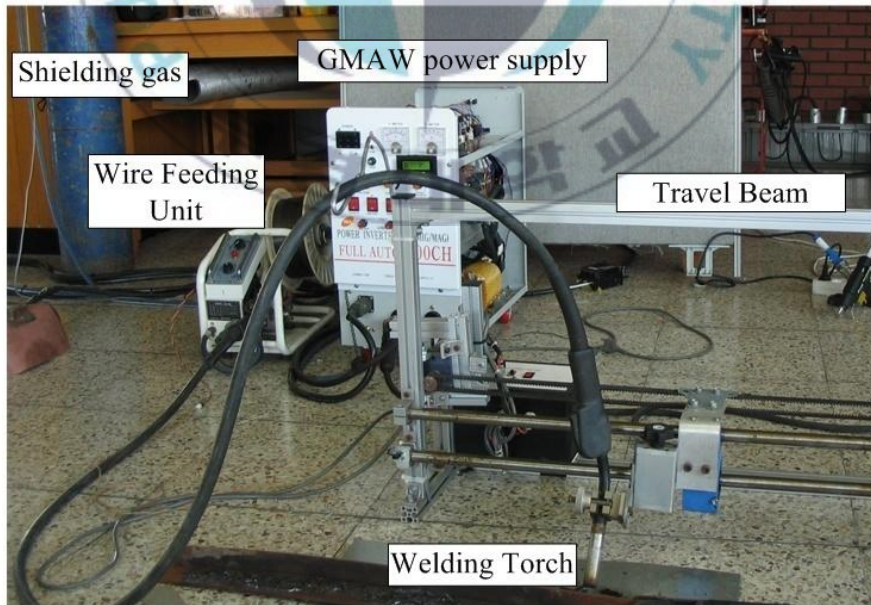


Fig. 2.24 GMAW system for experiment

Chapter 3. Control design using self-tuning Fuzzy PID

This chapter introduces welding current control of WFU in GMAW system using self-tuning Fuzzy PID (FPID). Firstly, introduction and the basic concept of this control method are given. Secondly, based on mathematics modeling of GMAW system in chapter 2, self-tuning Fuzzy PID and conventional PID methods are proposed. Finally, simulation and experiment results using proposed controllers are shown and compared.

3.1 Introduction

PID controller has been most widely used among controllers in modern industry because of its simple control structure. In GMAW system, a constant welding current is achieved by controlling the wire-feed speed. It is possible to use a conventional PID to control the wire-feed speed of the WFU. However, conventional PID controllers do not yield reasonable performance over a wide range of operating conditions because of the fixed gains used. Thus, the PID parameters need to be automatically adjusted by a fuzzy set [42].

This chapter presents a new closed-loop control method based on a self-tuning Fuzzy PID controller. The presented control method is compared to the conventional PID control.

3.2 Model of WFU

In previous chapter, mathematical modeling of WFU related with GMAW process was given. In this GMAW system, a DC servomotor is utilized to control the DC motor of the WFU, which controls the electrode feed-rate to maintain the welding arc.

The dynamic relationship between the angular velocity and the voltage applied to the DC motor of WFU in Eq. (2.26) are:

$$\frac{\dot{\theta}}{V_m} = \frac{k_T}{(D_{ratio}J_L + J_m)L_{am}s^2 + (L_{am}b_m + D_{ratio}R_{am}J_L + R_{am}J_m)s + (R_{am}b_m + k_e k_T)} \quad (3.1)$$

To change the angular velocity into linear velocity, Eq. (3.2) is used.

$$W_f = \dot{\theta}b' \quad (3.2)$$

$$b' = \frac{D_{mtr}}{2} \times 60 \quad (3.3)$$

where W_f is electrode feed rate [m/min], $\dot{\theta}$ is angular velocity of the motor [rad/s], and b' is conversion ratio from angular velocity into linear velocity, and rotor diameter of the motor, D_{mtr} .

Combining Eqs. (3.1) and (3.2) yields:

$$\begin{aligned} G_m(s) &= \frac{W_f(s)}{V_m(s)} \\ &= \frac{k_T}{(D_{ratio}J_L + J_m)L_{am}s^2 + (L_{am}b_m + D_{ratio}R_{am}J_L + R_{am}J_m)s + (R_{am}b_m + k_e k_T)} \end{aligned} \quad (3.4)$$

where $V_m(s)$ represents the DC voltage applied to the DC motor of the WFU [V].

DC motor of the WFU can be expressed as a second-order dynamic equation as follows:

$$G_m(s) = \frac{W_f(s)}{V_m(s)} = \frac{b_0}{s^2 + a_1s + a_0} \quad (3.5)$$

where

$$b_0 = \frac{b'k_T}{L_{am}(D_{ratio}J_L + J_m)} \quad a_1 = \frac{L_{am}b_m + R_{am}D_{ratio}J_L + R_{am}J_m}{L_{am}(D_{ratio}J_L + J_m)} \quad a_0 = \frac{R_{am}b_m + k_e k_T}{L_{am}(D_{ratio}J_L + J_m)}$$

The purpose of controlling the WFU is to change the electrode feed-rate for tracking the set value, I_s [A]. In the GMAW process, the electrode feed-rate must be equal to the electrode melting-rate to maintain a stable arc length.

$$W_f = M_R \quad (3.6)$$

where M_R is the electrode melting-rate.

The electrode melting-rate can be expressed as a function of welding current, I_w [A], and arc voltage, V_{arc} [V], as follows:

$$M_R = M_{Ri}I_w - M_{Rv}V_{arc} \quad (3.7)$$

where M_{Ri} and M_{Rv} are the coefficient ratios of the melting-rate to the welding current and arc voltage, respectively.

From Eqs. (3.6) and (3.7), the electrode feed-rate can be expressed as:

$$W_f(s) = M_{Ri}I_w - M_{Rv}V_{arc} \quad (3.8)$$

From Eq. (3.8), the welding current can be expressed as:

$$I_w = \frac{W_f(s)}{M_{Ri}} + \frac{M_{Rv}V_{arc}}{M_{Ri}} = \frac{1}{M_{Ri}}(W_f(s) + \Delta G) \quad (3.9)$$

where ΔG denotes $M_{Rv}V_{arc}$.

In fact, the welding current influences the electrode feed- rate much more than the arc voltage. If the arc voltage is considered as a disturbance in Eq. (3.9), the block diagram for an open loop transfer function of the WFU is shown in Fig. 3.1.

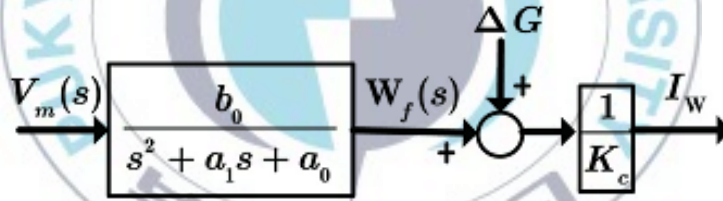


Fig. 3.1 Block diagram for an open loop transfer function of the WFU

If ΔG is considered to be a disturbance of the system, from Eq. (3.9) the transfer function $G(s)$ of the WFU between $V_m(s)$ and I_w can be obtained as follows:

$$G(s) = \frac{I_w(s)}{V_m(s)} = \frac{1}{K_c} \left[\frac{W_f(s)}{V_m(s)} + \frac{\Delta G(s)}{V_m(s)} \right] \quad (3.10)$$

By combining Eqs. (3.5) and (3.10), the transfer function of WFU in second order dynamic equations is obtained as:

$$G(s) = \frac{I_w(s)}{V_m(s)} = \frac{1}{K_c} \left[\frac{b_0}{(s^2 + a_1s + a_0)} + \Delta G_d \right] \quad (3.11)$$

where ΔG_d denotes $\Delta G(s)/V_m(s)$.

3.3 Controller design

Self-tuning Fuzzy PID controller means that the three gains K_p , K_I and K_D of PID controller are tuned by using fuzzy tuner.[4, 36]. The coefficients of the conventional PID controller are not often properly tuned for the nonlinear plant with unpredictable parameter variations due to its fixed gains. Hence, it is necessary to automatically tune the PID gains even in the nonlinear plant. The controller signal is chosen as V_m can be expressed in the time domain as:

$$u = V_m = K_p e + K_I \int e dt + K_D \frac{de}{dt} \quad (3.12)$$

$$e = I_s - I_w \quad (3.13)$$

$$K_I = K_p / T_I \quad (3.14)$$

$$K_D = K_p T_D \quad (3.15)$$

where e is the tracking error between the welding current and its setting value; T_I and T_D are the integral time coefficient and derivative time

coefficient, respectively, and K_p , K_i , K_d are the proportional gain, integral gain, and derivative gain, respectively.

Fig. 3.2 shows a conventional PID controller [52]].

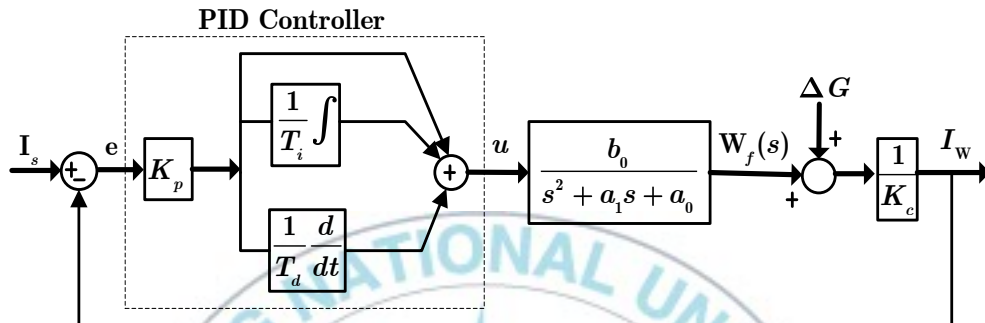


Fig. 3.2 Conventional PID controller

This chapter proposes a self-tuning Fuzzy PID controller. Fuzzy control provides a formal methodology for representing, manipulating and implementing a human's heuristic knowledge about how to control a system. This is also a convenient method for constructing nonlinear controllers by using heuristic information obtained from experience. Therefore, the advantages of fuzzy and PID controllers can be incorporated into a controller in order to achieve high control performance. The proposed controller in this chapter has two inputs and three outputs. The error e and its derivative \dot{e} are used as inputs. The tuning-gains, K_p , K_i and K_d , are the outputs. The fuzzy controller is added to the conventional PID controller to adjust the gains of the PID controller.

A new controller applied by the fuzzy controller is given as follows:

$$u = K_{pf}e + K_{if} \int edt + K_{df} \frac{de}{dt} \quad (3.16)$$

where

$$\begin{cases} K_{pf} = K_{tp}K_p \\ K_{if} = K_{ti}K_I \\ K_{df} = K_{td}K_D \end{cases} \quad (3.17)$$

where K_{pf} , K_{if} and K_{df} denote the changeable gains of the new controller;

K_p , K_I and K_D are the fixed values from the conventional PID controller; and

K_{tp} , K_{ti} and K_{td} are the tuning-gains from the fuzzy controller.

Fig. 3.3 shows the proposed self-tuning Fuzzy PID controller. K_{er} and $K_{\Delta er}$ are scaling gains that make the inputs satisfy the operational ranges.

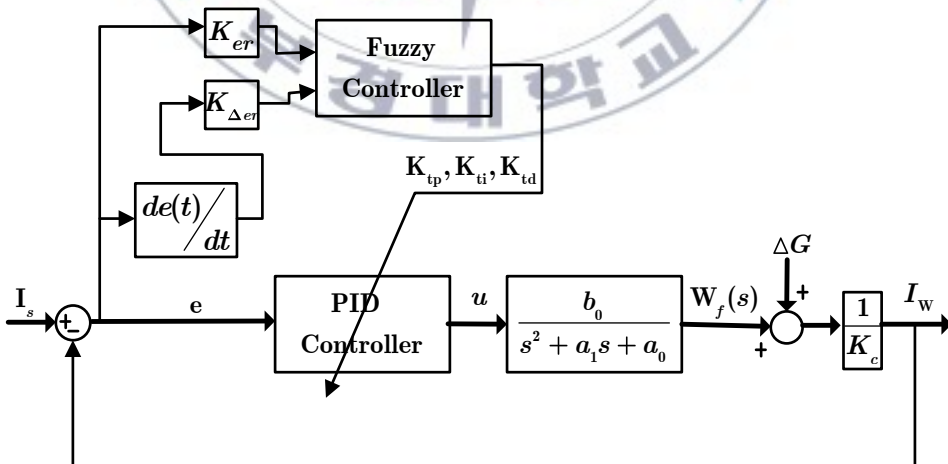


Fig. 3.3 Self-tuning Fuzzy PID controller

The general structure of fuzzy logic control is represented in Fig. 3.4.

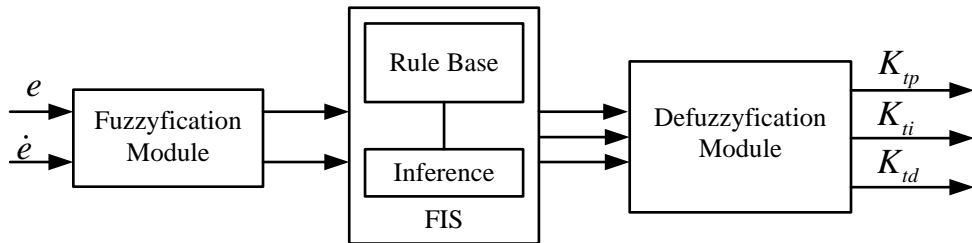


Fig. 3.4 Fuzzy logic control structure

To apply the fuzzy logic control in this system, the following step should be considered [10, 14, 19].

3.3.1 Normalization

In order to obtain feasible rule bases with high inference efficiency, the input error and its derivative must be normalized over interval -1 and 1 and output PID parameters must be normalized over the interval 0 and 1.

3.3.2 Fuzzification

After the input range becomes from -1 to 1, the next process is fuzzification. For each input variable, five membership functions are used. NB, NS, ZE, PS, and PB are Negative Big, Negative Small, Zero, Positive Small and Positive Big, respectively. The membership functions of the fuzzy inputs are shown in Fig. 3.5.

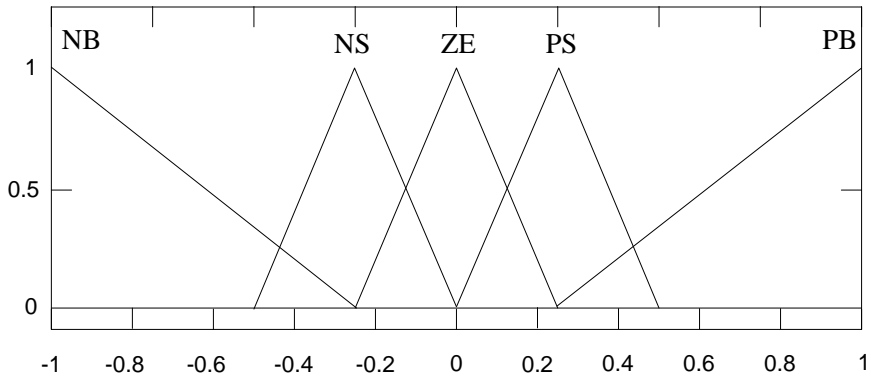


Fig. 3.5 Membership functions of input (e, \dot{e})

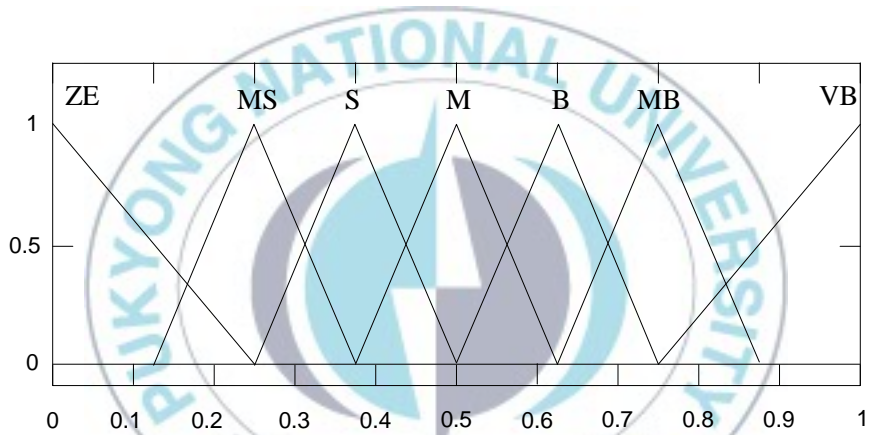


Fig. 3.6 Membership functions of output (K_p, K_i and K_d)

The output ranges from -1 to 1. For each output variable, seven membership functions are used. ZE, MS, S, M, B, MB, and VB are Zero, Medium small, Small, Medium, Big, Medium Big and Very Big, respectively. The membership functions of the fuzzy outputs are shown in Fig. 3.6.

3.3.3 Fuzzy rule and fuzzy inference

The behavior of a fuzzy system is characterized by a set of linguistic rules which constitute a rule base. It represents some linguistic relationship of input and output; the product of the input fuzzy region and the output fuzzy region. Using the fuzzy sets of input and output variables, fuzzy rules are composed as follows:

Rule i^{th} : If e is A_i and \dot{e} is B_i , then K_p is C_i , K_{ii} is D_i ,

and K_{id} is E_i , where A_i and B_i are the linguistic label inputs

and C_i , D_i , and E_i are the linguistic label outputs.

Tables 3.1 - 3.3 show the control rules used for the proposed self-tuning Fuzzy PID controller.

Table 3.1 Rule bases for determining gain K_p

\dot{e}/e	NB	NS	ZE	PS	PB
NB	VB	VB	VB	VB	VB
NS	B	B	B	MB	VB
ZE	ZE	ZE	MS	S	S
PS	B	B	B	MB	VB
PB	VB	VB	VB	VB	VB

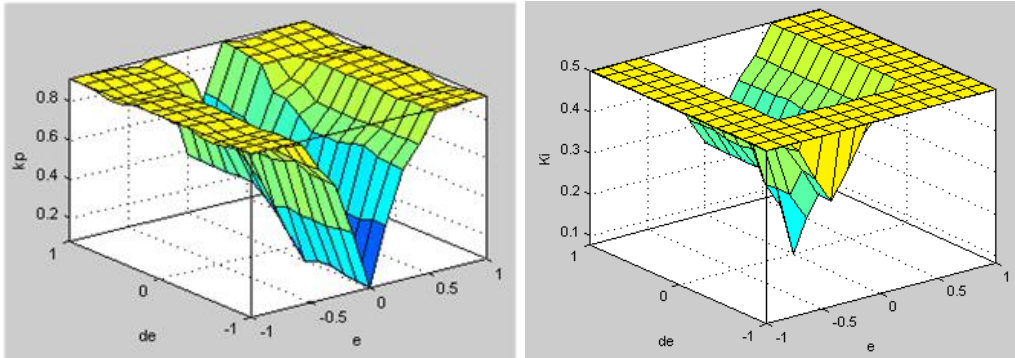
Table 3.2 Rule bases for determining gain K_{ii}

\dot{e}/e	NB	NS	ZE	PS	PB
NB	M	M	M	M	M
NS	S	S	S	S	S
ZE	MS	MS	ZE	MS	MS
PS	S	S	S	S	S
PB	M	M	M	M	M

Table 3.3 Rule bases for determining gain K_{td}

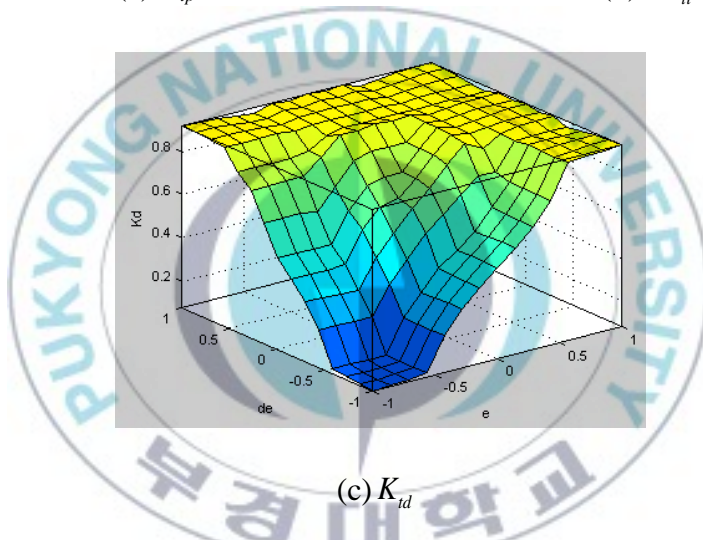
\dot{e}/e	NB	NS	ZE	PS	PB
NB	ZE	S	M	MB	VB
NS	S	B	MB	VB	VB
ZE	M	MB	MB	VB	VB
PS	B	VB	VB	VB	VB
PB	VB	VB	VB	VB	VB

As a result, the rule sets are established and shown on the surfaces in Fig. 3.7.



(a) K_{ip}

(b) K_{ii}



(c) K_{id}

Fig. 3.7 Rule surface views

3.3.4 Defuzzification

There are many defuzzification techniques but primarily only three of them are in common use.

- a. Maximum defuzzification technique

This method gives the output with the highest membership function. This

defuzzification technique is very fast but is only accurate for peaked output.

b. Centroid defuzzification technique

This method is also known as center of gravity or center of area defuzzification. This technique was developed by Sugeno in 1985. This is the most commonly used technique and very accurate.

c. Weighted average defuzzification technique

In this method, the output is obtained by the weighted average of the each output of the set of rules stored in the knowledge base of the system. This method is computationally faster and easier and gives fairly accurate result.

In this dissertation, the “centroid” method is used for defuzzification to obtain K_p , K_i and K_{id} .

3.4 Simulation and experimental results

3.4.1 Identification of parameters for transfer function

To verify the effectiveness of the proposed controller, simulation and experiment is done. The parameters of the DC motor for simulation are given in Table 3.4.

Table 3.4 Numerical values of DC motor of WFU

Parameters	Values	Units
k_e	51×10^{-3}	[Vs/rad]
k_T	5.06×10^{-2}	[Nm/A]
R_{am}	1.0	[Ω]
L_{am}	0.9×10^{-3}	[H]
J_m	1.624×10^{-4}	[kgm ²]
b_m	5.6×10^{-5}	[Nms]

Before doing simulation, some parameters should be calculated. The transfer function in Eq. (3.5) can be rewritten as follows:

$$G_m(s) = \frac{W_f(s)}{V_m(s)} = \frac{b_0}{s^2 + a_1s + a_0} \quad (3.18)$$

For the specific WFU, the wire feed roll diameter $D_{roll} = 25 \times 10^{-2} (m)$, the rotor diameter of motor $D_{mtr} = 4 \times 10^{-2} (m)$, the mass of feed roll $M_L = 10(kg)$.

The moment inertia of the wire feed rate, J_L , the ratio between the diameter of motor and wire feed roll, D_{ratio} , and the ratio between the electrode feed-rate and angular velocity of the DC motor is given as:

$$J_L = \frac{M_L \times (D_{roll} / 2)^2}{2} = 0.078$$

$$D_{ratio} = \frac{D_{mtr}}{D_{roll}} = 0.16 \quad (3.19)$$

$$b' = \frac{D_{mtr}}{2} \times 60 = 1.2$$

The parameters of transfer function, $G_m(s)$, can be calculated as follows:

$$b_0 = \frac{b' k_T}{L_{am} (D_{ratio} J_L + J_m)} = 5370.2 \quad (3.20)$$

$$a_1 = \frac{L_{am} b_m + R_{am} D_{ratio} J_L + R_{am} J_m}{L_{am} (D_{ratio} J_L + J_m)} = 1111.1 \quad (3.21)$$

$$a_0 = \frac{R_{am} b_m + k_e k_T}{L_{am} (D_{ratio} J_L + J_m)} = 231.53 \quad (3.22)$$

The nominal mathematical model of transfer function, $G_m(s)$, is as follows:

$$G_m(s) = \frac{5370.2}{s^2 + 1111.1s + 231.53} \quad (3.23)$$

The value of M_{Ri} depends on the diameter of the welding electrode. Based on the experimental results, M_{Ri} can be approximated as falling in the range of 0.041~0.046 for a 1.2mm aluminum electrode. In this dissertation, $M_{Ri} = 0.043$ is chosen.

3.4.2 Simulation and experimental results

To verify the effectiveness of the proposed controllers, simulation and experimental results are performed for the developed GMAW system. Comparison of the conventional PID controller and self-tuning Fuzzy PID controller for controlling the wire feed speed of the WFU is presented. Table 3.5 shows the welding condition for the experiment.

Table 3.5 Welding condition for the experiment

No	Parameter	Value
1	Metal workpiece type	Steel
2	Metal workpiece thickness	2 mm
3	Metal joint type	Butt joint
4	Filler wire size	1.2 mm
5	Welding current setting	110 A
6	Welding voltage setting	22 V
7	Shielding gas type	CO ₂
8	Gas flow rate	15 L/min
9	Distance between contact tip and workpiece	16mm
10	Torch travel speed	5 mm/sec

Figs. 3.8 - 3.11 show that the simulation responses for the step type of current for both controllers without disturbance ($\Delta G_d = 0$). The gain values set

for the conventional PID ($K_p = 0.2$, $K_I = 0.02$, and $K_D = 0.01$) and the scaling gains ($K_e = 0.05$ and $K_{\Delta e} = 0.0017$) are obtained from experiments with the real model.

Fig. 3.8 shows how the tuning-gains, K_p , K_i and K_d , vary online with the output of the system. In the beginning, K_p & K_d gain's value is 0.92, and K_i gain's value is 0.5. After 0.05 second, the value of gains is changing according to the current error. Finally, after 0.2 seconds, the tuning-gains become constant. The gains value after steady state is $K_p = 0.33$, $K_i = 0.14$ and $K_d = 0.78$.

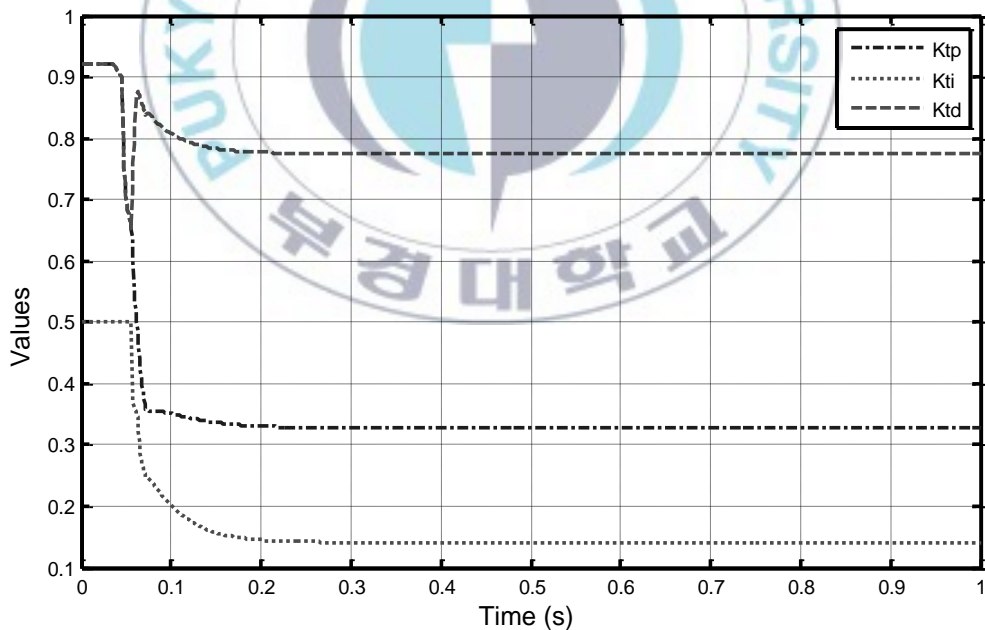


Fig. 3.8 Tuning-gains

Fig. 3.9 shows that the control performance of the system using the self-tuning Fuzzy PID(FPID) compared with conventional PID controller. The figure shows that the magnitude of both controllers starts at maximum of 24V in the beginning and is decreased gradually. The control input voltage in FPID controller reaches steady state of 0.22V more quickly than that in conventional PID controller.

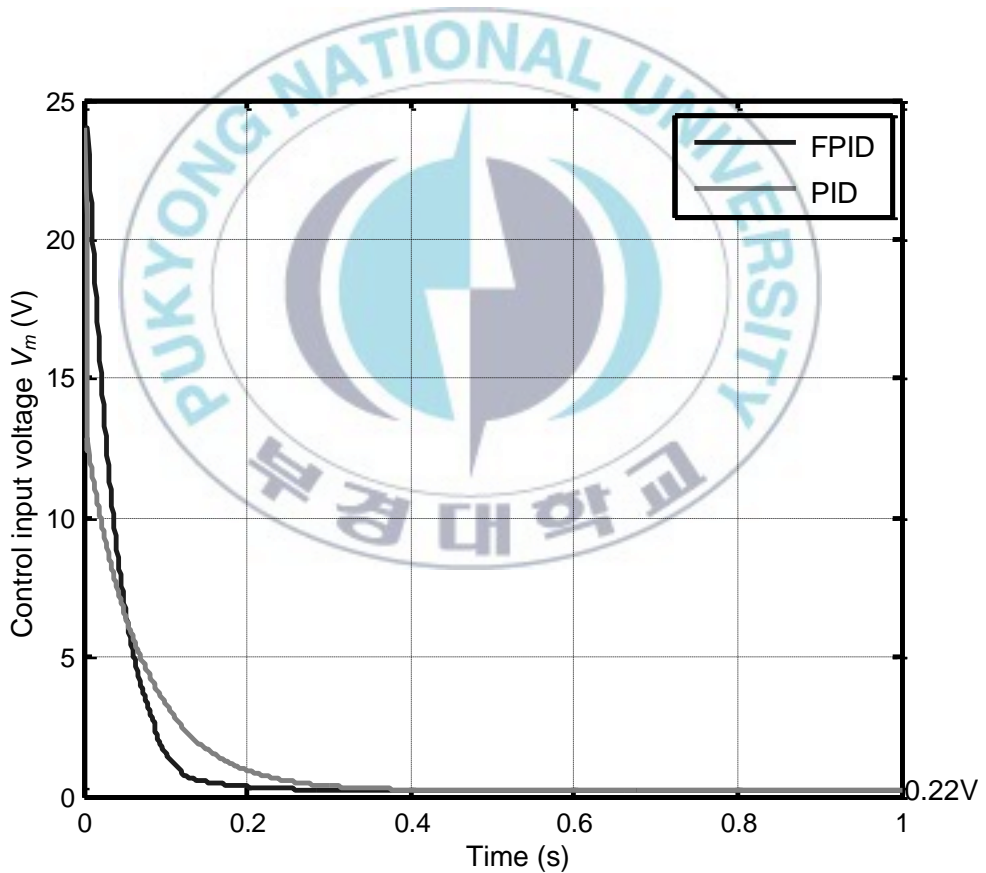


Fig. 3.9 Control voltage of Wire Feeding Unit in simulation

Fig. 3.10 shows the output current, I_w , in simulation using the self-tuning Fuzzy PID compared with conventional PID controller. The welding current performance using self-tuning Fuzzy PID is better than that using the conventional PID with regard to not only the rising time but also the settling time and steady state error. In both controllers, output welding current reaches its setting value of 110A at steady state.

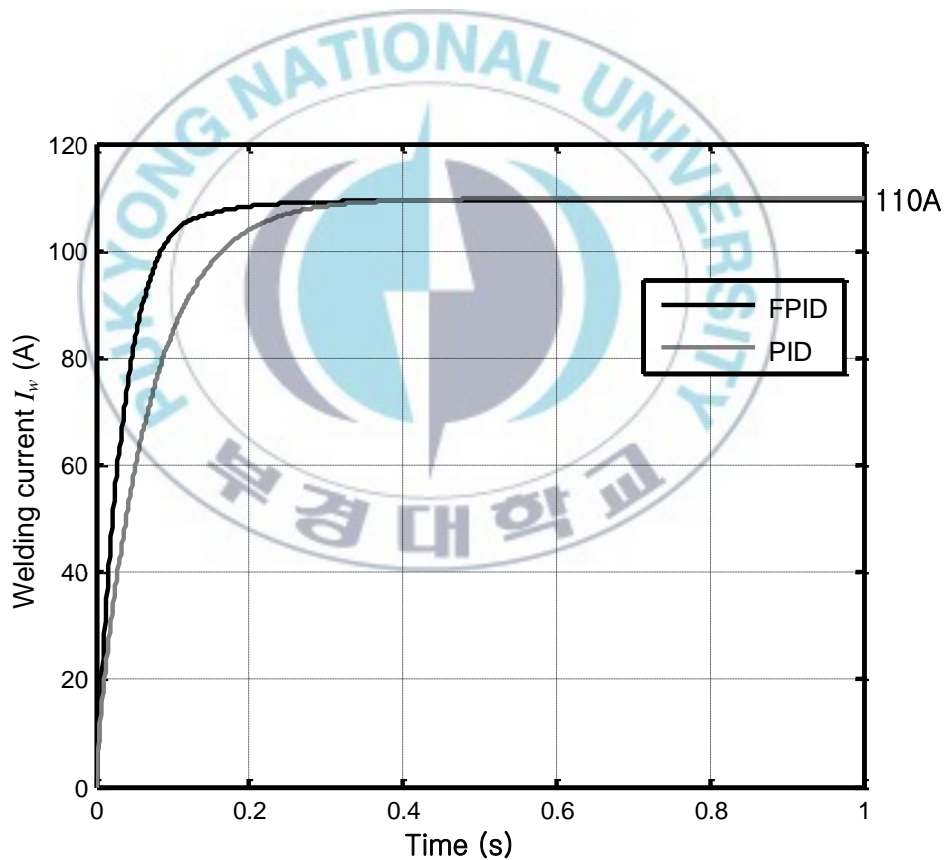


Fig. 3.10 Output current in simulation

Fig. 3.11 shows the welding current error, e_i , in simulation. The welding current error using self-tuning Fuzzy PID converges to zero after 0.3 seconds. On the other hand, the welding current error using conventional PID controller becomes zero after 0.4 seconds.

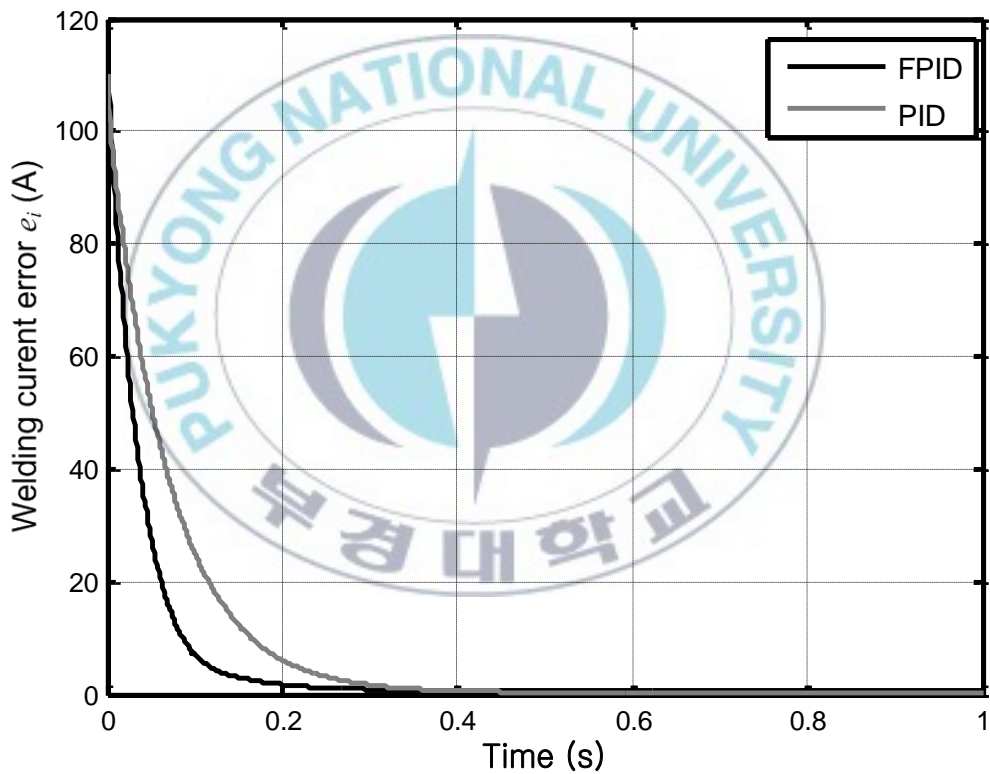


Fig. 3.11 Welding current error in simulation

Next, to prove the effectiveness of the proposed controller, a disturbance scheme shown in Fig. 3.12 is excited. The excited disturbance is given as:

$$\Delta G = A \sin(\omega t) + Rnd(t)$$

where $A = 2$, $\omega = 2\pi/8$, and $Rnd(t)$ is the white noise signal.

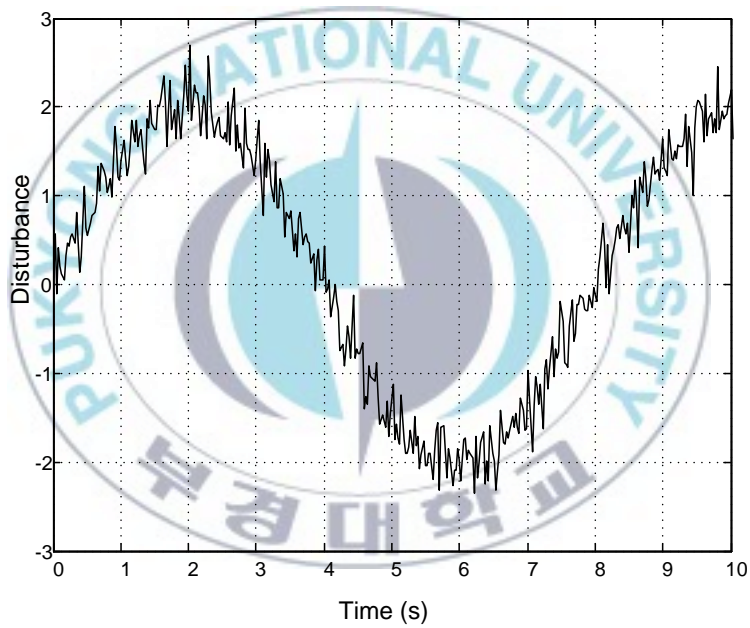


Fig. 3.12 Disturbance applied to GMAW system

Fig. 3.13 shows the output welding currents of the self-tuning Fuzzy PID controller and the conventional PID controller. The current output is bounded around $110 \pm 1\text{A}$ with the self-tuning Fuzzy PID controller and around $110 \pm 6\text{A}$ with the conventional PID controller. It is obvious that the proposed controller achieves the better tracking response than the conventional PID controller.

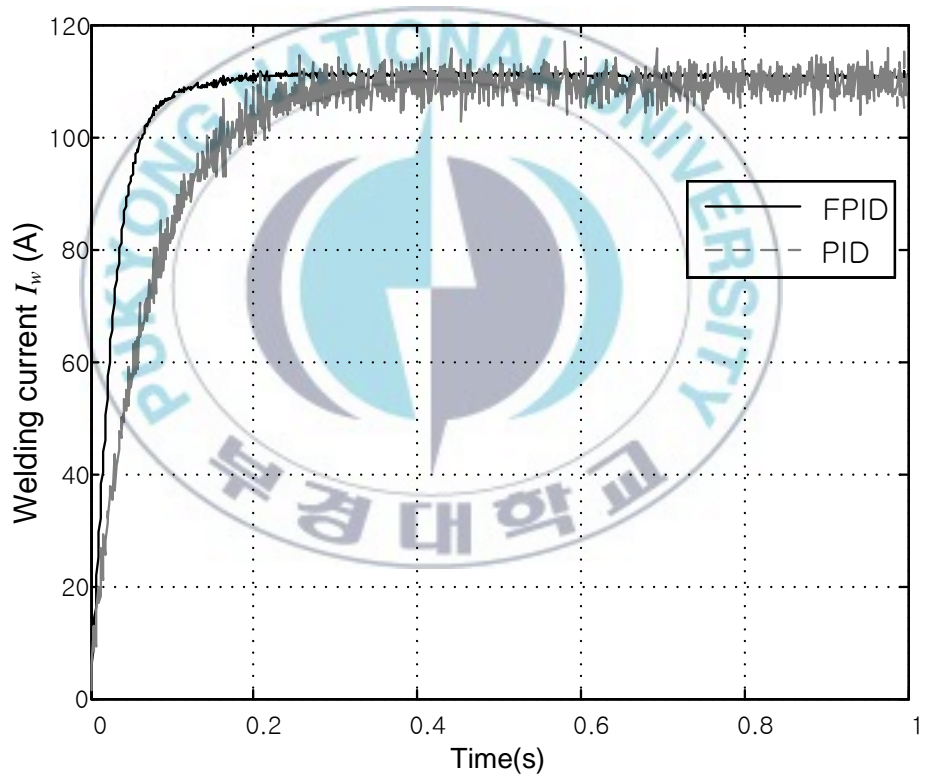


Fig. 3.13 Simulation results for developed GMAW with disturbance

Fig. 3.14 shows the tuning-gains, K_p , K_i and K_d , with disturbance. After 0.1 second, the tracking error is bounded around zero but is not equal to zero. Therefore, the tuning-gains still vary to compensate the error caused by disturbance.

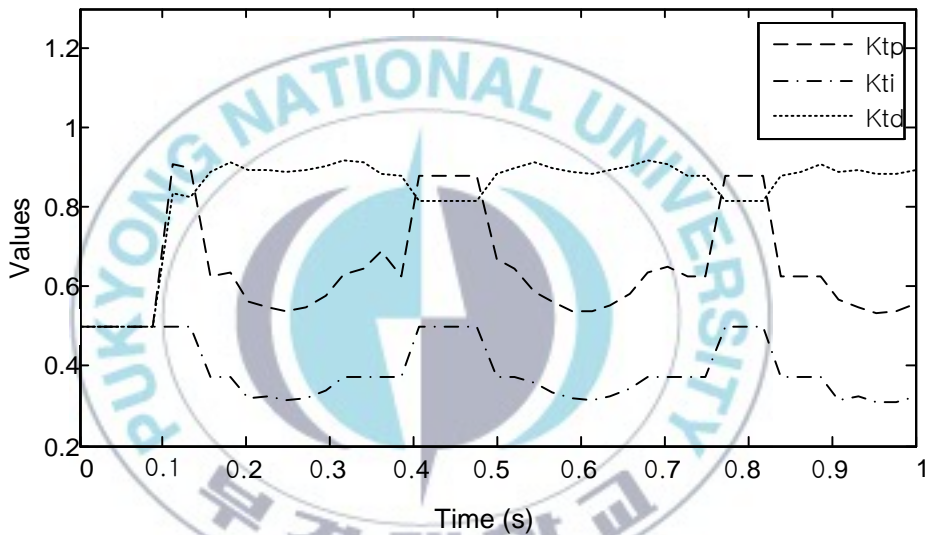


Fig. 3.14 Tuning-gains with disturbance

The experimental results for the welding current and voltage are shown in Fig. 3.15. These results show that the output values are stable and track the setting values of 110A and 22V very well during the welding process.

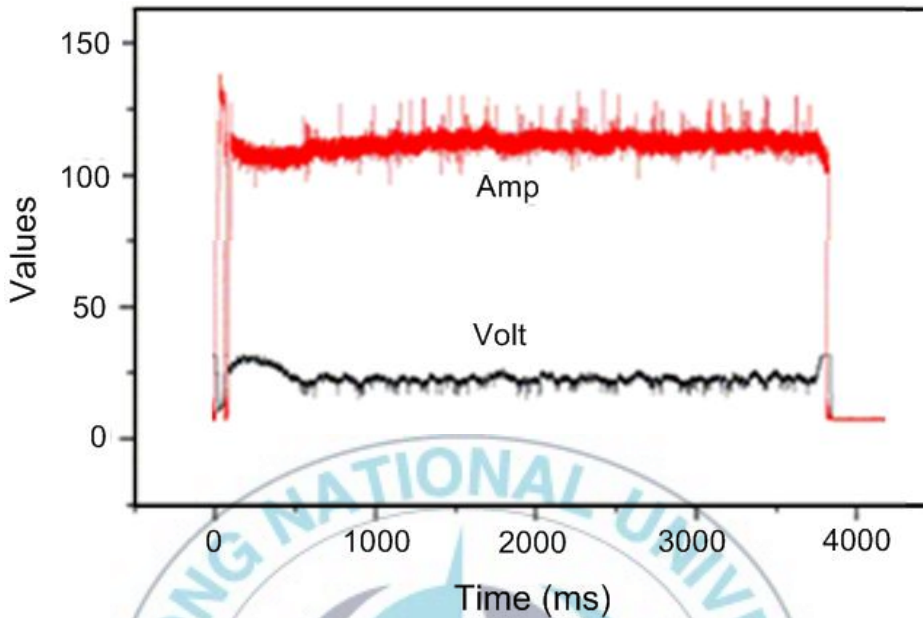


Fig. 3.15 Experimental results for developed GMAW

Fig. 3.16 and Fig. 3.17 show welding results by FPID and the PID [11], respectively. These results show that the FPID's performance is better than the PID's.



Fig. 3.16 Welding result by FPID

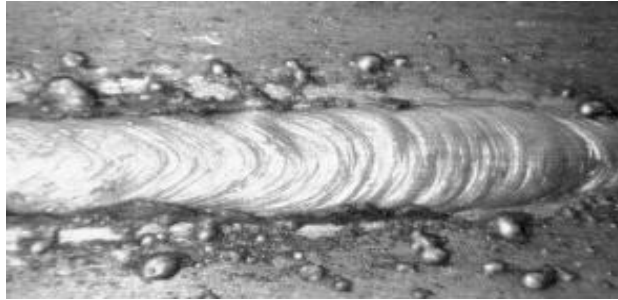


Fig. 3.17 Welding result by PID

3.5 Summary

This chapter proposed a new method for developing digital GMAW system. The PS-GMAW is a constant voltage power supply. A constant arc current is maintained by controlling the wire-feed rate. A self-tuning Fuzzy PID controller is developed and successfully applied to the WFU. To design the controller, the welding error and its derivative is defined and then fuzzy logic control is applied to determine the tuning gains automatically. This tuning-gains are applied to change the gains of PID controller. Simulation and experiment are carried out to evaluate the effectiveness of the proposed control method for the GMAW system. Furthermore, the simulation and experimental results shows that the self-tuning Fuzzy PID(FPID) can achieve good tracking in comparison with the conventional PID controller even in noisy condition. The simulation result shows that the system with FPID makes the welding current be stable around 110A after 0.3 seconds. On the other hand, the system with conventional PID makes the welding current be stable after 0.4 seconds.

Chapter 4. Control design using Fuzzy Sliding Mode Control

This chapter introduces the voltage control using proportional controller and current control using Fuzzy Sliding Mode Control. The control system is tested through simulation and experiment to verify the effectiveness of control system. In this chapter, the simulation and experimental results are analyzed and discussed.

4.1 Introduction

In this chapter, to control arc voltage of GMAW, proportional controller is proposed based on Gas Metal Arc Welding Power Supply's mathematics modeling. To control welding current, Fuzzy Sliding Mode Control method is proposed based on Wire Feeding Unit's mathematical modeling. By combining the flexibility of fuzzy logic control method and robustness of Sliding Mode Control method, a new control method is proposed to control GMAW welding process. Furthermore, to verify the effectiveness of the proposed controllers, the proposed controllers are compared with the conventional PID controller using simulation and experimental results.

4.2 Controller design

4.2.1 Design of voltage controller for Gas Metal Arc Welding Power Supply

Based on mathematical modeling of Gas Metal Arc Welding Power Supply(PS-GMAW), the arc voltage controller is designed. From Eq. (2.1), arc voltage is written as follows:

$$V_{arc} = V_{oc} - L_s \frac{dI_w}{dt} - (R_L + R_s) I_w \quad (4.1)$$

Because the values of electrode resistance, R_L , source resistance, R_s and inductance, L_s , in this system is very small, voltage drop by these parameters in PS-GMAW is considered as disturbance.

Therefore, Eq. (4.1) can be written as :

$$V_{arc} = V_{oc} - \Delta D \quad (4.2)$$

where

$$\Delta D = L_s \frac{dI_w}{dt} + (R_L + R_s) I_w \text{ is considered as disturbance.}$$

Furthermore, Eq. (4.1) shows that the value of arc voltage, V_{arc} , is directly related to the open circuit voltage of PS-GMAW, V_{oc} . Therefore, in this dissertation, proportional controller is proposed to control the arc voltage of PS-GMAW.

Because of the GMAW power supply using high frequency transformer, the average output voltage of GMAW power supply can be expressed as follows:

$$V_{oc} = 2 \times D \times V_t \quad (4.3)$$

where D is duty of PMW that ranges from 0 to 48%, V_t is output voltage of transformer. In this GMAW system, maximum output voltage of transformer is 86V. The relationship between the PS-GMAW controller U_u and D can be written as:

$$D = U_u \times \frac{0.48}{256} = \frac{3}{1600} U_u \quad (4.4)$$

By combining Eqs. (4.2) – (4.4), the relationship between controller and output becomes:

$$V_{arc} = \left(2 \times \frac{3}{1600} U_u \times 86 \right) - \Delta D = \frac{129}{400} U_u - \Delta D \quad (4.5)$$

Error voltage e_u is defined as:

$$e_u(t) = (V_s - V_{arc}) \quad (4.6)$$

where V_s is the constant setting voltage for welding machines.

The proposed proportional controller can be updated as:

$$U_{u(k)} = U_{u(k-1)} + K_{pp} \times e_{u(k-1)} \quad (4.7)$$

where K_{pp} are positive constant values. $U_{u(k-1)}$ and $e_{u(k-1)}$ are the values of controller and the error at $(k-1)^{th}$ time, respectively.

4.2.2 Design of current controller for Wire Feeding Unit

Based on mathematical modeling of the Wire Feeding Unit, the welding current controller is designed. Taking V_m as input, I_w , as output, and state

variables, $x_1 = W_f$ and $x_2 = \dot{W}_f$, state and output equations for Wire Feeding Unit are obtained from Eqs. (3.5) and (3.9) as follows:

$$\begin{bmatrix} \dot{x}_1 \\ \dot{x}_2 \end{bmatrix} = \begin{bmatrix} 0 & 1 \\ -a_0 & -a_1 \end{bmatrix} \begin{bmatrix} x_1 \\ x_2 \end{bmatrix} + \begin{bmatrix} 0 \\ b_0 \end{bmatrix} u_i \quad (4.8)$$

$$y = I_w = c[x_1 + \Delta G] \quad (4.9)$$

where $c = \frac{1}{M_{Ri}}$ and $\Delta G = M_{Rv} V_{arc}$

From transfer function of WFU Eq. (3.5), the following are obtained.

$$G_m(s) = \frac{W_f(s)}{V_m(s)} = \frac{b_0}{s^2 + a_1s + a_0}$$

$$W_f(s)(s^2 + a_1s + a_0) = V_m(s)b_0$$

$$s^2W_f(s) + a_1sW_f(s) + a_0W_f(s) = V_m(s)b_0$$

$$s^2W_f(s) = -a_1sW_f(s) - a_0W_f(s) + u_i(s)b_0$$

$$\ddot{W}_f = -a_1\dot{W}_f - a_0W_f + b_0u_i$$

$$\begin{cases} \dot{x}_1 = x_2 = \dot{W}_f \\ \dot{x}_2 = \ddot{W}_f = -a_1\dot{W}_f - a_0W_f + b_0u_i = -a_1x_2 - a_0x_1 + b_0u_i \end{cases} \quad (4.8a)$$

From Eq. (3.9), the output welding current is as follows:

$$y = I_w = \frac{1}{M_{Ri}} \times [W_f + \Delta G] = c \times [x_1 + \Delta G] \quad (4.10)$$

The current error e_i is defined as follows:

$$e_i = \frac{I_s - I_w}{c} = \frac{I_s - y}{c} = \frac{I_s}{c} - x_1 - \Delta G \quad (4.11)$$

where I_s is the constant setting current value.

$$x_1 = \frac{I_s}{c} - e_i - \Delta G \quad (4.12)$$

From Eq. (4.14), derivative of the error in Eq. (4.17) can be expressed as,

$$\dot{e}_i = -\dot{x}_1 - \Delta\dot{G} = -\frac{\dot{I}_w}{c} = -\frac{\dot{y}}{c} = -x_2 - \Delta\dot{G} \quad (4.13)$$

$$x_2 = -\dot{e}_i - \Delta\dot{G} \quad (4.14)$$

The second derivative of current error in Eq. (4.18) is expresses as follows:

$$\ddot{e}_i = -\dot{x}_2 - \Delta\ddot{G} \quad (4.15)$$

$$\dot{x}_2 = -\ddot{e}_i - \Delta\ddot{G} \quad (4.16)$$

Substituting Eq. (4.12), Eq. (4.14) and Eq. (4.15) in to Eq. (4.8a) yields:

$$-\Delta\ddot{G} - \ddot{e}_i + a_1(-\Delta\dot{G} - \dot{e}_i) + a_0\left(\frac{I_s}{c} - \Delta G - e_i\right) = b_0 u_i \quad (4.17)$$

$$\begin{aligned} \ddot{e}_i &= -a_1 \dot{e}_i + a_0\left(\frac{I_s}{c} - e_i\right) - b_0 u_i - \Delta\ddot{G} - a_1 \Delta\dot{G} - a_0 \Delta G \\ &= -a_1 \dot{e}_i + a_0\left(\frac{I_s}{c} - e_i\right) - b_0 u_i + \bar{d} \end{aligned} \quad (4.18)$$

where $\bar{d} = -\Delta\ddot{G} - a_1 \Delta\dot{G} - a_0 \Delta G$ is bounded value.

Sliding surface is defined to design sliding mode controller as follows [4, 53]:

$$S = \dot{e}_i(t) + \lambda e_i(t) \quad (4.19)$$

where λ is positive constant value.

Derivative of sliding surface can be calculated as follows:

$$\dot{S} = \ddot{e}_i + \lambda \dot{e}_i = [(\lambda - a_1)\dot{e}_i + \frac{a_0}{c}(I_s - ce_i) - b_0 u_i] + \bar{d} \quad (4.20)$$

Lyapunov function is defined as:

$$V = \frac{1}{2} S^2 \quad (4.21)$$

For system stability, derivative of Lyapunov function must be satisfied with :

$$\dot{V} = S\dot{S} \leq 0 \quad (4.22)$$

This dissertation uses Fuzzy Sliding Mode Control (FSMC) method proposed by from [6, 11, 18, 69]. The rule base of the FSMC can be constructed based on Lyapunov's stability in Eq. (4.22).

$$\dot{V} = S\dot{S} = S \left[(\lambda - a_1)\dot{e}_i + \frac{a_0}{c}(I_s - ce_i) - b_0 u_i \right] + S\bar{d} \leq 0 \quad (4.23)$$

From Eq. (4.19), the error, e_i , converges to zero along the trajectory of $S = 0$. From Eq. (4.23), it is seen that if $S < 0$, then decreasing u_i results in decreasing of $S\dot{S}$, and vice versa. Hence, the control variable, u_i , can be designed in an attempt to satisfy the reachability condition to ideal sliding mode $S\dot{S} < 0$.

Fuzzy control rules are as follows:

NB is Negative Big, NM is Negative Medium, NS is Negative Small, ZE/Z is Zero, PS is Positive Small, PM is Positive Medium, and PB is Positive Big, and their universe of discourse are all assigned to be $\{-6, 6\}$.

Membership functions for these fuzzy sets corresponding to S , \dot{S} or \dot{u}_i are defined in Fig. 4.1.

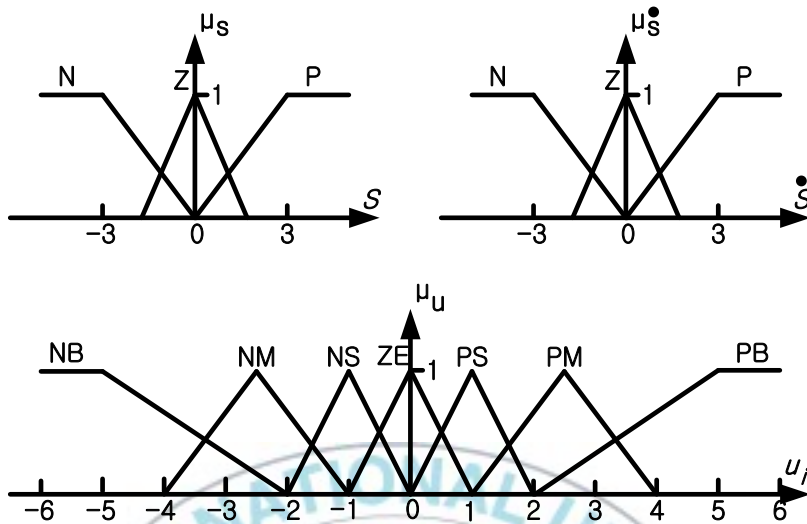


Fig.4.1 Membership functions

The fuzzy control rule base is shown in Table 4.1.

Table 4.1 Rulebase of FSMC

u_i		\dot{s}		
		P	Z	N
s	P	PB	PM	PS
	Z	PS	ZE	NS
	N	NS	NM	NB

Then it applies the Mamdani's mini-operation fuzzy implication and adopts the center of area as defuzzification method to construct the rule set shown as surface in Fig. 4.2.

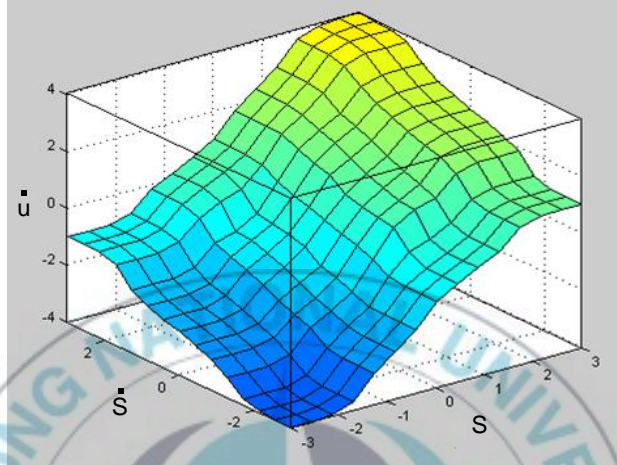


Fig.4.2 Rule surface of SFMC

The block diagram of the proposed controller is shown in Fig. 4.3. In Fig. 4.3, the proportional controller controls the inverter and Fuzzy Sliding Mode Controller controls the DC motor of WFU separately.

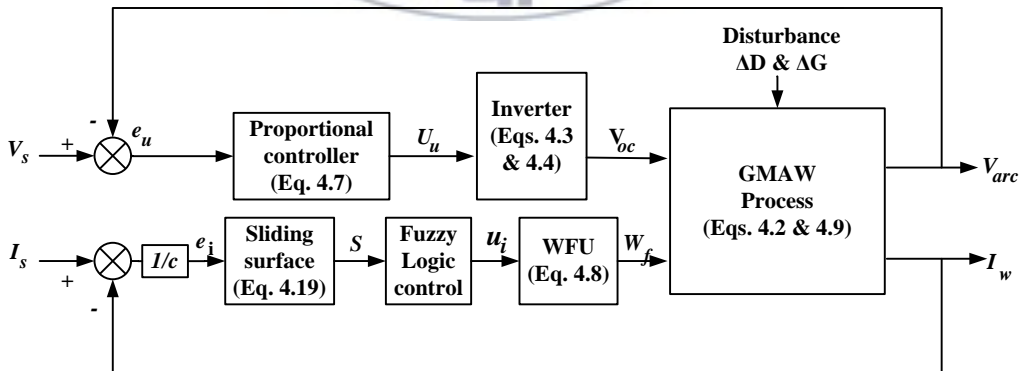


Fig.4.3 Block diagram of GMAW control system.

4.3 Simulation and experimental results

4.3.1 Identification of parameters for the transfer function

The parameters of the DC motor of WFU for simulation are given in Table 3.4. The transfer function in Eq. (3.5) can be written as follows:

$$G_m(s) = \frac{W_f(s)}{V_m(s)} = \frac{b_0}{s^2 + a_1s + a_0} \quad (4.22)$$

In this system, the diameter of the motor, D_{mtr} , is 4×10^{-2} (m). The ratio between the electrode feed-rate and the angular velocity of DC motor of WFU is given as:

$$b' = \frac{W_f}{\dot{\theta}} = \frac{D_{mtr}}{2} \times 60 = 1.2 \quad (4.23)$$

The parameters of transfer function of Eq. (3.5), can be calculate as follows:

$$b_0 = \frac{b'k_T}{L_{am}(D_{ratio}J_L + J_m)} = 5370.2 \quad (4.24)$$

$$a_1 = \frac{L_{am}b_m + R_{am}D_{ratio}J_L + R_{am}J_m}{L_{am}(D_{ratio}J_L + J_m)} = 1111.1 \quad (4.25)$$

$$a_0 = \frac{R_{am}b_m + k_e k_T}{L_{am}(D_{ratio}J_L + J_m)} = 231.53 \quad (4.26)$$

From Eqs. (4.23 - 4.27), the transfer function, $G_m(s)$, in nominal model is as follows:

$$G_m(s) = \frac{W_f(s)}{V_m(s)} = \frac{5370.2}{s^2 + 1111.1s + 231.53} \quad (4.27)$$

The M_{Ri} in Eq. (4.9) depends on a diameter of welding electrode. Based on experimental results, the gain, M_{Ri} , can be approximated ranging from 0.041~0.046 for 1.2mm aluminum electrode. In this dissertation, $M_{Ri} = 0.043$ is chosen.

4.3.2 Simulation results

To verify the effectiveness of the proposed controller, simulation is done. Numerical values and initial conditions used in simulation of the proposed controllers shown in Table 4.2.

Table 4.2 Numerical values of parameters and initial conditions

Gains	Value	Gains	Value
M_{Ri}	0.043	R_L	0.036 Ω
M_{Rv}	0.14	R_s	0.004 Ω
K_{pp}	0.51	λ	350
L_s	0.14mH	$u_i(0)$	0V
$x_1(0)$	0	$u_u(0)$	69digit num
$x_2(0)$	0	$V_{arc}(0)$	22.5V

To verify the effectiveness of the proposed controllers, the proposed controllers are compared with PID controller through simulation and experiment. Figs. 4.4 – 4.8 shows that the simulation responses for both controllers without disturbances($\Delta G = 0$ and $\Delta D = 0$). Parameters of PID controller are derived

using ziegler-nichols method. From this method, PID gains, $K_P= 0.2$, $K_I= 0.02$ and $K_D = 0.012$, are chosen for simulation. The setting current is 110A, setting voltage is 22V and electrode diameter 1.2mm.

Fig. 4.4 shows simulation responses of signal control, u_i , for PID controller and FSMC. In the FSMC and PID controllers, at the beginning of welding, the control voltage is increased rapidly to shorten the rising time of welding current. Control input voltage of WFU at steady state is 0.22V. The control input voltage of Fuzzy Sliding Mode Control (FSMC) reaches steady state condition at 0.17seconds. On the other hand, conventional PID reaches steady state condition after 0.37seconds.

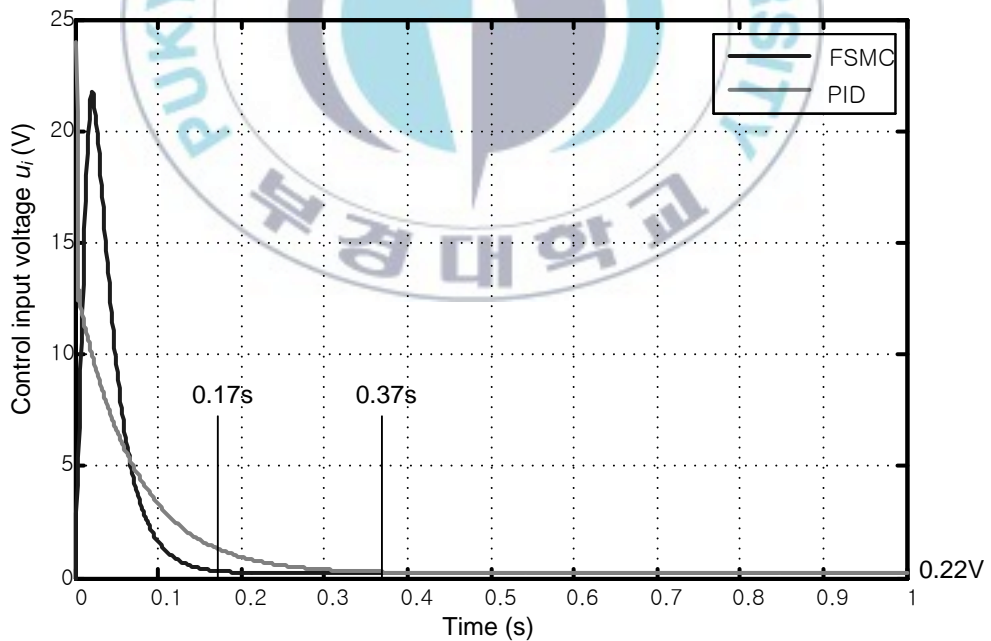


Fig. 4.4 Control voltage of Wire Feeding Unit in simulation

Fig. 4.5 shows output current, I_w , in simulation to track the setting current of 110A. The performance of rising time, settling time and steady state error of the output current of GMAW is better using the proposed Fuzzy Sliding Mode Controller than using conventional PID controller. The FSMC makes the system reach the steady state condition after 0.17 seconds. PID controller needs 0.37 seconds to reach steady state condition. Furthermore, the rising time of FSMC is shorter than that of PID controller.

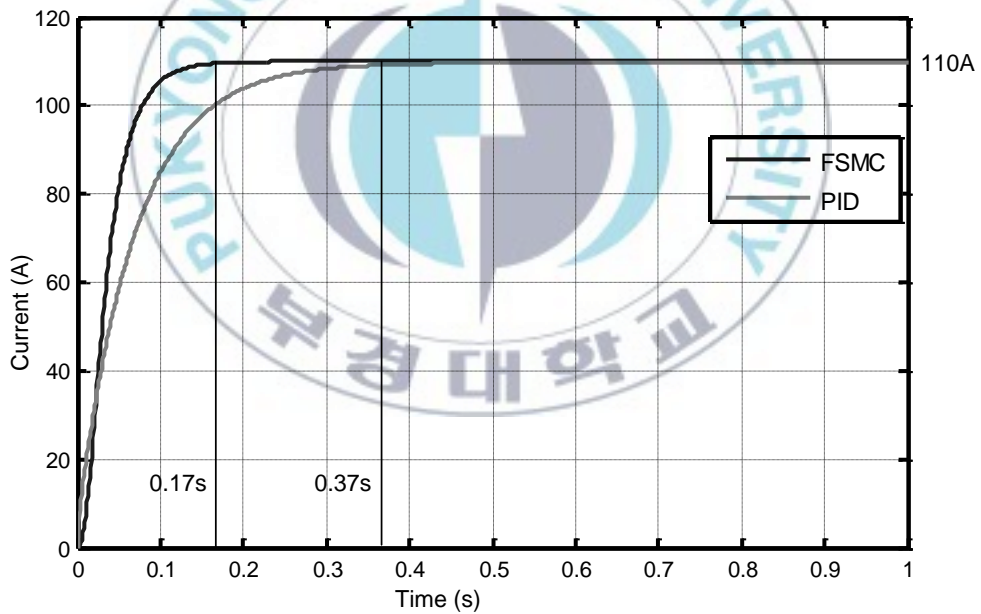


Fig. 4.5 Output current in simulation.

The welding current errors, e_i , for both controllers are shown in Fig. 4.6. The current error of FSMC is decreased rapidly and becomes zero after 0.17 seconds. On the other hand, the current error of PID controller is decreased and becomes zero after 0.37 seconds.

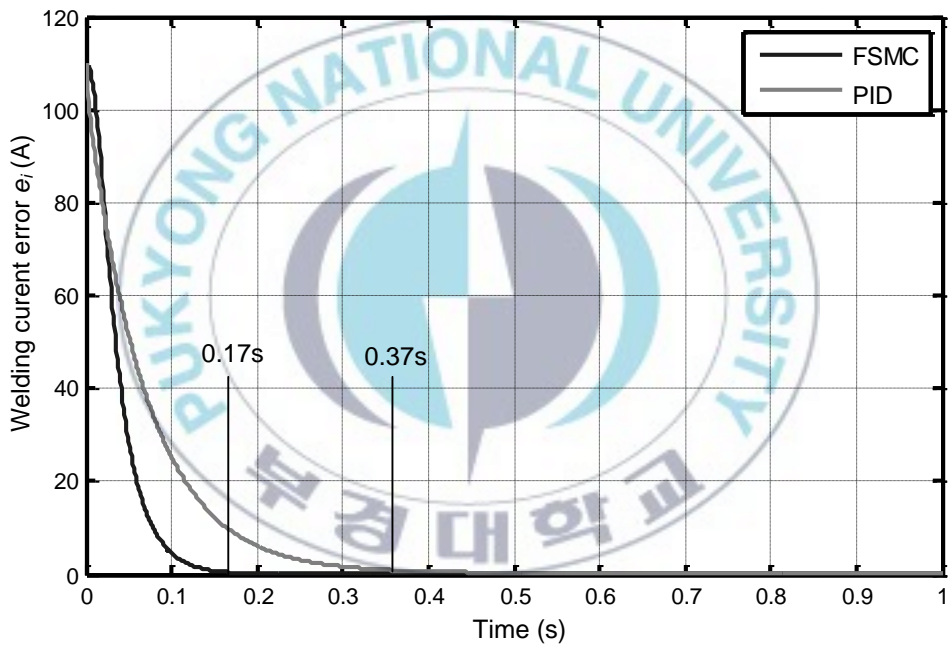


Fig. 4.6 Welding current error in simulation.

Fig. 4.7 shows that reachability condition to the sliding surface $S\dot{S} < 0$ is proven for FSMC.

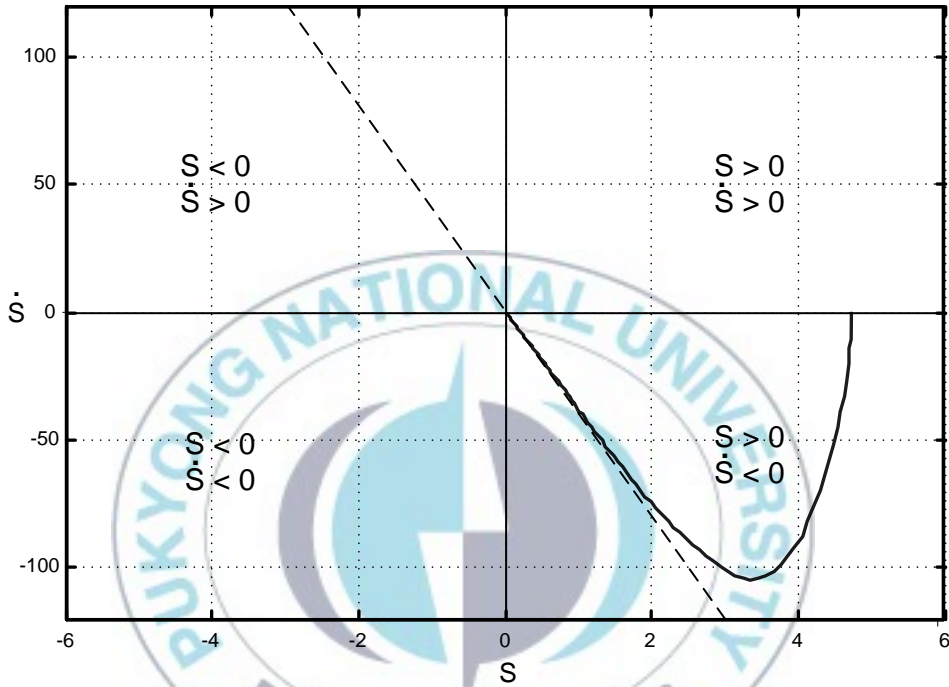


Fig. 4.7 Sliding surface in simulation.

Fig. 4.8 shows that the simulation results of output welding current and voltage are 110A and 22V, respectively. Fig. 4.8 shows that the welding voltage, V_{arc} , is stable after 0.03 seconds and welding current, I_w , is stable after 0.17 seconds. Arc voltage and welding current at steady state are 22V and 110A, respectively.

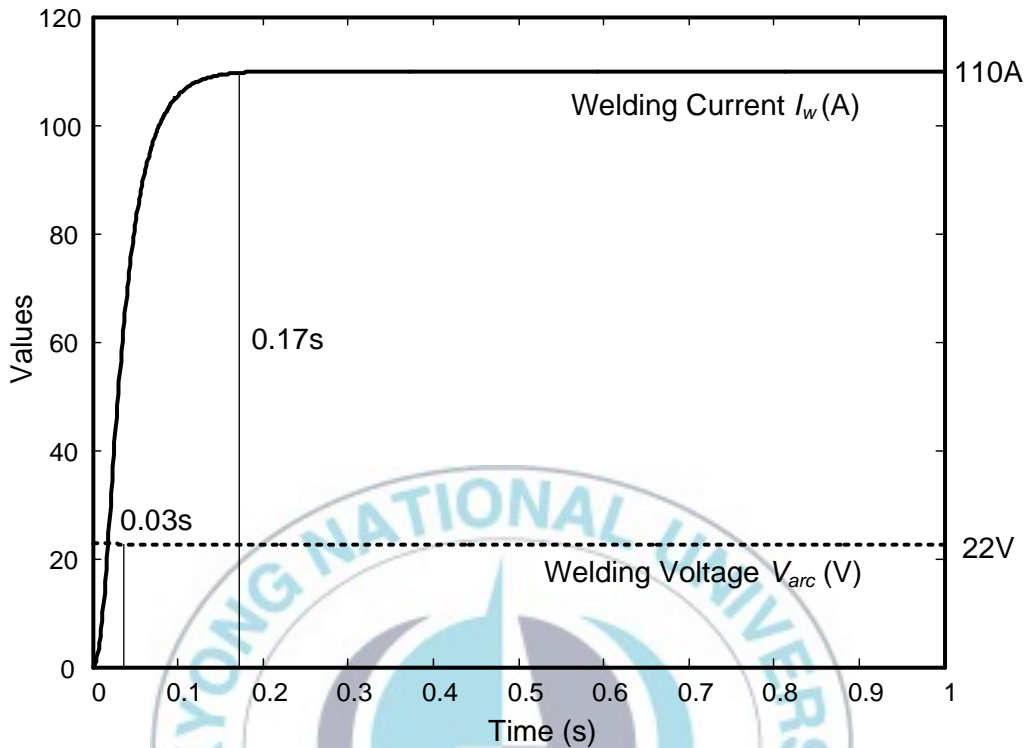


Fig. 4.8 Output welding voltage and current in simulation.

4.3.3 Experimental results

The welding condition for the experiment is shown in Table 3.5.

Fig. 4.9 shows the control input voltage of Wire Feeding Unit from experiment using PID controller. The control input voltage in experiment is bounded along that in simulation. In the beginning, control input voltage of WFU is maximum, then decreased and bounded around 0.22 ± 0.03 V at steady state condition after 0.37 seconds.

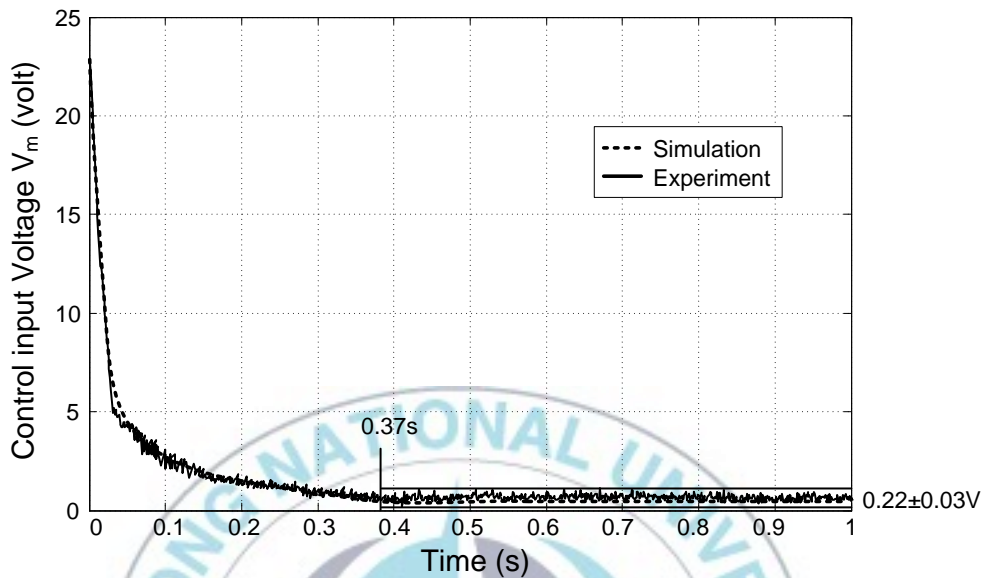


Fig. 4.9 Control input voltage of Wire Feeding Unit using PID controller

The simulation and experimental results of welding current and welding voltage using PID controller are shown in Fig. 4.10. The voltage setting is 22V and current setting is 110A. The experimental result is bounded along the simulation results. At steady state condition, the output welding current is $110 \pm 6A$ and output welding voltage is bounded around $22 \pm 1V$. Simulation results and experimental results show that the welding voltage, V_{arc} , is stable after 0.1 second and welding current, I_w , is stable after 0.37 seconds.

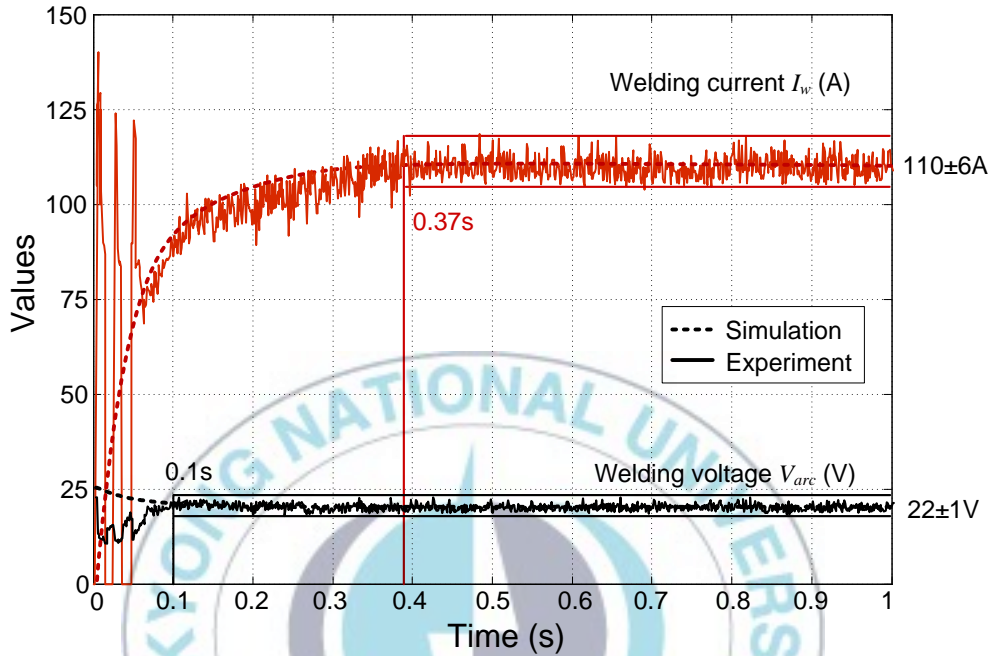


Fig. 4.10 Welding current and welding voltage using PID controller.

Fig. 4.11 shows the welding current error of GMAW system from simulation and experiment using PID controller. Experiment results are bounded around simulations results. In the beginning, the current error is changed rapidly. The current error using PID controller is decreased and becomes zero after 0.37 seconds. The welding current error is bounded around $0\pm 6A$.

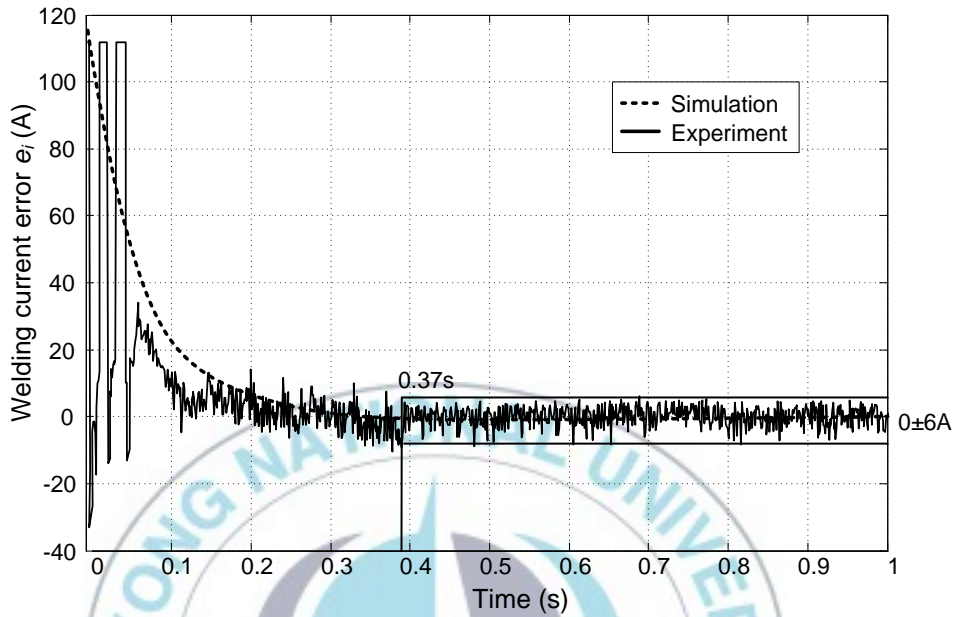


Fig. 4.11 Welding current error using PID controller

Fig. 4.12 shows the control voltage of Wire Feeding Unit from experiment using FSMC controller. The control input voltage in experiment is bounded around that in simulation. It changes rapidly at the beginning rising time. At steady state condition after 0.17 seconds, the control voltage of WFU in experiment is bounded around 0.22 ± 0.03 V.

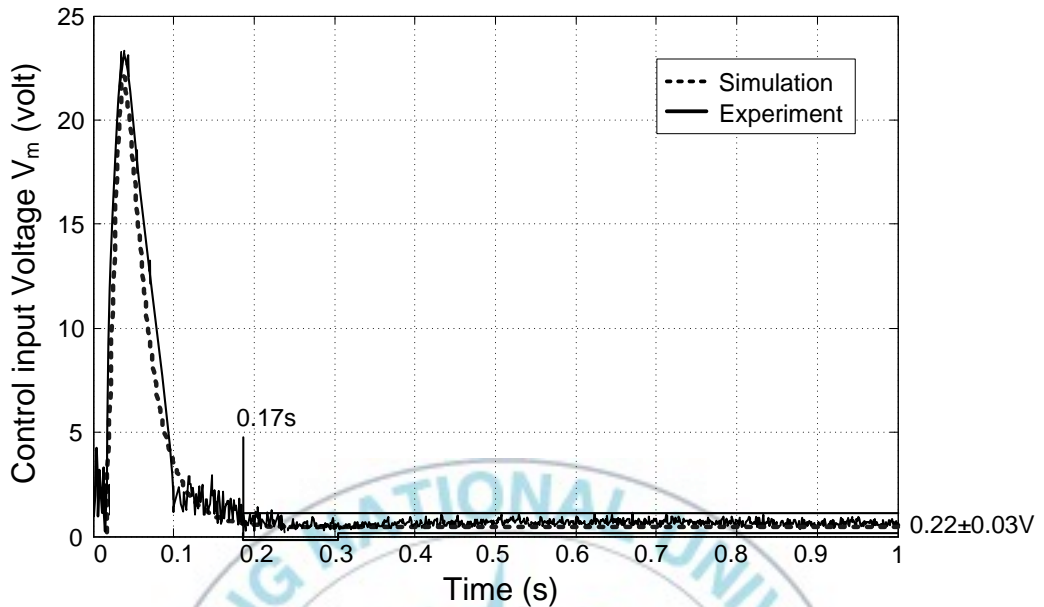


Fig. 4.12 Wire Feeding Unit control input of voltage using FSMC

The experimental results of welding current and welding voltage using FSMC are shown in Fig. 4.13. The voltage setting is 22V and current setting is 110A. It is shown that FSMC is successfully controlling the welding current and voltage during welding process. The experimental result is bounded around the simulation results. At the beginning of welding, the control voltage is increased rapidly to shorten the rising time of welding current and then decreased rapidly. Simulation and experimental results show that the welding arc voltage, V_{arc} , is stable after 0.03 seconds and welding current, I_w , is stable after 0.17 seconds. At steady state condition, the welding current is bounded around $110\pm 6A$ and the welding voltage is bounded around $22\pm 1V$.

In the beginning of welding process, the welding current has big changes during short circuit condition. After taking sometimes, the welding arc is produced and then welding current follows the setting point.

The welding current noise occurs because of the droplet transfer during the welding process. On the other hand, the welding voltage noise occurs because of the welding current noise.

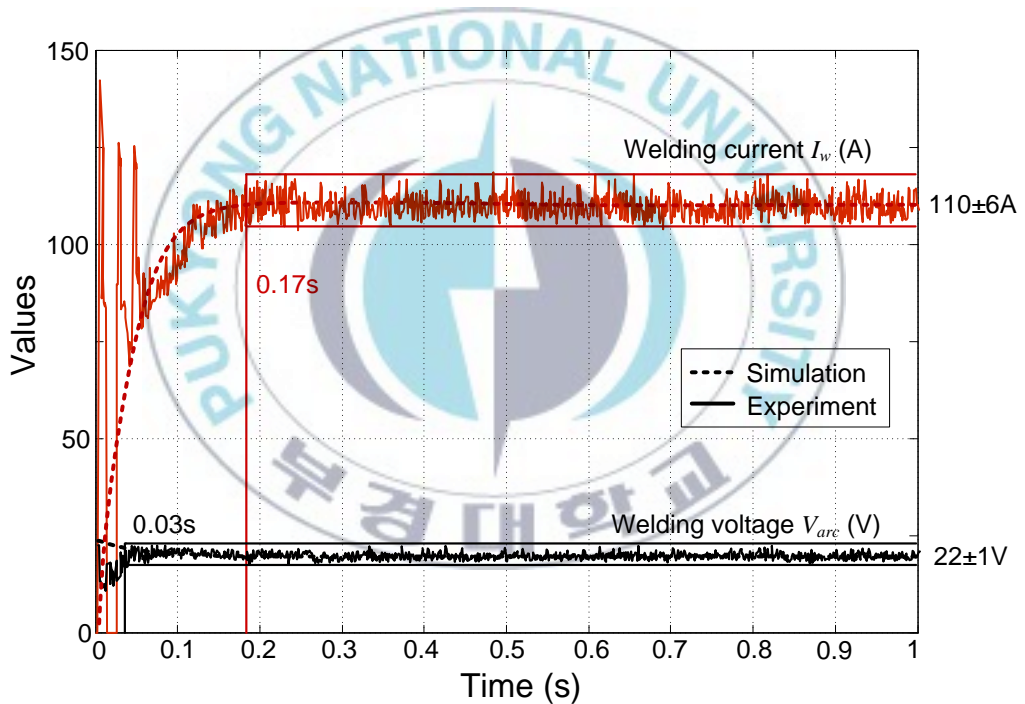


Fig. 4.13 Welding current and welding voltage using FSMC

Fig. 4.14 shows the welding current error in the simulation and experiment result using FSMC. The experimental result is bounded around the simulation

result. In simulation and experiment, the current error of FSMC becomes zero after 0.17 seconds. At the steady state condition, the error is bounded around $0 \pm 6A$. The experiment results show that the system is stable even if there is disturbance.

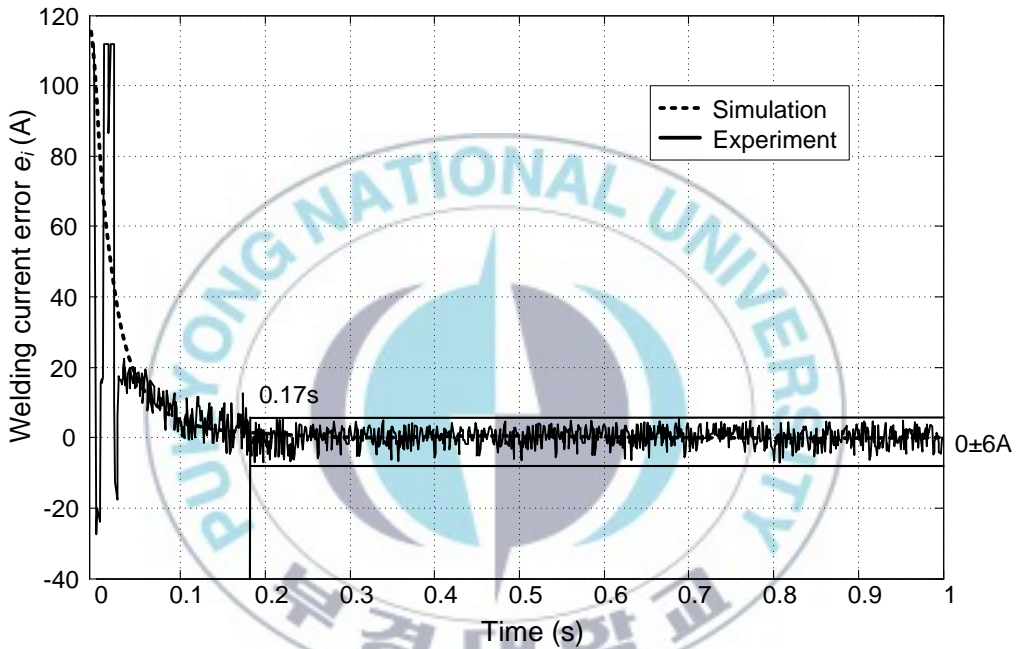


Fig. 4.14 Welding current error using FSMC

Fig. 4.15 shows the sliding surface for simulation and experimental results. In FSMC, reachability condition to the sliding surface $S\dot{S} < 0$ in experiment is proven. The difference between simulation and experimental results occurs because of the disturbance.

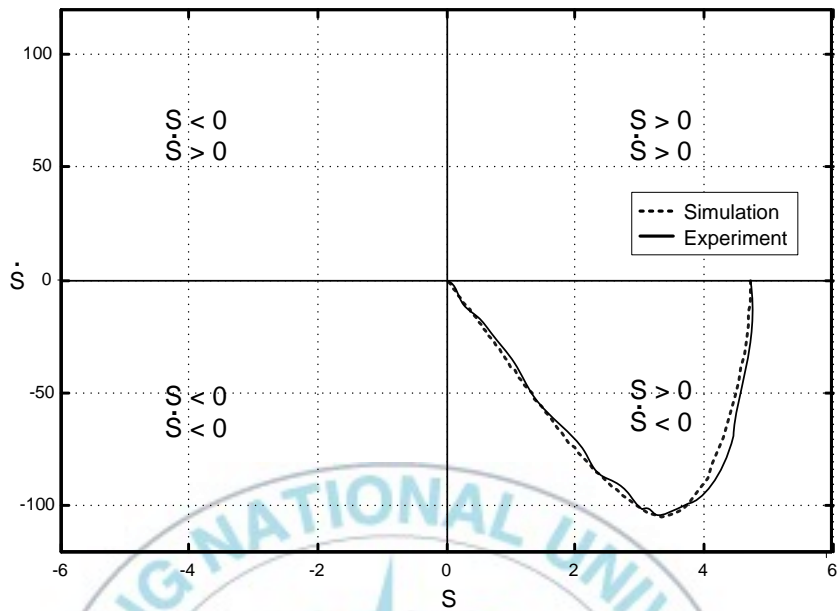
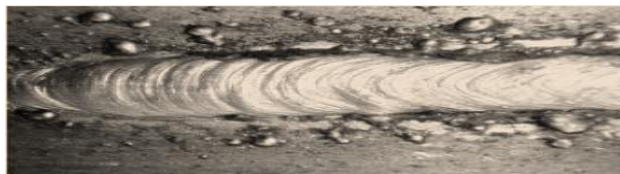


Fig. 4.15 Sliding surface

Furthermore, the welding results of GMAW using FSMC (a) and PID (b) are shown in Fig. 4.16. The pictures show that the welding result using the FMSC in Fig. 4.16 (a) is nicer and neater than that using PID controller in Fig. 4.16 (b).



(a) FSMC



(b) PID

Fig. 4.16 Welding results of GMAW

4.4 Summary

Based on the dynamics models of GMAW, a hybridized controller was proposed by combining proportional controller for voltage control of PS-GMAW and Fuzzy Sliding Mode Controller (FSMC) for current control of WFU. A control law is obtained by using sliding mode control technique and then modified the control input using values obtained from fuzzy controller. The system stability is guaranteed by using Lyapunov stability theory. The proposed hybridized controller tracks its setting value and keeps constant voltage and current of a Gas Metal Arc Welding (GMAW). Simulation results show that the performance of rising time, settling time and steady state error of the output current of GMAW is better using proposed controllers than using conventional PID controller. The arc voltage is stable at 22V after 0.03 seconds. The FSMC makes the system reach the steady state condition at 110A after 0.17 seconds. PID controller needs 0.37 seconds to reach steady state condition. Furthermore, experimental results show that the welding current and voltage are successfully controlled by the proposed controller and the welding result in proposed controllers is nicer and neater than that in PID controller.

Chapter 5. Kalman filter

In previous chapters, self-tuning Fuzzy PID(FPID) and Fuzzy Sliding Mode Control(FSMC) was proposed to control the welding parameter. Although those controllers successfully control the parameter, the welding result can be better if the noise from feedback is reduced. Therefore, in this chapter, the Kalman filter is proposed to reduce the effect of the noise. To verify the effectiveness of the Kalman filter, simulation is done in close loop system using FPID and FSMC in previous chapters.

5.1 Introduction

To control the welding quality, welding current and arc voltage are important parameters due to its influence to weld geometry, weld metallurgical characteristics, weld stability, weld defect and strength. Welding current can be measured by using hall current sensor or series of resistance. Measuring arc voltage is difficult due to the variation of arc length. The arc length can be measured using laser, welding voice and emitted light. Those methods need expensive sensors [46, 51]. So, in this dissertation, to calculate the arc voltage, the voltage between contact tip and work piece is measured under the condition that the variation of wire feeding rate is considered as process noise. In the welding process, measurement noise and process noise can reduce the performance of controller [38].

This dissertation proposes Kalman filter as an observer to estimate the welding current and arc voltage, and reduces the process noise due to variation of arc length and measurement noise of the sensors. To estimate the welding output, the wire feed rate must be known. To simplify the system, the wire feed rate can be observed using Kalman filter. The estimated welding current and arc voltage can be applied as feedback to control the welding output.

The Kalman filter uses a series of measurements observed over time that contains noise and other inaccuracies. It produces estimates of unknown variables that tend to be more precise than those based on a single measurement alone. The algorithm works in a two-step process. In prediction step, the Kalman filter produces estimates of the present state variables along with their uncertainties. Then, these estimates are updated using a weighting factor by Kalman gain. When estimates have higher certainty, more weight is given to estimates. Because of the algorithm's recursive nature, it can run in real time using only the present input measurements and the previously calculated state; no additional past information is required. From a theoretical standpoint, the main assumption of the Kalman filter is that the underlying system is a linear dynamical system and that all error terms and measurements have a Gaussian distribution.

5.2 Kalman filter design

Most systems are described with continuous-time dynamics. However, state estimation and control algorithms are implemented in digital electronics [28]. So,

to design a Kalman filter, firstly, the discrete stochastic process must be considered. It means that continuously time-varying state is sampled at spaced intervals of time to create the sequence $x(k)$, $k \in \{0,1,2,3,\dots\}$.

The state space for GMAW system without disturbance from Eqs. (4.8) - (4.10) is considered as follows:

$$\dot{x} = Ax + Bu \quad (5.1)$$

$$y = Cx \quad (5.2)$$

$$A = \begin{bmatrix} 0 & 1 \\ -a_0 & -a_1 \end{bmatrix} B = \begin{bmatrix} 0 \\ b_0 \end{bmatrix} C = [c \quad 0]$$

where $x \in R^2 = [x_1 \quad x_2]^T = [W_f \quad \dot{W}_f]^T$ is the state vector, $y = I_w$ is the scalar output, and $u = V_m$ is the scalar controller for WFU and $c = 1/M_{Ri}$.

The GMAW system can be modeled as linear dynamical discrete-time system:

$$x(k+1) = Fx(k) + Gu(k) \quad (5.3)$$

$$y(k) = Hx(k) \quad (5.4)$$

where

$$x(k) = [x_1(k) \quad x_2(k)]^T \quad (5.5)$$

$$y(k) = y_1(k)$$

Proof of Eqs. (5.6) - (5.8) refers to Appendix A.

$$F = e^{AT} \approx I + AT = \begin{bmatrix} 1 & T \\ -a_0T & 1 - a_1T \end{bmatrix} \quad (5.6)$$

$$G = e^{AT} \int_0^T e^{-At} dt B = A^{-1} (e^{AT} - I) B \approx BT = \begin{bmatrix} 0 \\ b_0 T \end{bmatrix} \quad (5.7)$$

$$H = C = [c \ 0] \quad (5.8)$$

From Eqs. (5.3) and (5.4), the linear dynamical discrete-time system with the process noise and measurement noise becomes:

$$x(k+1) = Fx(k) + Gu(k) + v(k) \quad (5.9)$$

$$y(k) = Hx(k) + w(k) \quad (5.10)$$

The state vector, $x(k) \in \mathbb{R}^n$, denotes the full system state. The input vector, $u(k) \in \mathbb{R}^m$, represents the GMAW system input such as PS-GMAW duty cycle and DC motor voltage for WFU. The output vector, $y(k) \in \mathbb{R}^p$, represents the GMAW system output measured by the system sensors such as welding current and arc voltage. The system matrix, $F(k) \in \mathbb{R}^{n \times n}$, is system matrix of the GMAW system. $G(k) \in \mathbb{R}^{n \times m}$ is input matrix. The $v(k) \in \mathbb{R}^n$ is called the process noise vector and is assumed to be white Gaussian noise with zero mean and covariance matrix, $V(k)$. The process noise is used to calculate unmodeled disturbance that affects the system dynamics. The matrix, $H(k) \in \mathbb{R}^{p \times n}$, is output matrix. The measurement noise vector, $w(k) \in \mathbb{R}^p$, is assumed to be white Gaussian noise with zero mean and covariance matrix, $W(k)$. It is assumed that $H(k)$ is full rank for all k although it may not be

square.

From Eq. (5.1), the matrix A and C is known. This system is observable, because its observability matrix has full rank. The unmeasured states are observed and estimated through measuring the accessible output. In GMAW, the electrode feed rate, W_f , is not measured directly. In this dissertation, Kalman filter estimates the electrode feed rate, W_f . Then, the welding current and arc voltage are computed based on the estimation result. Moreover, the welding process noise due to the variation of wire feeding rate and measurement noise is changed.

The Kalman algorithm works in a two steps process [13, 40]:

1. Prediction:

In first step, states are predicted based on their previously estimated values and then their covariances are computed. Relations related to this step are presented by:

$$\hat{x}(k+1|k) = F(k)\hat{x}(k|k) + G(k)u(k) \quad (5.11)$$

$$P(k+1|k) = F(k)P(k|k)F(k)^T + V(k) \quad (5.12)$$

where $\hat{x}(k+1|k)$ is predicted state, and $P(k+1|k)$ is predicted covariance matrix.

2. Update:

In the second step, at first, gain of the Kalman filter, K , is computed and then the predicted states are updated by the new measurements. The state covariances are also updated in this stage. The following relations describe

the update step.

$$\hat{x}(k+1|k+1) = \hat{x}(k+1|k) + K\varepsilon \quad (5.13)$$

$$P(k+1|k+1) = P(k+1|k) - KH(k+1)P(k+1|k) \quad (5.14)$$

where

$$\varepsilon = y(k+1) - H(k+1)\hat{x}(k+1|k) \quad (5.15)$$

$$S = H(k+1)P(k+1|k)H(k+1)^T + W(k+1) \quad (5.16)$$

$$K = P(k+1|k)H(k+1)^T S^{-1} \quad (5.17)$$

where $\hat{x}(k+1|k+1)$ is estimated state, K is Kalman gain, ε is error between prediction and measurement, and $P(k+1|k+1)$ is update equation for covariance matrix.

Those equations provide the optimal estimate of x in the sense that the expected value of error between $x(k)$ and $\hat{x}(k|k)$ is minimized at every k . One can view Kalman gain, K , as the weighting factor that takes account the relationship between the accuracy of predicted estimate and the measurement noise. If K is large, the sensor reading is more believable than the prediction and the Kalman filter weights the sensor readings highly when it computes the updated estimate. If K is small, the sensor reading is unbelievable and measurement results do not have much influence in the update step.

The process noise vector, $v(k)$, represents the noise that disturbs the welding process. In GMAW process, the noise happens because of disturbance caused by changing the distance between contact tip and work piece, voltage

noise in PS-GMAW and the friction in Wire Feeding Unit.

The covariance matrix of vector with k independent observations $Z = [z_1, \dots, z_k]^T$ of p dimensional random variable $Z_p \in \mathbb{R}^{p \times 1}$ (a $p \times 1$ column-vector) is

$$\text{cov}(X) = E\langle (X)(X)^T \rangle = \frac{1}{k} \sum_{i=1}^k (z_i - \bar{z})(z_i - \bar{z})^T \quad (5.18)$$

where $X = Z - \bar{z}$, E means expectation, \bar{z} means average of z ($\bar{z} = E(z)$), z_i is the i^{th} observation of Z , and $\bar{z} = \frac{1}{k} \sum_{i=1}^k z_i$ is the sampled mean value.

In Kalman filter, the noises are assumed to be white Gaussian noise with zero mean ($\bar{z} = 0$).

If each value of vector Z is assumed to be constant ($z_i = z$), Eq. (5.18) is reduced as :

$$\text{cov}(X) = \frac{1}{k} \sum_{i=1}^k (z_i - 0)(z_i - 0)^T = \frac{k}{k} (z)(z)^T = (z)(z)^T \quad (5.19)$$

The process noise vector is denoted by:

$$v(k) = \begin{bmatrix} \tau_1 \\ \tau_2 \end{bmatrix} \quad (5.20)$$

The covariance matrix of the process noise vector from Eqs. (5.19) and (5.20) is:

$$V(k) = \text{cov}(v(k)) = E\langle v(k) v(k)^T \rangle = v(k) v(k)^T$$

$$= \begin{bmatrix} \tau_1 \\ \tau_2 \end{bmatrix} \begin{bmatrix} \tau_1 & \tau_2 \end{bmatrix} = \begin{bmatrix} \tau_1^2 & \tau_1 \tau_2 \\ \tau_1 \tau_2 & \tau_2^2 \end{bmatrix} \quad (5.21)$$

The measurement noise vector, $w(k)$, represents the noise that disturbs the measurement process. In GMAW process, the measurement noise is caused by the accuracy of the sensors and electrical circuit. The measurement noise vector is denoted by:

$$w(k) = [\tau_3] \quad (5.22)$$

The covariance matrix of the measurement noise vector from Eqs. (5.19) and (5.22) is:

$$W(k) = \text{cov}(w(k)) = E \langle w(k) w(k)^T \rangle = w(k) w(k)^T = [\tau_3][\tau_3]^T = [\tau_3^2] \quad (5.23)$$

By using estimated state, $\hat{x}(k+1|k+1)$, the estimated output for feedback can be calculated using:

$$\hat{y}(k+1|k+1) = H\hat{x}(k+1|k+1) \quad (5.24)$$

where $\hat{y}(k+1|k+1) = \hat{I}_w(k+1|k+1)$

The estimated arc voltage is calculated using:

$$\hat{V}_{arc}(k+1|k+1) = \frac{129}{400} U_u - \Delta\hat{D} \quad (5.25)$$

where $\Delta\hat{D} = L_s \frac{d\hat{I}_w}{dt} + (R_L + R_s)\hat{I}_w$ and $\hat{I}_w = \hat{I}_w(k+1|k+1)$

5.3 Simulation results

The simulation is based on states in proposed GMAW system. In simulation, firstly, the Kalman filter is used to estimate the arc voltage and welding current in open loop condition. The purpose of this simulation is to verify the effectiveness of Kalman filter reducing the effect of the noises. Secondly, the Kalman filter is to estimate the arc voltage and welding current in closed loop condition using FPID and FSMC. The aim of this simulation is to verify the effectiveness of Kalman filter applied in closed loop condition.

All parameters values and initial conditions for simulation is shown in Table 5.1.

Table 5.1 Parameter values and initial conditions

Gains	Value	Gains	Value
M_{Ri}	0.043	R_L	0.036Ω
M_{Rv}	0.14	R_s	0.004Ω
K_{pp}	0.51	λ	350
L_s	0.14mH	$u_i(0)$	0V
$x_1(0)$	0	$u_u(0)$	69 digit num
$x_2(0)$	0	$V_{arc}(0)$	22.5V

The parameters in transfer function can be calculated as follows:

$$b_0 = \frac{b'k_T}{L_{am}(D_{ratio}J_L + J_m)} = 5370.2 \quad (5.26)$$

$$a_1 = \frac{L_{am}b_m + R_{am}D_{ratio}J_L + R_{am}J_m}{L_{am}(D_{ratio}J_L + J_m)} = 1111.1 \quad (5.27)$$

$$a_0 = \frac{R_{am}b_m + k_e k_T}{L_{am}(D_{ratio}J_L + J_m)} = 231.53 \quad (5.28)$$

The Kalman filter algorithm can be applied in the discrete time process of GMAW system. Firstly, the process noise and measurement noise must be assumed.

Using Eq. (5.21), the covariance matrix of process noise is calculated. In this simulation, the process noise vector is assumed as $\tau_1 = 1 \times 10^{-3}$, $\tau_2 = 1 \times 10^{-3}$ and sampling time $T=1\text{ms}$. Therefore, the covariance matrix of the process noise vector is:

$$V(k) = \begin{bmatrix} 1 \times 10^{-6} & 1 \times 10^{-6} \\ 1 \times 10^{-6} & 1 \times 10^{-6} \end{bmatrix}$$

Using Eq. (5.23), the covariance matrix of measurement noise is calculated. For this simulation, the measurement noise vector is assumed as $\tau_3 = 10$, the covariance matrix of the measurement noise vector is:

$$W(k) = [\tau_3^2] = [100]$$

The initial condition of error covariance matrix, $P(k)$, is chosen as:

$$P(k) = \begin{bmatrix} 1 & 0 & 0 \\ 0 & 1 & 0 \\ 0 & 0 & 1 \end{bmatrix}$$

5.3.1 Kalman filter applied in self-tuning Fuzzy PID controller

To verify the effectiveness of Kalman filter in closed loop GMAW system, the simulation using the self-tuning Fuzzy PID controller (FPID) in previous chapter is done. Fig. 5.1 shows block diagram of GMAW system for Kalman filter applied to self-tuning Fuzzy PID controller.

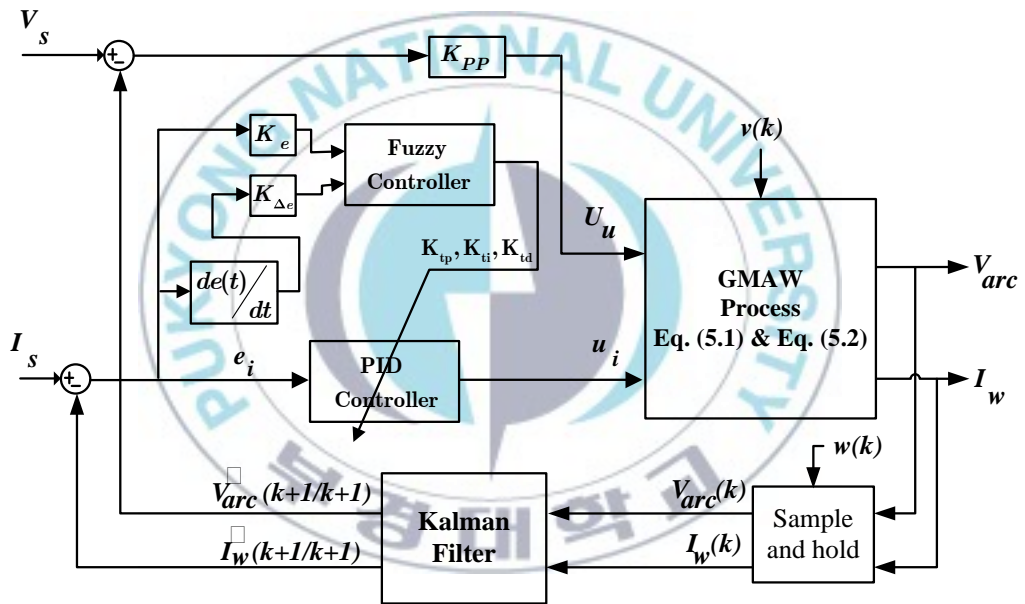


Fig. 5.1 Block diagram of GMAW system applying Kalman filter to self-tuning Fuzzy PID controller

The simulation results of Kalman filter applied to self-tuning Fuzzy PID controller are shown in Figs. 5.2– 5.7.

Fig. 5.2 shows the control voltage input of Wire Feeding Unit using Kalman filter to self-tuning Fuzzy PID controller in simulation. There is noise in the control voltage without applying Kalman filter. This noise caused by the derivative gain, K_D , amplifies the derivative of error. In noisy signal, the derivative of noise becomes bigger and the control signal has bigger noise. In control voltage using Kalman filter, the noise is reduced significantly. So the control noise is also reduced. After 0.25 seconds, average control input voltage of WFU goes to 0.22V.

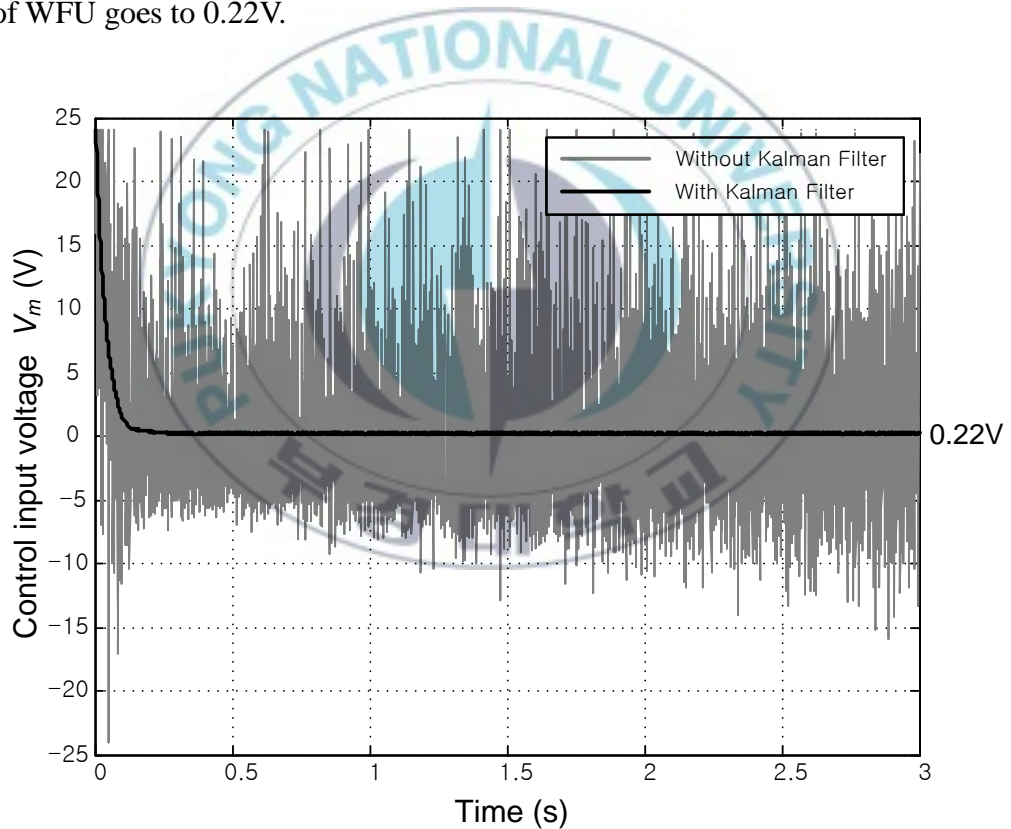


Fig. 5.2 Control input voltage of Wire Feeding Unit with/ without applying Kalman filter to self-tuning Fuzzy PID controller in simulation

Fig. 5.3 shows the output current, I_w , in simulation with/ without applying Kalman filter to self-tuning Fuzzy PID controller. The output current without applying Kalman filter can't reach its setting value of 110A and is not smooth due to the disturbance of the noise. On the other hand, the output current using Kalman filter is smoother. The noise in output current using Kalman filter is reduced. Therefore, the controller can track the output current to its setting value of 110A easily.

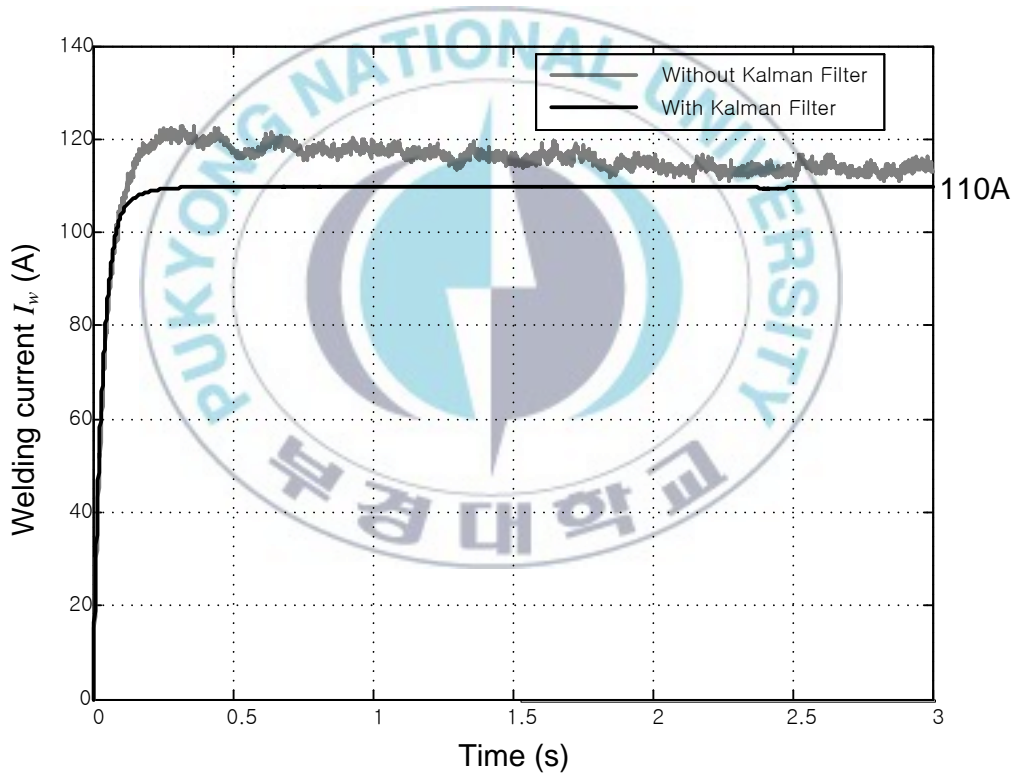


Fig. 5.3 Output current in simulation with/ without applying Kalman filter to self-tuning Fuzzy PID controller

Fig. 5.4 shows the welding current error, e_i , in simulation with/ without applying Kalman filter to self-tuning Fuzzy PID controller. The simulation result shows that the welding current error using Kalman filter becomes zero after 0.25 seconds. On the other hand, the welding current error without applying Kalman filter never becomes zero because of the noise.

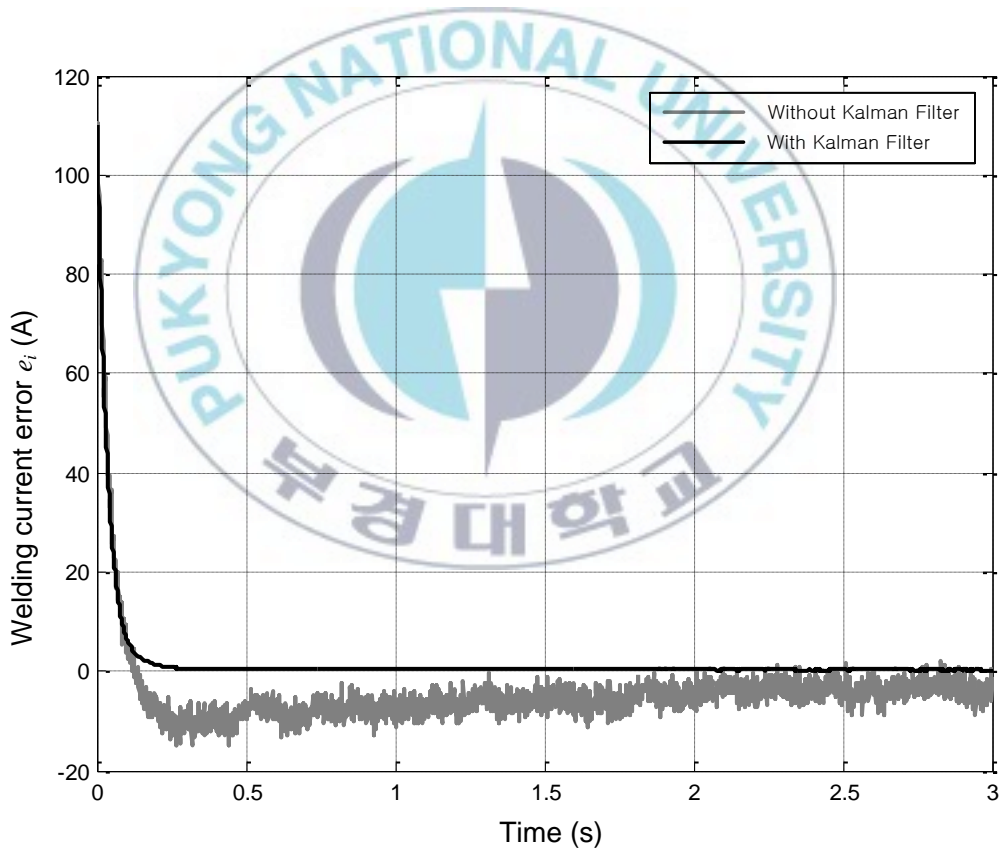


Fig. 5.4 Welding current error with/ without applying Kalman filter applied to self-tuning Fuzzy PID controller in simulation

Fig. 5.5 shows the PS-GMAW voltage controller with/ without applying Kalman filter to self-tuning Fuzzy PID controller in simulation. Without applying Kalman filter, there is noise that causes the output voltage to become chattering. Simulation using Kalman filter shows that PS-GMAW control voltage can smoothly control the output voltage of welding machines. After 0.25 seconds, the output value of arc voltage controller reaches 68.4.

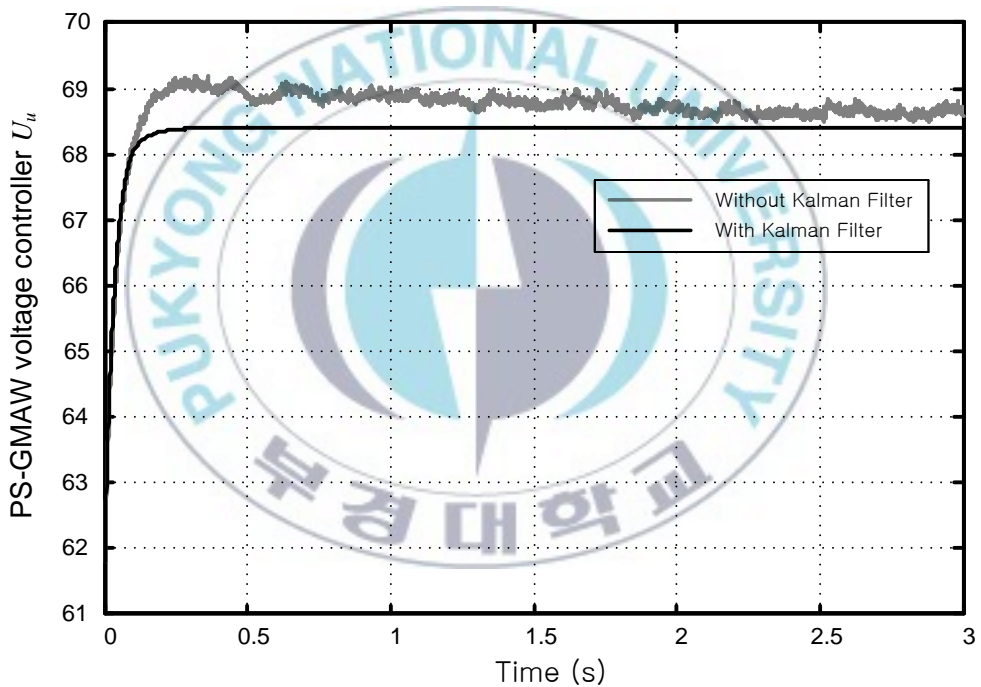


Fig. 5.5 PS-GMAW voltage controller with/ without applying Kalman filter to self-tuning Fuzzy PID controller in simulation

Fig. 5.6 shows the arc voltage, V_{arc} , in simulation with/ without applying Kalman filter to self-tuning Fuzzy PID controller simulation. In simulation without applying Kalman filter, the signal has noise due to noisy control signal. In filtered simulation using Kalman filter, the output arc voltage is smooth. After 0.25 seconds, the output arc voltage goes to 22V.

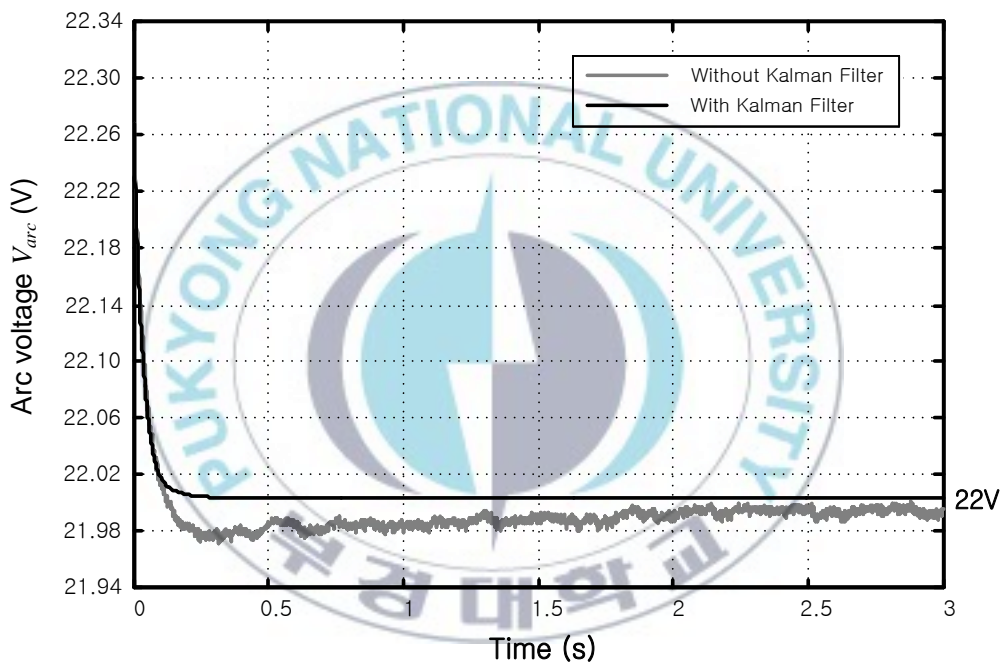


Fig. 5.6 Arc voltage in simulation with/ without applying Kalman filter to self-tuning Fuzzy PID controller

Fig. 5.7 shows the arc voltage error, e_u , in simulation with/ without applying Kalman filter to self-tuning Fuzzy PID controller. The error in simulation with applying Kalman filter becomes zero after 0.25 seconds. The error in simulation without applying Kalman filter can not go to zero.

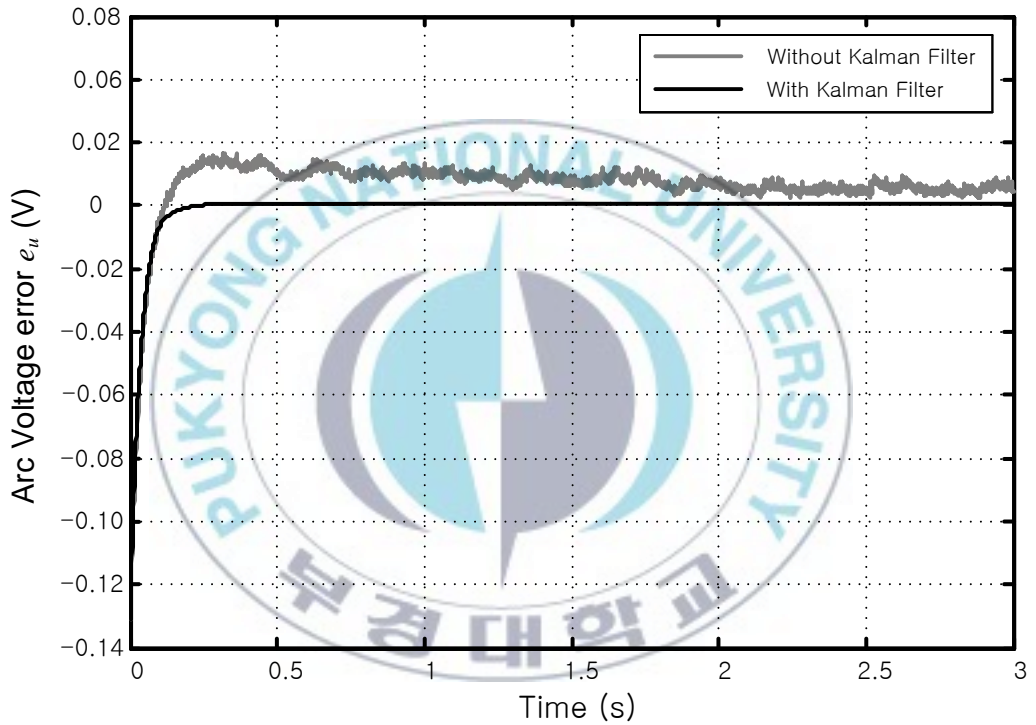


Fig. 5.7 Arc voltage error in simulation with/ without applying Kalman filter to self-tuning Fuzzy PID controller

5.3.2 Kalman filter applied on Fuzzy Sliding Mode Control

Fig. 5.8 shows block diagram of GMAW system applying Kalman filter to Fuzzy Sliding Mode Control.

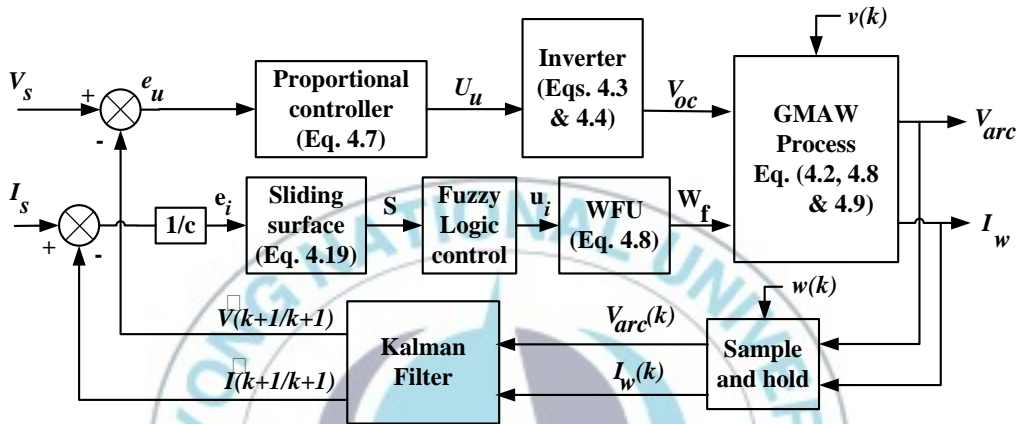


Fig. 5.8 Block diagram of GMAW system applying Kalman filter to Fuzzy Sliding Mode Control

The simulation result of Kalman filter applied to Fuzzy Sliding Mode Control is shown in Figs. 5.9 – 5.13.

Fig. 5.9 shows the control input voltage, V_m , of Wire Feeding Unit with/without applying Kalman filter to Fuzzy Sliding Mode Control simulation. In simulation without Kalman filter, the control signal has oscillation with -5V – +5V after 0.2 seconds. This is caused by unfiltered feedback noise. Control signal applying Kalman filter to FSMC goes to 0.22V after 0.25 seconds.

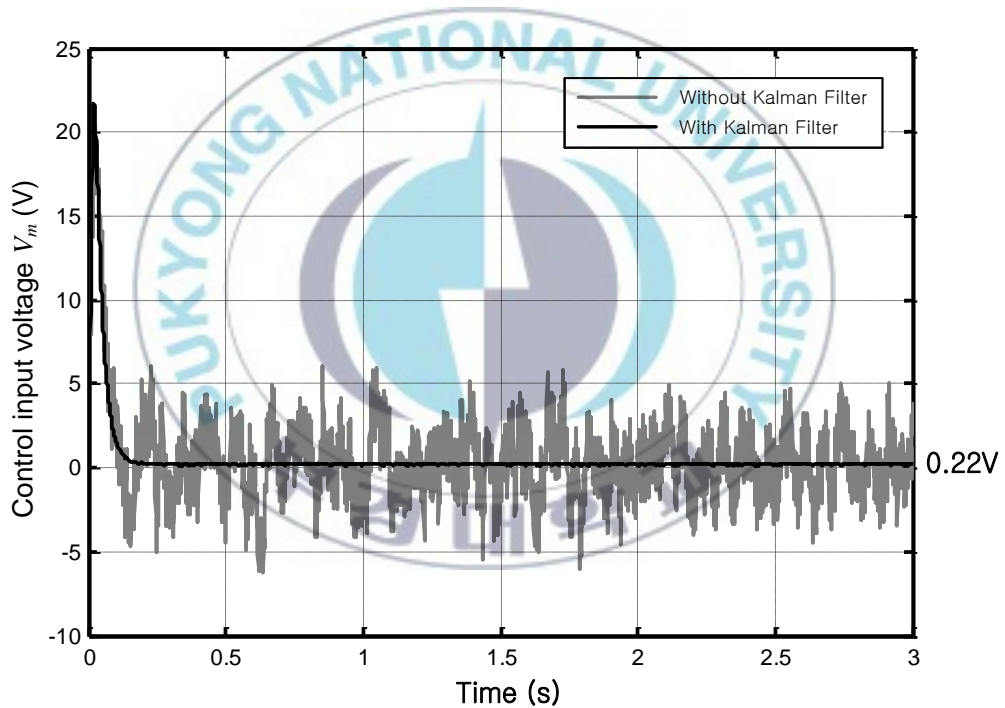


Fig. 5.9 Wire Feeding Unit control voltage with/ without applying Kalman filter to Fuzzy Sliding Mode Control in simulation

Fig. 5.10 shows the output current, I_w , in simulation with/ without applying Kalman filter to Fuzzy Sliding Mode Control. The output current using Kalman filter is stable after 0.15 seconds and bounded around 110A. On the other hand, the output current without applying Kalman filter have bigger oscillation around 110A than that with applying Kalman filter and is stable after more than 0.5 seconds.

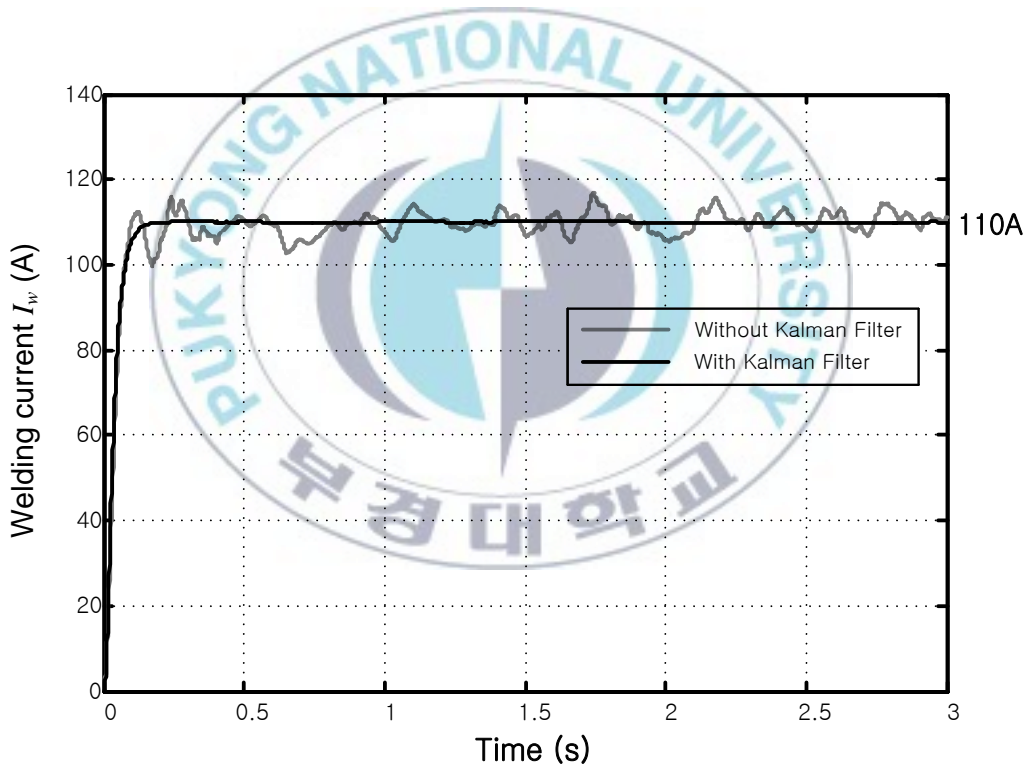


Fig. 5.10 Output current in simulation with/ without applying Kalman filter to Fuzzy Sliding Mode Control in simulation

Fig. 5.11 shows the welding current error, e_i , in simulation with/without applying Kalman filter to Fuzzy Sliding Mode Control. In simulation using Kalman filter, the output error becomes zero after 0.15 seconds. On the other hand, the error in simulation without applying Kalman filter is oscillated and bounded around $0 \pm 8A$ after 0.5 seconds.

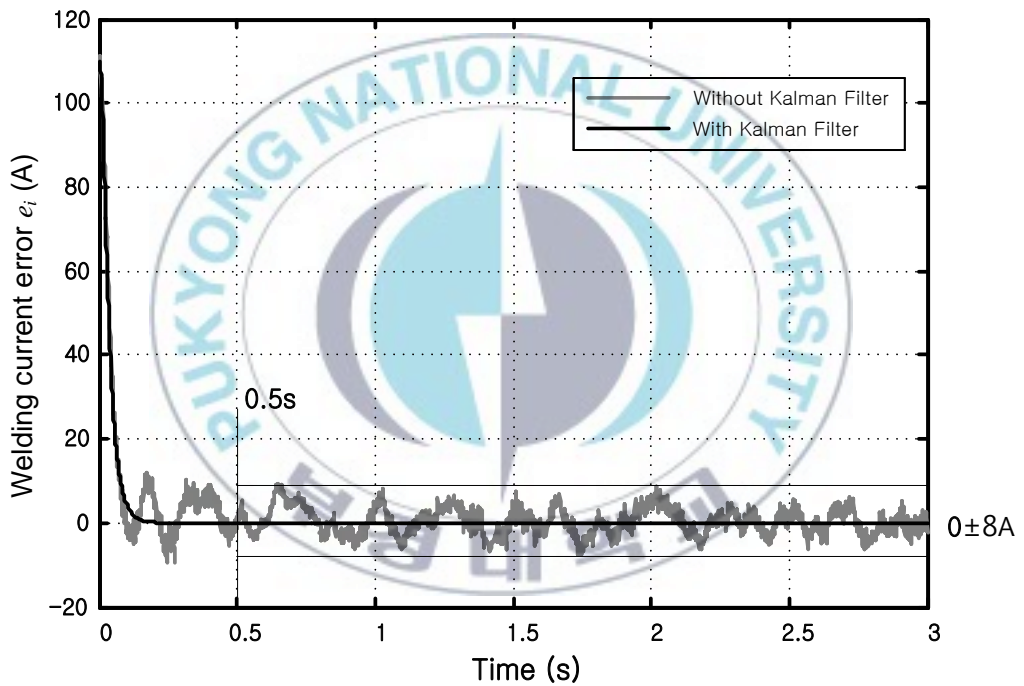


Fig. 5.11 Welding current error in simulation with/ without applying Kalman filter to Fuzzy Sliding Mode Control

Fig. 5.12 shows the arc voltage, V_{arc} , in simulation with/without applying Kalman filter to Fuzzy Sliding Mode Control. The Arc voltage, V_{arc} , with applying Kalman filter becomes stable and goes to 22V after 0.15 seconds. The Arc voltage without applying Kalman filter is also bounded around 22V with chattering after 0.15 seconds.

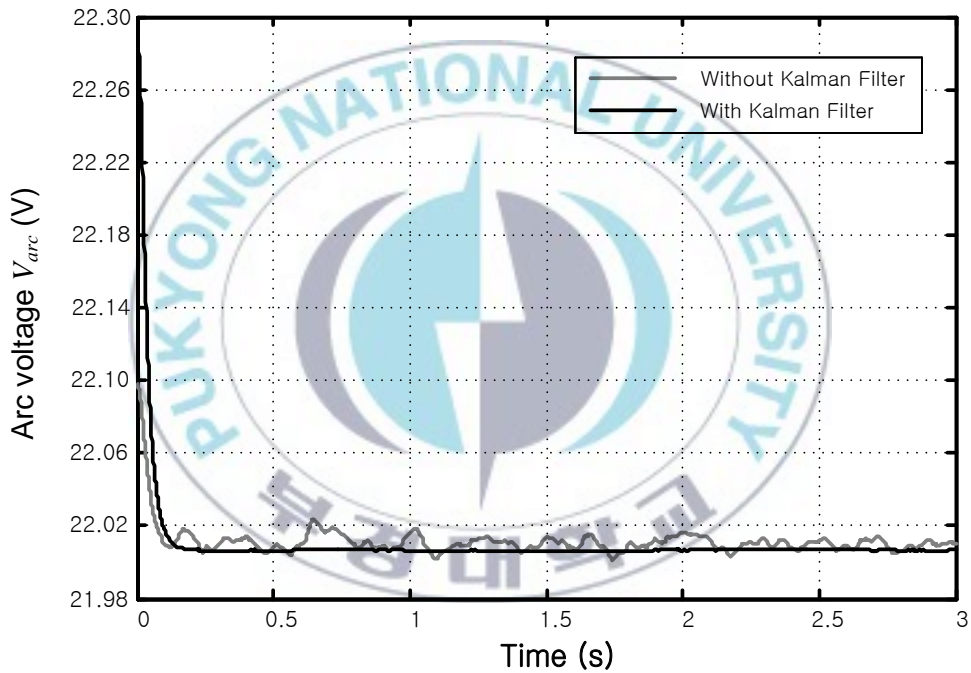


Fig. 5.12 Arc voltage in simulation with/ without applying Kalman filter to Fuzzy Sliding Mode Control

Fig. 5.13 shows the arc voltage, V_{arc} , in simulation with/ without applying Kalman filter to Fuzzy Sliding Mode Control. With applying Kalman filter, error becomes zero after 0.15 seconds. On the other hand, without applying Kalman filter, error becomes zero after 0.15 seconds and has oscillation around zero.

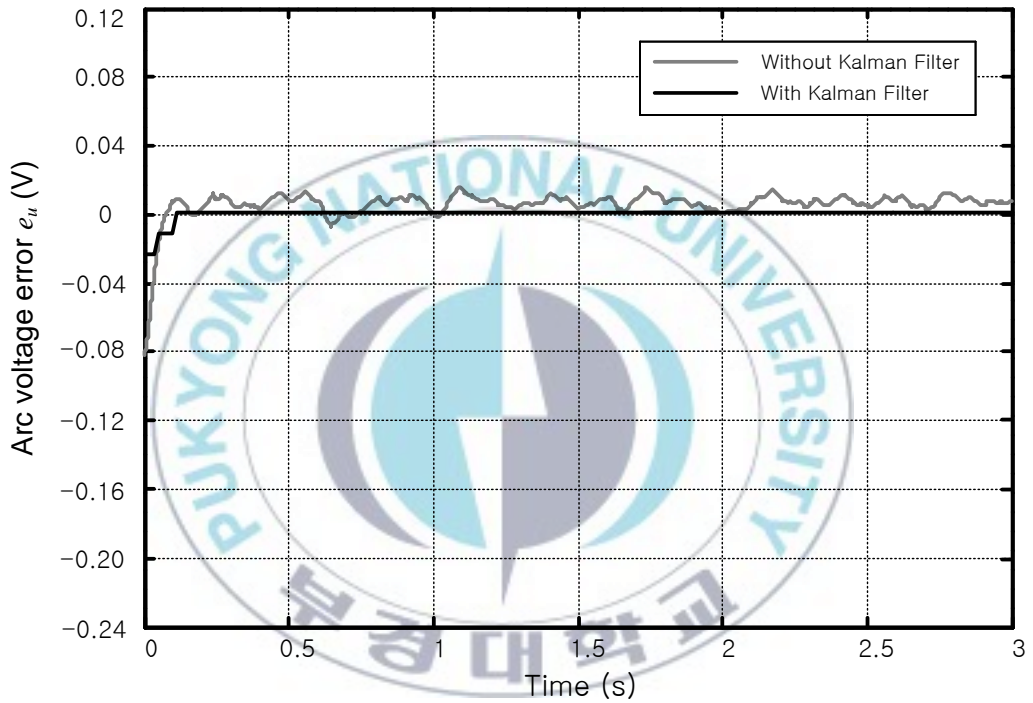


Fig. 5.13 Arc voltage in simulation with/ without applying Kalman filter to Fuzzy Sliding Mode Control

5.4 Summary

To reduce the process noise and measurement noise of GMAW system, Kalman filter is proposed as a digital filter. Based on the linear discrete-time system of GMAW, Kalman filter is designed. The Kalman filter works in 2 steps, prediction and update. The estimated outputs are updated each sample time step and approaches the real values eventually. To verify the effectiveness of Kalman filter, the simulation is done in closed loop condition. Closed loop simulation shows that the Kalman filter effectively reduces the noises. The simulation results applying Kalman filter to Fuzzy Sliding Mode Control show better performance than those applying Kalman filter to self-tuning Fuzzy PID. By combining the Kalman filter with self-tuning FuzzyPID controller and Fuzzy Sliding Mode Control, the simulation result shows that the Kalman filter reduces the noise effectively. The system performance with applying Kalman filter is better than that without applying Kalman filter. The simulation result using self-tuning Fuzzy PID shows that error using Kalman filter becomes zero after 0.25 seconds. On the other hand, the error without applying Kalman filter never becomes zero because of the noise. The output current in simulation applying Kalman filter to Fuzzy Sliding Mode Control is stable after 0.15 seconds and bounded around 110A. On the other hand, the output current without applying Kalman filter has oscillation and is stable after 0.5 seconds. The arc voltage in simulation applying Kalman filter to Fuzzy Sliding Mode Control becomes stable and goes to 22V after 0.15 seconds. On the other hand, the arc voltage without applying Kalman filter is bounded around 22V with chattering after 0.15 seconds.

Chapter 6. Conclusions and future works

6.1 Conclusions

This dissertation proposes modeling and controlling digital Gas Metal Arc Welding (GMAW) system. This system consists of PS-GMAW, Wire Feeding Unit (WFU), shielding gas and travel beam. The objective of this dissertation is to present modeling and innovative control algorithms for digital GMAW system. The conclusions of the dissertation are summarized as follows:

1. The basic concepts of welding machines, mathematical modeling of GMAW system and the prototype of GMAW system for experiment are given. The PS-GMAW is developed based on DSP TMS320F28335 technology, IGBT drive, motor drive and sensors such as current sensor and voltage sensor.
2. Mathematics modeling of PS-GMAW based on Kirchoff's current law and mathematics modeling for DC motor of WFU based on Newton's law and Kirchoff's voltage law are presented.
3. Self-tuning Fuzzy PID controller is applied for developing a digital GMAW system. The PS-GMAW is a constant voltage power supply. Its control system is developed based on the incorporation of DSP and IC TL494. A constant arc current is maintained by controlling the electrode feed rate. A self-tuning Fuzzy PID controller is proposed to control the welding current by controlling the electrode feed rate of WFU. A control law is obtained by

modifying the gains of conventional PID using tuning gains obtained from fuzzy controller. The fuzzy tuning gain is obtained from fuzzyfying the current error e and its derivative \dot{e} . Then, based on fuzzy rule base, the tuning gain is determined. The proposed controller shows that the welding current can tracks the setting current 110A after 0.25 seconds. The control law keeps the welding current stable and makes the current error go to zero. Simulation and experiment are carried out to evaluate the effectiveness of proposed control method for GMAW system. The self-tuning Fuzzy PID based on mathematical modeling is used in simulation using Kalman filter in chapter 5.

4. Based on the dynamics models of GMAW, the hybridized controller is proposed by combining proportional controller and Fuzzy Sliding Mode Controller. A control law is obtained by using sliding mode control technique and then modified the control input using values obtained from fuzzy controller. The system stability is guaranteed by using Lyapunov stability theory. The proposed hybridized controller tracks its setting value at 110A/22V after 0.15 seconds and keeps constant voltage and current GMAW. Simulation results show that the performance of rising time, settling time and steady state error of the output current of GMAW is better using proposed controllers than using conventional PID controller. Furthermore, experiment results show that the welding current and voltage are successfully controlled by the proposed controllers.
5. To reduce the process noise and measurement noise of GMAW system, Kalman filter is proposed as a digital filter. Based on the linear discrete-time

system of GMAW, Kalman filter is designed. The Kalman filter works in 2 steps, prediction and update. The estimated outputs are updated each sample time step and approaches the real values eventually. To verify the effectiveness of Kalman filter, the simulation is done. Furthermore, by combining the Kalman filter with self-tuning Fuzzy PID controller and Fuzzy Sliding Mode Control, the simulation results show that the Kalman filter reduces the noise effectively and the system performance applying Kalman filter is better than that without applying Kalman filter. The simulation results applying Kalman filter to FSMC show better performance than those applying Kalman filter to FPID.

6. Table 6.1 shows the proposed controller's advantages that can solve the problems of conventional controllers.

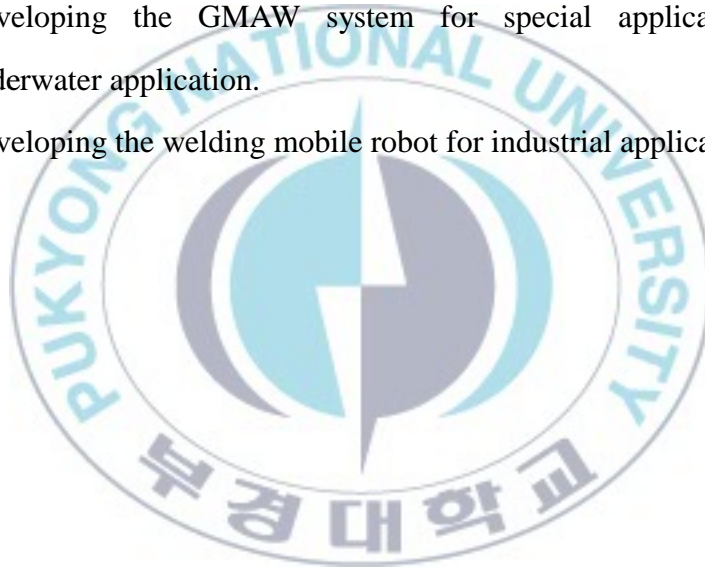
Table 6.1 Advantages of proposed controllers

Proposed controller	Advantages
Fuzzy PID control	Self-tuning parameters : getting the best parameters automatically in real time
Fuzzy Sliding Mode Control	Guarantee of stability for closed-loop system, No chattering phenomenon
Kalman filter	No delay time compare with band width filter, Removal of only noise from real data and no loss of data

6.2 Future works

This dissertation only focuses on the innovative algorithm to control the welding current and arc voltage of digital Gas metal Arc Welding. There are some future works as follows:

- ❖ Improving mathematical modeling to get more accurate simulation result.
- ❖ Developing better algorithm such as robust control to control the welding parameter and improve the welding quality.
- ❖ Developing the GMAW system for special application such as underwater application.
- ❖ Developing the welding mobile robot for industrial application.



References

- [1]. American Welding Society “Welding handbook 9th edition Vol.1-5”, Danver, American Welding Society, 2001.
- [2]. A. Scotti, V. Ponomarev and W. Lucas, “A scientific application oriented classification for metal transfer modes in GMA welding”, Journal of Materials Processing Technology, Vol. 212, pp. 1406-1413, 2011.
- [3]. A. Verma and M.M. Gor, “Actuator design for arc welding robot”, Journal of Science and Technology, Vol.6, pp. 48-53, 2010.
- [4]. A. Visioli, “Practical PID control”, London, Springer-verlag, 2006.
- [5]. B. O. Kam, S.M. Cho and S.B. Kim, “A study on bead height control of GMAW by short circuit time ratio”, Vol. 16, pp. 53-59, 2002.
- [6]. C. Edwards and S.K. Spurgeon., “Sliding mode control theory and applications”, Taylor & Francis, UK, 1998.
- [7]. C. Kim, M. Kang and S. Bae, “Statistical analysis of welding industry of South Korea”, Journal of Achievements in Materials and Manufacturing Engineering, Vol. 36, Issue 2, 2009.
- [8]. C. Voicu and L.R. Mistodie, “Corelationbetween drops dynamics and the GMAW-P arc stability”, The Annals of ‘Dunarea se Jos’ University of Galaty, Vol. 5, pp. 4.19-422, 2009.

- [9]. C. C. Kung and C.C. Liao, "Fuzzy sliding mode controller design for tracking control of non-linear system", American Control Conference, Baltimore, pp. 180-184, 1994.
- [10]. C. T. Leondes, "Fuzzy logic and expert systems applications", California, Academic Press Limited, 1998.
- [11]. C. Y. Lee, P. C. Tung and W. H. Chu, "Adaptive fuzzy sliding mode control for an automatic arc welding system", International Journal of Advance Manufacturing Technology, Vol. 29, pp. 481-489, 2006.
- [12]. C. Y. Lee, "The rise of Korean automobile industry", International Journal of Multidisciplinary Research, Vol. 1, Issue 6, pp. 428-439, 2011.
- [13]. D. Simon, "Optimal state estimation Kalman, H_{∞} and nonlinear approaches", New Jersey, John Willey and Sons, 2006.
- [14]. D. Q. Truong and K.K. Ahn, "Force control for hydraulic load simulator using self-tuning grey predictor fuzzy PID controller", International Symposium on Electrical & Electronics Engineering, pp. 86-91, 2009.
- [15]. D. S. Naidu, S. Ozcelik and K.L. Moore "Modeling, sensing and control of gas metal arc welding", Elsevier Science Ltd., UK, 2003.
- [16]. E. Karadeniz, U. Ozsarac and C. Yildiz, "The effect of process parameters on penetration in gas metal arc welding processes", Material and Design, Vol. 28, pp. 649-656, 2007.

- [17]. F. Ding, H. Jiankang, S. Yu and L. Lihui, "Fuzzy PID control of wire extension in pulsed MIG welding for aluminum alloy", 2010 Seventh International Conference on Fuzzy Systems and Knowledge Discovery, pp. 686-690, 2010.
- [18]. G. Bartolini and L. Fridman "Modern sliding mode control theory", Berlin, Springer-Verlag, 2008.
- [19]. G. Chen and T. T. Pham, "Introduction to fuzzy sets, fuzzy logic, and fuzzy control systems", Florida, CRC Press LLC, 2001.
- [20]. H. Terasaki and S.W. Simpson, "Circuit simulation for gas metal arc welding system", The 47th Midwest Symposium on Circuit and System, Vol. 3, pp. 387-390, 2004.
- [21]. H.L. Saunders, "MIG/MAG welding guide for gas metal arc welding (GMAW)", American Society for Metals, 1997.
- [22]. I. Gertsovich and N. Svanberg, "Analysis of MIG welding with aim on quality", Blekinge Institute of Technology, Sweden, 2008.
- [23]. J. Hu and H.L. Tsai, "Effects of current on droplet generation and arc plasma in gas metal arc welding", Journal of Applied Physics, Vol. 100, No. 053304, 2006.

- [24]. J.J. Lowke, “Physical basis for the transition from globular to spray modes in gas metal arc welding”, *Journal of Physics D: Applied Physics*, Vol. 42, 2009.
- [25]. J.P. Planckaert, E.H. Djermoune, D. Brie, F. Briand, and F. Richard, “Modeling of MIG/MAG welding with experimental validation using an active contour algorithm applied on high speed movies”, *Applied Mathematical Modeling*, Vol. 34, pp. 1004-1020, 2010.
- [26]. J.S. Gho, Y.M. Chae, K.S. Kim, C.Y. Won, H.S. Mok and G.H. Choe, “A study on the effect of wire feeding speed controller in inverter arc welding machine”, *Power Electronics and Drive Systems*, 1999, PEDS '99, Vol. 1, pp. 394-398, 1999.
- [27]. J.S. Thomsen, “Advanced control methods for optimization of arc welding“, Aalborg University, Denmark, 2004.
- [28]. K. Ogata, “Discrete-time control systems”, Prentice-Hall Inc., New Jersey, 1995.
- [29]. K.H. Shin and P.S. Ciccantell, “The steel and ship building industries of South Korea”, *American Sociological Association*, Vol. 15, pp. 167-192, 2009.

- [30]. K.K Ahn and B.K Nguyen, "Position control of shape memory alloy actuators using self-tuning fuzzy PID controller", *International Journal of Control, Automation, and Systems*, Vol. 4, No. 6, pp. 756-762, 2006.
- [31]. K.L. Moore, D.S. Naidu, R. Yender and J. Tyler, "Gas metal arc welding control: Part I Modeling and analysis", *Nonlinear Analysis Theory, Methods & Applications*, Vol. 30 No. 5, pp. 3101-3111, 1997.
- [32]. K.L. Moore, M.A. Abdelrahman and D.S. Naidu, "Gas metal arc welding control: Part II Control strategy", *Nonlinear Analysis*, Vol. 35, pp. 85-93, 1999.
- [33]. M. Abdelrahman, "Feedback linearization control of current and arc length in GMAW system", *Proceeding of the American Control Conference*, Philadelphia, 1998.
- [34]. M. Jafari and Z. Malekjamshidi, "Design of a new intelligent current controller for a welding machine", *Industrial Electronics & Applications (ISIEA)*, pp. 264-268. 2010.
- [35]. M. Lanzetta, M. Santochi and G. Tantussi, "Online control of robotized gas metal arc welding", *CIRPS Annals- Manufacturing Technology*, Vol. 50, pp. 13-16, 2001.
- [36]. M.A. Johnson and M.H. Moradi, "PID control new identification and design methods", London, Springer-Verlag, 2005.

- [37]. M.D. Ngo, V.H. Duy, N.T. Phuong, H.K. Kim and S.B. Kim, "Development of digital gas metal arc welding system", Journal of Material Processing Technology, Vol. 189, pp. 384-391, 2007.
- [38]. M.M. Anzehee, M. Haeri and A.R.D Tipi, "Gas metal arc welding process control based on arc length and arc voltage", International Conference on Control, Automation and Systems, 2010.
- [39]. M.M. Anzehee and M. Haeri, "Welding current and arc voltage control in a GMAW process using ARMarkov based MPC", Control Engineering Practice, Vol. 19, pp. 1408-1422, 2011.
- [40]. M.S. Grewal and A.P. Andrews, "Kalman filtering theory and practice using MATLAB", New Jersey, John Willey and Sons, 2008.
- [41]. P. Jiluan, "Arc welding control", Cambridge England, Wooden Publishing Limited, 2003.
- [42]. P. J. Modenesi and R.I. Reis, "A model for melting rate phenomena in GMA welding", Journal of Material Processing Technology, Vol. 189, pp. 199-205, 2007.
- [43]. P. K. Gosh, L. Dorn, S. Kulkarni and F. Hofmann, "Arc characteristics and behavior of metal transfer in pulsed current GMA welding of stainless steel", Journal of Materials Processing Technology, Vol. 209, pp. 1262-1274, 2009.

- [44]. P. V. Junhor, D.M.B. da Silva, M.V.S. Barreto and A.C. Pereira, “Control of machine of welding MIG using controller fuzzy”, Electric Machines and Drives, 2005 IEEE International Conference, pp. 1845-1849, 2005.
- [45]. R. Blondeau, “Metallurgy and mechanics of welding”, Hoboken, John Wiley & sons, 2008.
- [46]. S. Kodama, Y. Ikuno, Y. Ichiyama and N. Baba, “Process modeling of short-circuiting GMA welding and its application to arc sensor control”, Nippon Steel Technical Report, No, 95, 2007.
- [47]. S. Mishra and T. Debroy, “A heat-transfer and fluid-flow based model to obtain a specific weld geometry using various combination of welding variables”, Journal of Applied Physics, Vol. 98, 2005.
- [48]. S. Yu, M.B. Yuan, D.J. Xin and D.X. Chao, “Optimal switching function discrete slidingmode control based on unmatched uncertainties states observer”, WSEAS Transactions on System and Control, Vol. 5, pp. 291-300, Vol. 5, 2010.
- [49]. S.K. Jeong, G.Y. Lee, W.K. Lee and S.B. Kim, “Development of high speed rotating arc sensor and seam tracking controller for welding robot”, Industrial Electronics, 2001. Proceedings. ISIE 2001. IEEE, Vol. 2, pp. 845-850, 2001.

- [50]. T.J. Kim, J.P. lee, B.D, Min, D.W. Yooand C.U. Kim. “Characteristics of pulse MIG arc welding with a wire melting rate change by current polarity effect”, Journal of Electrical Engineering and Technology, Vol. 2, pp. 366-372, 2007.
- [51]. T.P. Quinn, C. Smith, C.N. McCowan, E. Blachowiakand R.B. Madigan,“Arc sensing for defects in constant-voltage gas metal arc welding”, Welding Journal, Vol. 78, pp. 322-328, 1999.
- [52]. V.D. Yurkevich, “Advances in PID control”, Rijeka, InTech 2011, pp. 299-306, 2007.
- [53]. W. Perruquetti and J.P. Barbot, “Sliding mode control engineering”, New York, Marcel Dekker, Inc, 2002.
- [54]. W.H. Chu and P.C. Tung “Development of an automatic arc welding system using a sliding mode control”, International Journal of Machine Tools &Manufacture, Vol. 45, pp. 933-939, 2004.
- [55]. W.P. Aung, “Analysis on modeling and simulink of DC motor and its driving system used for wheeled mobile robot”, World Academy of Science, Engineering and Technology, Vol. 32
- [56]. X. Huang and S. Chen, “SVM-based fuzzy modeling for the arc welding process”, Materials Science and Engineering, Vol. 427, pp. 181-187, 2006.

- [57]. X. Liu, "Dual bypass gas metal arc welding process and control", University of Kentucky, USA, 2008.
- [58]. Y.M. Zhang and Y.C. Liu, "Modeling and control of quasi-keyhole arc welding process", *Control Engineering Practice*, Vol. 11, pp. 1401-1411, 2003.
- [59]. Y.M. Chae, Y.T. Jang, M. Milan, J.S. Ghoand G.H. Choe, "A novel mixed current and voltage control scheme for inverter arc welding machines". *Applied Power Electronics Conference and Exposition 2001*, Vol. 1, pp. 308-313, 2001.
- [60]. Z. H. Rao, S. M. Liao and H. L. Tsai, "Effects of shielding gas compositions on arc plasma and metal transfer in gas metal arc welding", *Journal of Applied Physics*, Vol. 107, 2010.
- [61]. A. Anders, "Tracking down the origin of arc plasma Science-II. Early continuous discharges", *IEEE Transactions on Plasma Science*, Vol. 31, pp. 1060-1069, 2003.
- [62]. H. B. Cary and S. C. Helzer, "Modern welding technology", Upper Saddle River, Pearson Education, New Jersey, 2005.

Publication and Conference

A. International Journal

- [1] S. M. Shin, J. H. Suh, J. S. Im, H. R. Yoo and S. B. Kim, “Development of third-party damage monitoring system for natural gas pipeline”, KSME International Journal, Vol.17, No.10, pp. 1423-1430, 2003.
- [2] V. T. Dinh, H. Nguyen, S. M. Shin, H. K. Kim, S. B. Kim and G. S. Byun, “Tracking control of omnidirectional mobile platform with disturbance using differential sliding mode controller”, International Journal of Precision Engineering and Manufacturing, Vol. 13, No. 1, pp. 1-10, Jan. 2012.

B. Domestic Proceeding

- [1] 신승목, 전양배, 김춘식, 윤수호, 김상봉, “토목 구조물의 정밀 변위 측정 시스템의 개발 및 그 응용”, ICCAS 2001, International Conference on Control, Automation and Systems, pp. 1931-1934, Jeju, 2001.10.
- [2] 박성재, 신승목, 김상봉, 윤지근, “Development of emergency generator controller in automatic switch board”, 2002 춘계 학술 대회 논문집, 한국동력기계공학회, pp. 209-216, 2002.5.

- [3] 박성재, 신승목, 이채규, 김상봉, “교량 구조물의 정밀 계측 시스템 개발”, 2003 년도 춘계 학술 대회 강연 및 논문집, 대한기계학회, pp. 857-862, 2003.4.23-25
- [4] 신승목, 서진호, 띠, 김상봉, “음향 전파 모델을 이용한 천연가스 배관용 타공사 모니터링 시스템의 개발”, 2003 년도 춘계 학술 대회 강연 및 논문집, 대한기계학회, pp. 905-910, 2003.4.23-25

C. International Proceeding

- [1] S.M. Shin, C. Hur, C.S. Kim, S.H. Yoon and S.B. Kim, “Development of real time monitoring and forecasting/emergency system for land slide of road”, ICCAS 2001, International Conference on Control, Automation and Systems, pp.1023-1026, Jeju, 2001.10
- [2] S.M. Shin, H.R. Yoo, J.S. Im and S.B. Kim, “Development of third-party damage monitoring system for natural gas pipeline”, Proceedings of the 8th Conference on Science and Technology, Control & Automation, pp.119-124, Vietnam National University, HCM City, April, 2002.
- [3] S.M. Shin, J.H. Suhand S.B. Kim, “Real-time monitoring system to detect third-party damage on natural gas pipeline using acoustic detection method”, 2004 International Conference on Dynamics, Instrumentation

and Control, pp.1-10, Nanjing Association for Science and Technology,
China, 2004.



Appendix A

Discretization

Exponential function has the following relationship :

$$e^{At} = I + At + \frac{1}{2!} A^2 t^2 + \dots + \frac{1}{n!} A^n t^n + \dots = \sum_{k=0}^{\infty} \frac{A^k t^k}{k!} \quad (\text{A.1})$$

$$\begin{aligned} \frac{d}{dt} e^{At} &= A + A^2 t + \frac{A^3 t^2}{2!} + \dots + \frac{A^n t^{n-1}}{(n-1)!} + \dots \\ &= A \left[I + At + \frac{A^2 t^2}{2!} + \dots + \frac{A^{n-1} t^{n-1}}{(n-1)!} + \dots \right] = A e^{At} \end{aligned} \quad (\text{A.2})$$

A continuous time state equation and output equation are :

$$\dot{x}(t) = Ax(t) + Bu(t) \quad (\text{A.3})$$

$$y(t) = Cx(t) \quad (\text{A.4})$$

From Eq.(A.3), the following is obtained :

$$\dot{x}(t) - Ax(t) = Bu(t) \quad (\text{A.5})$$

Multiplying e^{-At} in both side of Eq. (A.5) is as follows :

$$e^{-At} [\dot{x}(t) - Ax(t)] = \frac{d}{dt} [e^{-At} x(t)] = e^{-At} Bu(t) \quad (\text{A.6})$$

Integrating Eq.(A.5) between 0 and t gives :

$$e^{-At} x(t) = x(0) + \int_0^t e^{-A\tau} Bu(\tau) d\tau \quad (\text{A.7})$$

Therefore, solution of continuous-time state equation of Eq. (A.3) is :

$$x(t) = e^{At} x(0) + \int_0^t e^{A(t-\tau)} Bu(\tau) d\tau = e^{At} x(0) + e^{At} \int_0^t e^{-A\tau} Bu(\tau) d\tau \quad (\text{A.8})$$

Discrete time state equation of Eq. (A.8) putting $t = kT$ and $u(t) = u(kT)$ for $kT \leq t \leq kT + T$ is obtained as,

$$x(kT) = e^{Akt} x(0) + e^{Akt} \int_0^{kT} e^{-A\tau} Bu(\tau) d\tau \quad (\text{A.9})$$

For $t = (k+1)T$, the following is obtained from Eq. (A.8).

$$x((k+1)T) = e^{A(k+1)T} x(0) + e^{A(k+1)T} \int_0^{(k+1)T} e^{-A\tau} Bu(\tau) d\tau \quad (\text{A.10})$$

Multiplying e^{AT} in the both side of Eq. (A.9) and subtracting it from Eq. (A.10) gives:

$$x((k+1)T) = e^{AT} x(kT) + e^{A(k+1)T} \int_{kT}^{(k+1)T} e^{-A\tau} Bu(\tau) d\tau \quad (\text{A.11})$$

From discrete-time state equation of Eq.(A.11) that $u(\tau) = u(kT)$, $x(0)$ is the value of the state at time $t = t_0$, $x(k)$ is the value of the state at time $t_0 + Tk, T$ is defined to be the sampling time, and $t = \tau - kT$, the following is obtained :

$$\begin{aligned} x((k+1)T) &= e^{AT} x(kT) + e^{AT} \int_0^T e^{-At} Bu(kT) dt \\ &= e^{AT} x(kT) + \int_0^T e^{A(T-t)} B dt u(kT) \end{aligned} \quad (\text{A.12})$$

Eqs. (A.3) and (A.4) can be expressed as a discrete time system as follows :

$$x(k+1) = Fx(k) + Gu(k) \quad (\text{A.13})$$

$$y(k) = Hx(k) \quad (\text{A.14})$$

If Eqs.(A.13) and (A.14) compared to Eqs. (A.4) and (A.12), respectively,

the the following is obtained:

$$F = e^{AT} \quad (\text{A.15})$$

$$G = \left(\int_0^T e^{A(T-t)} \right) B dt = A^{-1} (e^{AT} - I) B \quad (\text{A.16})$$

$$H = C \quad (\text{A.17})$$

Using Taylor series, Eqs. (A.15) and (A.16) are reduced as:

$$F = e^{AT} = I + AT + \frac{A^2 T^2}{2!} + \frac{A^3 T^3}{3!} + \dots + \frac{A^n T^n}{n!} \dots \quad (\text{A.18})$$

$$G = \int_0^T e^{A(T-t)} dt B = - \int_T^0 e^{A\tau} d\tau B = \int_0^T e^{A\tau} d\tau B$$

$$= \left[A\tau + \frac{A^2 \tau^2}{2!} + \frac{A^3 \tau^3}{3!} + \dots + \frac{A^n \tau^n}{n!} \dots \right]_0^T B \quad (\text{A.19})$$

$$= A^{-1} \left[AT + \frac{A^2 T^2}{2!} + \frac{A^3 T^3}{3!} + \dots + \frac{A^n T^n}{n!} \dots \right] B \quad (\text{A.20})$$

$$= A^{-1} [e^{AT} - I] B \quad (\text{A.21})$$

where $\tau = T - t$ and $-dt = d\tau$

Eqs. (A.18) and (A.20) taking $n = 1$ becomes

$$F = e^{AT} = I + AT \quad (\text{A.22})$$

$$G = A^{-1} [AT] B = TB \quad (\text{A.23})$$

Using Eqs. (A.22)- (A.23), the discrete time equations of GMAW is obtained as follows:

$$x(k+1) = (I + AT)x(k) + BTu(k) \quad (\text{A.24})$$

$$= \left(\begin{bmatrix} 1 & 0 \\ 0 & 1 \end{bmatrix} + \begin{bmatrix} 0 & 1 \\ -a_0 & -a_1 \end{bmatrix} T \right) x(k) + \begin{bmatrix} 0 \\ b_0 \end{bmatrix} Tu(k) \quad (\text{A.25})$$

$$= \left(\begin{bmatrix} 1 & T \\ -a_0 T & 1 - a_1 T \end{bmatrix} \right) x(k) + \begin{bmatrix} 0 \\ b_0 T \end{bmatrix} u(k) = Fx(k) + Gu(k) \quad (\text{A.26})$$

$$y(k) = Hx(k) = Cx(k) = [c \ 0]x(k) \quad (\text{A.27})$$

From Eqs. (A.26) and (A.27), the following are obtained.

$$F = \begin{bmatrix} 1 & T \\ -a_0 T & 1 - a_1 T \end{bmatrix}, G = \begin{bmatrix} 0 \\ b_0 T \end{bmatrix}, H = [c \ 0] \quad (\text{A.28})$$

